Universidade de Brasília
Instituto de Geociências
Programa de Pós-graduação em Geologia

Evolução geológica de migmatitos da Zona de Cisalhamento Patos, Província Borborema, NE do Brasil: Abordagem integrada U-Pb, Lu-Hf e Sm-Nd

Geological evolution of migmatites from the Patos Shear Zone, Borborema Province, NE Brazil: Integrated U-Pb, Lu-Hf, and Sm-Nd approach

FRANKIE JAMES SERRANO FACHETTI

Orientador: Prof. Dr. Reinhardt Adolfo Fuck

Tese de Doutorado Nº 204

Brasília, dezembro/2023

Universidade de Brasília
Instituto de Geociências
Programa de Pós-graduação em Geologia

Evolução geológica de migmatitos da Zona de Cisalhamento Patos, Província Borborema, NE do Brasil: Abordagem integrada U-Pb, Lu-Hf e Sm-Nd

Geological evolution of migmatites from the Patos Shear Zone, Borborema Province, NE Brazil: Integrated U-Pb, Lu-Hf, and Sm-Nd approach

FRANKIE JAMES SERRANO FACHETTI

Tese apresentada ao Programa de Pós-Graduação em Geologia – Instituto de Geociências – IG da Universidade de Brasília – UnB como requisito parcial obrigatório para a obtenção do título de Doutor em Geologia.

Área de concentração: Geologia Regional

Orientador: Prof. Dr. Reinhardt Adolfo Fuck

Comissão Examinadora:

Prof. Dr. Nilson Francischini Botelho (IG/UnB)
Prof. Dr. Ticiano José Saraiva dos Santos (UNICAMP)
Prof. Dr. Lauro Cezar Montefalco de Lira Santos (UFPE)

Ficha catalográfica elaborada automaticamente,
com os dados fornecidos pelo(a) autor(a)

Fe FACHETTI, FRANKIE JAMES SERRANO
Evolução geológica de migmatitos da Zona de Cisalhamento Patos, Província Borborema, NE do Brasil: Abordagem integrada U-Pb, Lu-Hf e Sm-Nd / FRANKIE JAMES SERRANO FACHETTI; orientador Reinhardt Adolfo Fuck. -- Brasília, 2023.
135 p.

Tese(Doutorado em Geologia) -- Universidade de Brasília, 2023.

1. retrabalho crustal. 2. evolução crustal. 3. colisão continental. 4. migmatização. 5. isotopos de U-Pb, Lu-Hf e Sm-Nd . I. Fuck, Reinhardt Adolfo , orient. II. Título.

AGRADECIMENTOS

Após uma jornada de anos, celebramos a conquista deste trabalho que agora se materializa. Quero expressar minha gratidão a todos que desempenharam um papel crucial nesse percurso. À minha amada família - Olga, Geraldo, Fabiana, Flávio, Ítalo, Davi e Welliton - vocês foram o meu porto seguro nos momentos desafiadores.

Agradeço imensamente aos Professores Elton e Fuck pela paciência, orientações sagazes e valiosos ensinamentos que moldaram este trabalho. Também estendo minha gratidão aos Professores Ana, Carlos Humberto, Roberta, Nilson, Endel, Guilherme e Gustavo pelo apoio técnico que foi essencial para o sucesso deste projeto.

Quero reconhecer meus colegas de jornada, Alanielson, Pedro, Dhener, Francisco, Newton, Larissa, Carol, Letícia, Juliana, Ingrid, Gabriel, Cesar, Gilson, Marcelo, Rodrigo, Ravena, Carlos, Manu e Paola. Somente nós compreendemos os desafios superados e as vitórias conquistadas ao longo do caminho.

E não posso deixar de expressar minha profunda gratidão ao Presidente da República Federativa do Brasil, Luiz Inácio Lula da Silva. Sua visão e implementação de políticas públicas revolucionaram o perfil socioeconômico dos estudantes do ensino superior no país, desempenhando um papel fundamental em minha trajetória acadêmica. O presente trabalho foi realizado com apoio da Coordenação de Aperfeiçoamento de Pessoal de Nível Superior-Brasil (CAPES) - Código de Financiamento 001.

A cada um que fez parte desta jornada, meu sincero obrigado. Este trabalho é resultado do esforço coletivo que enriqueceu não apenas meu conhecimento, mas também minha jornada pessoal e profissional. Que cada nome aqui mencionado seja um reflexo do meu profundo apreço e reconhecimento por suas contribuições inestimáveis.

RESUMO

A configuração tectônica da Província Borborema exibe complexo arcabouço estrutural, definido por história policíclica desde o Arqueano até o final do Neoproterozóico. Diferentes blocos crustais foram acrescidos, amalgamados e retrabalhados, formando um conjunto de sub províncias, cada qual com história evolutiva distinta, separadas por um sistema de zonas de cisalhamento interconectadas. A Zona de Cisalhamento Patos corresponde a extensa estrutura de mais de 400 km de comprimento, orientação E-W, separando o Domínio Rio Grande do Norte e a Zona Transversal a sul, no estado da Paraíba. No corredor de cisalhamento, cuja cinemática é essencialmente dextral, afloram migmatitos, granitos foliados, gnaisses diversos e faixas de milonitos, afetados em maior ou menor grau de deformação. Neste trabalho são apresentados resultados de diferentes fases de migmatização nas rochas que se encontram na faixa definida pelo Lineamento de Patos. O principal objetivo foi determinar a sequência de eventos que permitiu estabelecer diferentes fases de geração de migmatitos em rochas submetidas a diferentes eventos de fusão parcial e retrabalhamento crustal. Idades U-Pb de 3.5 e 3.3 Ga são interpretadas como sendo as idades de cristalização dos protólitos dos migmatitos no Paleoarqueano. Idades meso-neoarqueanas encontradas nas rochas datadas mostram história complexa, marcada por magmatismo e deformação em 3.2, 3.0 e 2.65 Ga, com fases de geração de migmatitos contemporâneos. Novo pulso de eventos magmáticos com migmatização associada se desenvolve no Paleoproterozóico, com idades de 2.2, 2.1 e 2.0 Ga. Por fim, um evento em 575 Ma é bem evidente na geração de migmatitos róseos avermelhados, com magmatismo granítico rico em K, cortando e injetando as rochas mais antigas. Assim, embora a Orogenia Brasiliana seja responsável pelo desenvolvimento das extensas zonas de cisalhamento transcorrentes na região, e o desenvolvimento do arcabouço tectônico do Lineamento Patos, os resultados obtidos mostram que foram preservados fragmentos de crosta antiga ao longo do mesmo. A semelhança entre as idades e a estruturação geológica dessas rochas permite concluir que as unidades de crosta paleoproterozóica do Cráton do São Francisco e os inliers adjacentes do embasamento, que carregam uma história tectônica semelhante, sejam consideradas como um sistema orogênico

coevo, possivelmente contínuo em sua formação, e sejam conhecidas como Orógeno Grande São Francisco.

Palavras-chave:
retrabalho crustal; crescimento crustal; colisão continental; evolução crustal; migmatização; isotopos de Hf-Nd; desequilíbrio.

ABSTRACT

The Patos Shear System (PSS) is a 20-40 km wide domain of anastomosing shear zones intercalated with non-mylonitic segments at the core of the Borborema Province, a transpressive Neoproterozoic orogen in NE Brazil, part of the reworked São Francisco Craton. We provide new U-Pb, Lu-Hf and Sm-Nd analyses for non-mylonitic basement migmatitic orthogneisses. Four magmatic events (~3.40, 3.26, 2.68-2.64 and 2.18 Ga), as well as three metamorphic/migmatization ones (~3.0, 2.1-2.0 Ga and 570-575 Ma) were evidenced. Metamorphism and leucosome injection at ~570-575 Ma attest the PSS was subjected to high heat from medium- to high-temperature dextral shearing. A distinct Paleoproterozoic (~2.1-2.0 Ga) migmatization event is probably related to the amalgamation of Neo-Paleoarchean blocks and an older ~3.0 Ga metamorphic event may represent crustal thickening induced by the collision between small Paleoarchean landmasses. Paleoarchean magmatic protoliths obtained here were emplaced concomitant with TTGs and high-K rocks regionally, and our Hf data from these rocks, after filtering for isotopic disequilibrium during anatexis, combined with a large compilation, point to an apparent mixing of magma derived from a CHUR-like reservoir with older crust, better reconciled, although not conclusively, with a stagnant-lid scenario dominated by plume activity. Hf data from 2.68-2.64 Ga old migmatites plot along a conspicuous Meso-Neoproterozoic “reworking array” and our preferred model is that magmatism between 2.9 and 2.6 Ga took place in an accretionary/collisional continental setting, following renewed juvenile additions between ~3.2 to 2.9 Ga. At last, the crystallization age of ~2.18 Ga of an orthogneiss is related to another Wilson Cycle. Our data point to reworking of Archean lithologies during the Paleoproterozoic, as evidenced by inherited Archean zircon grains, but ƐHf and ƐNd close to CHUR suggest involvement of more juvenile material as well, consistent with regional data, and the preferred scenario is that of subduction followed by collision.

Keywords:

crustal reworking; crustal growth; continental collision; crustal Evolution; migmatization; Hf-Nd isotopes and disequilibrium

SUMÁRIO

SUMÁRIO

CAPÍTULO 1

INTRODUÇÃO

1.1 Importância e justificativa da Tese

A compreensão das fontes e processos que possibilitaram a geração e o crescimento da crosta continental é uma das questões mais relevantes e desafiadoras da pesquisa geológica na história evolutiva da Terra. Principalmente pela escassez de rochas paleoarqueanas (> 3,5 Ga), o estudo isotópico e geoquímico das raras ocorrências de crosta antiga é estratégico para a compreensão da evolução geológica do planeta (Condie et al., 2000, 2010; Evans et al., 2011).

Nesse contexto, a Província Borborema exibe complexa evolução crustal, com diferentes episódios de geração de crosta continental, desde o Paleoarqueano até o Neoproterozoico (Almeida et al., 1981; Dantas et al., 2004, 2008; Van Schmus et al., 2008, 2011; Padilha et al., 2017; Oliveira e Medeiros, 2018). Ademais, diversos episódios e formação de cinturões orogênicos e tafrogênicos ocorreram durante o Riaciano até o Neoproterozoico (Brito Neves, 2011), culminando com processos colisionais e fusão de massas marcados pela instalação de zonas de cisalhamento e granitogênese sintectônica de ca. 575 Ma (Jardim de Sá, 1994; Van Schmus et al. 2003; Brito Neves et al., 2000; Souza et al., 2007; Hollanda et al., 2015; Santos et al., 2008, 2015).

Núcleos arqueanos na Província Borborema, retrabalhados durante orogêneses paleoproterozoicas entre 2,3 e 2,0 Ga, são registrados no Maciço São José do Campestre (Dantas et al., 2004, 2013), no Bloco Campo Grande (Ferreira et al., 2017), em São Tomé-RN (Ruiz et al., 2018), no Maciço Tróia-CE (Costa et al., 2015) e em unidades do Complexo Patos (Viegas et al., 2013), como altos do embasamento da Zona Transversal (Van Schmus et al., 2011; Brito Neves, 2011). A presença de tipos de rochas e idades tão distintas torna a Província Borborema uma área chave para o entendimento do Pré-Cambriano no Brasil.

1.2 Seleção da área e objetivos da pesquisa

O Lineamento Patos é uma das estruturas mais marcantes da Província Borborema, desenvolvido durante a Orogenia Brasiliana (Corsini et al., 1991; Santos et al., 2010; Viegas et al., 2013), representando um sistema de cisalhamento transcorrente de mais de 400 km de extensão, por 45 km de largura, que separa o Domínio Rio Grande do Norte (DGN) dos domínios da Zona Transversal, a sul (Brito Neves, 1975; Jardim de Sá, 1994; Santos, 1996; Costa, 2002), e constitui importante limite litosférico na Província Borborema (Van Schmus et al., 2008, 2011). As rochas que constituem a Zona de Cisalhamento Patos são gnaisses migmatíticos arqueanos que sofreram sucessivos eventos de retrabalhamento no Paleoproterozóico e Neoproterozóico (Costa, 2002; Viegas et al., 2013).

A presença de núcleos arqueanos retrabalhados por orogêneses mais jovens é uma feição expressiva dos complexos migmatíticos da Província Borborema, como Maciço São José do Campestre (MSJC) no Domínio Rio Grande do Norte, na Zona de Cisalhamento Patos e nas rochas do embasamento da Zona Transversal (Costa, 2002; Guimarães & Silva Filho 2000; Viegas et al. 2014).

Apesar dos estudos já realizados no Complexo Patos nas últimas décadas, percebe-se algumas lacunas no entendimento da evolução geodinâmica dessa região. Um dos principais problemas é a datação absoluta dos processos de fusão, migmatização e geração de rochas em complexos polideformados. As incertezas analíticas empregadas nos estudos pretéritos, realizados há 20 anos, baseadas principalmente no método ICP-TIMS, que embora seja muito preciso, não permitia a identificação de histórias complexas que registrem múltiplos episódios geológicos a que foram submetidas essas rochas (Costa, 2002)

O objetivo principal desta tese é a investigação dos processos relacionados à formação dos migmatitos e gnaisses que ocorrem ao longo da Zona de Cisalhamento Patos, com ênfase em métodos geocronológicos e geoquímica isotópica mais robustos.

Esta tese trás dados geoquímicos, isotópicos e geocronológicos inéditos sobre a evolução crustal e os processos de fusão parcial numa escala regional do limite entre o Domínio Rio Grande do Norte e a Zona Transversal da Província Borborema, respondendo especificamente aos seguintes questionamentos:

a) Qual é a idade de geração dos migmatitos da Zona de Cisalhamento Patos?
b) Qual o tipo do magmatismo da Zona de Cisalhamento Patos?
c) Por quais eventos tectono-metamórficos essa zona foi afetada ao longo do Arqueano e Proterozoico e seus respectivos ambientes?
d) Como se comportam os sistemas isotópicos U-Pb e Lu-Hf em terrenos migmatíticos polideformados?

A área de estudo está localizada no Centro-Oeste do Estado da Paraíba, na Região Nordeste do Brasil (Fig. 1). Os limites geográficos são os meridianos 36°30’ a Oeste, 37°40’ a Leste e os paralelos 6°52’ a Norte e 7°11’ a Sul, abrangendo parte das folhas topográficas SUDENE (escala 1:100.000) Patos (SB-24-ZD-I), Juazeirinho (SB-24-ZD-II), Jardim Seridó (SB-24-ZB-V), Serra Negra do Norte (SB-24-ZB-IV), Pombal (SB-24-ZA-VI) e Piancó (SB-24-ZC-III). Os principais municípios integrantes da área pesquisada são Patos, Juazeirinho, Catingueira, Teixeira e Santa Luzia.

O acesso é dado a partir de João Pessoa-PB pela BR-230, seguindo aproximadamente 230 km para oeste até o trevo subsequente a Juazeirinho, tomando a PB-228 por 95 km até o município de Patos-PB (Fig. 1).

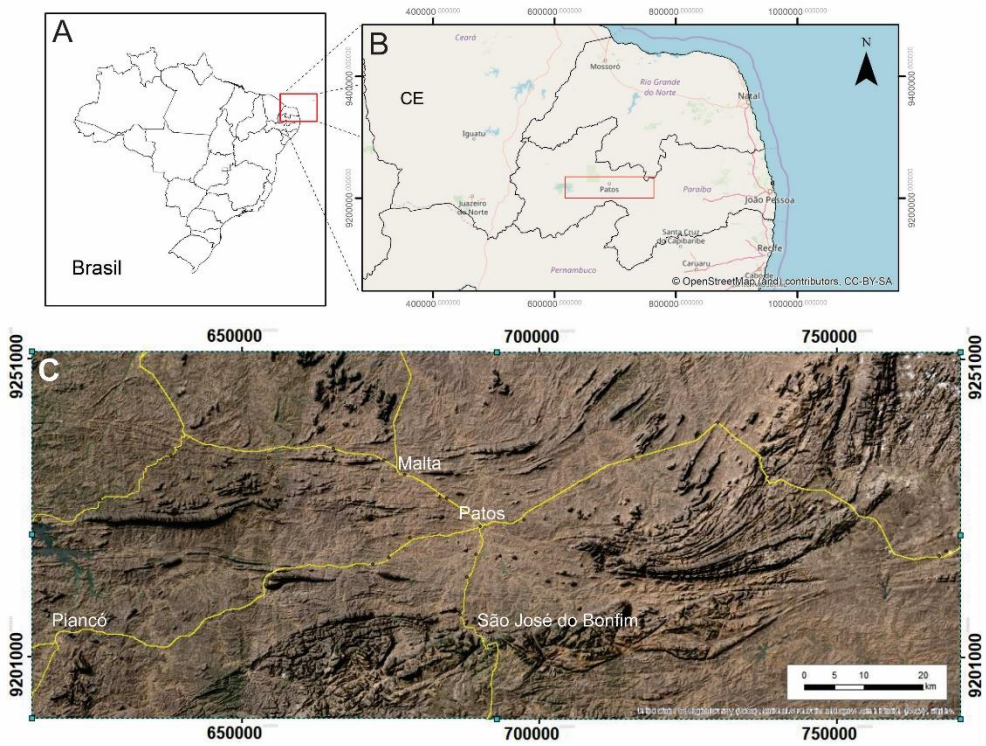

Figura 1. Mapa de localização e vias de acesso do Lineamento Patos. A) mapa do Brasil; B) Extremo nordeste do Brasil. Retângulo vermelho mostra o local da área estudada; C) Região do município de Patos-PB.

CAPÍTULO 2

Contexto Geológico

2.1 Província Borborema

A Província Borborema (Almeida et al., 1981), localizada no nordeste do Brasil, apresenta complexa evolução geológica pré-cambriana, marcada principalmente pela ocorrência de fragmentos crustais paleoarqueanos (3,5 Ga; Dantas et al., 2004), magmatismo juvenil Riaciano (2,25 – 2,15 Ga; Souza et al., 2007) e instalação de complexos sistemas de cisalhamentos com granitogênese neoproterozoica (ápice em 575 Ma; Van Schmus et al., 2011; Nascimento et al., 2015) durante a Orogenia Brasiliano-Panafricana (Caby, 1989; Arthaud et al., 2008; Van Schmus et al., 2008). A Província Borborema é compartimentada em sub-províncias, domínios, terrenos, blocos e maciços com histórias evolutivas distintas, separados por zonas de cisalhamentos regionais (Jardim de Sá, 1994; Santos, 1996; Brito Neves et al., 2000) (Fig. 2).

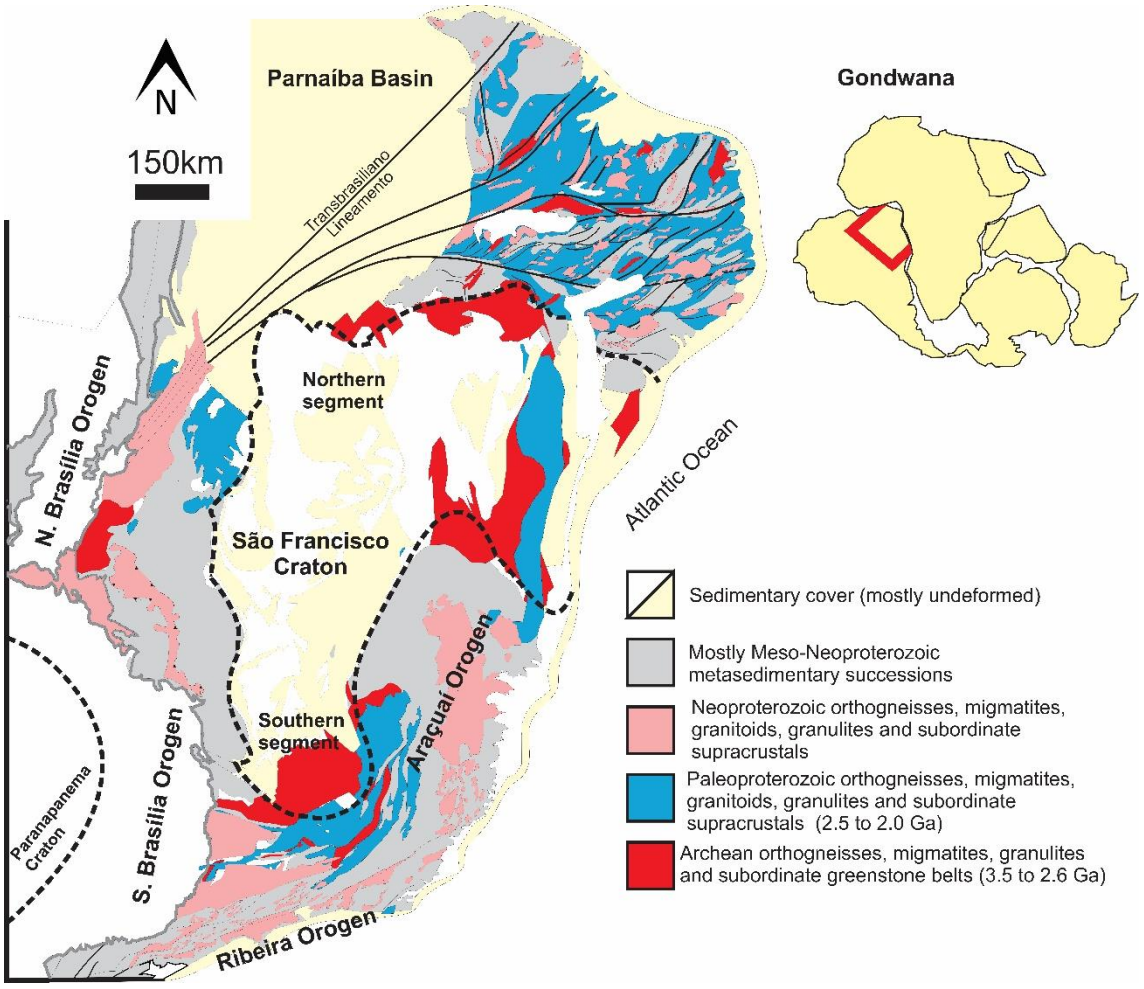

Figura 2. Mapa do Oriente da Plataforma Sul-Americana, mostrando as idades das unidades constituintes. Adaptado de Marimon et al. (2020) e Neves et al. (2021).

2.2 Lineamento Patos

O Lineamento Patos é uma mega zona de cisalhamento, orientada em trend W-E, com aproximadamente 400 km de comprimento, que separa o Domínio Rio Grande do Norte e a Zona Transversal (Santos, 1996). Compreende complexo corredor estrutural de cerca de 45 km de largura com cinemática dextral, que abriga diversas zonas de cisalhamento subordinadas, blocos e lentes desmembradas de fragmentos crustais com idades que variam do Arqueano (Costa, 2002) ao Neoproterozoico (Hollanda et al., 2015), num embasamento gnáissico-migmatítico predominantemente paleoproterozoico (Santos et al. 2010; Viegas et al 2013). Em reconstituições paleogeográficas corresponde, no Oeste Africano, ao Lineamento Adamoua (Costa, 2002; Arthaud et al., 2008; Viegas et al., 2013).

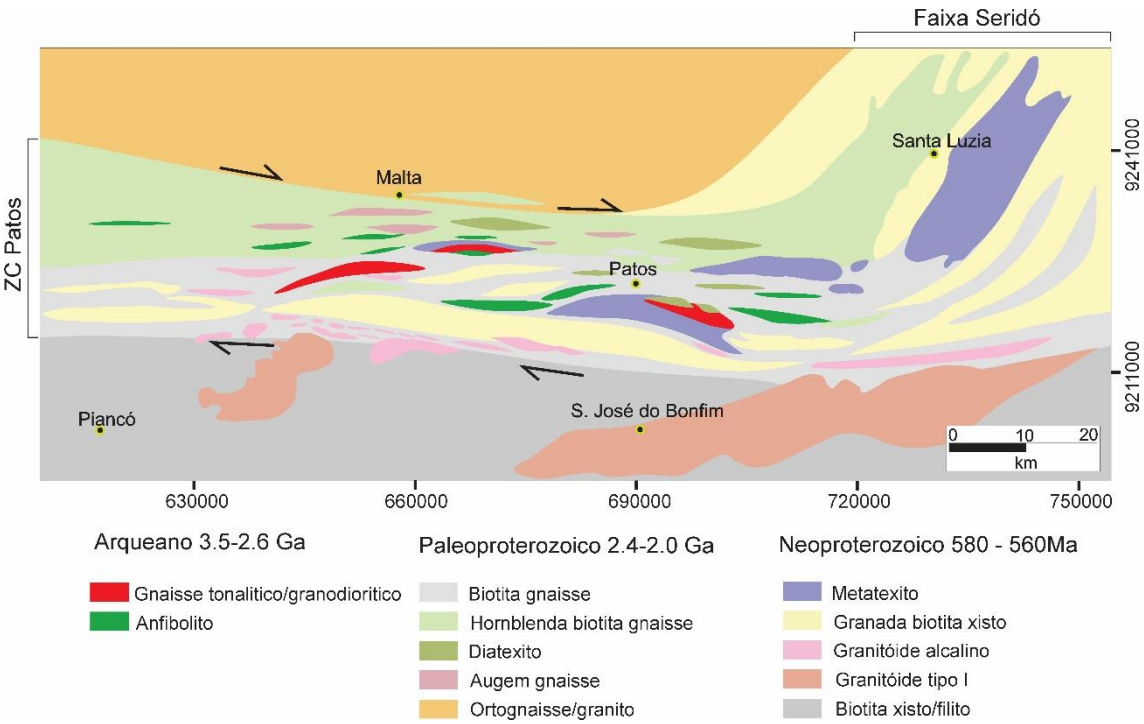

Figura 3. Mapa geológico da região de Patos-PB. ZC=zona de cisalhamento . Modificado de Viegas et al., (2014)

O embasamento do Lineamento Patos é constituído por complexos migmatito-gnáissicos de idade pré-cambriana, formados principalmente por rochas ortoderivadas que foram submetidas a múltiplos eventos de deformação e metamorfismo do fácies anfibolito superior ao fácies xisto verde (Scheid e Ferreira,1991; Costa et al., 2002). Os complexos são constituídos por migmatitos tonalíticos, granodioríticos e monzograníticos, gnaisses de composição granodiorítica, monzogranítica e quantidade subordinada de sienogranito (Ferreira e Santos, 2000; Santos et al., 2006), com forte estruturação W-E, formado por um sistema conjugado de zonas de cisalhamento secundárias entre a Zona Cisalhamento Patos e Malta (Fig. 4).

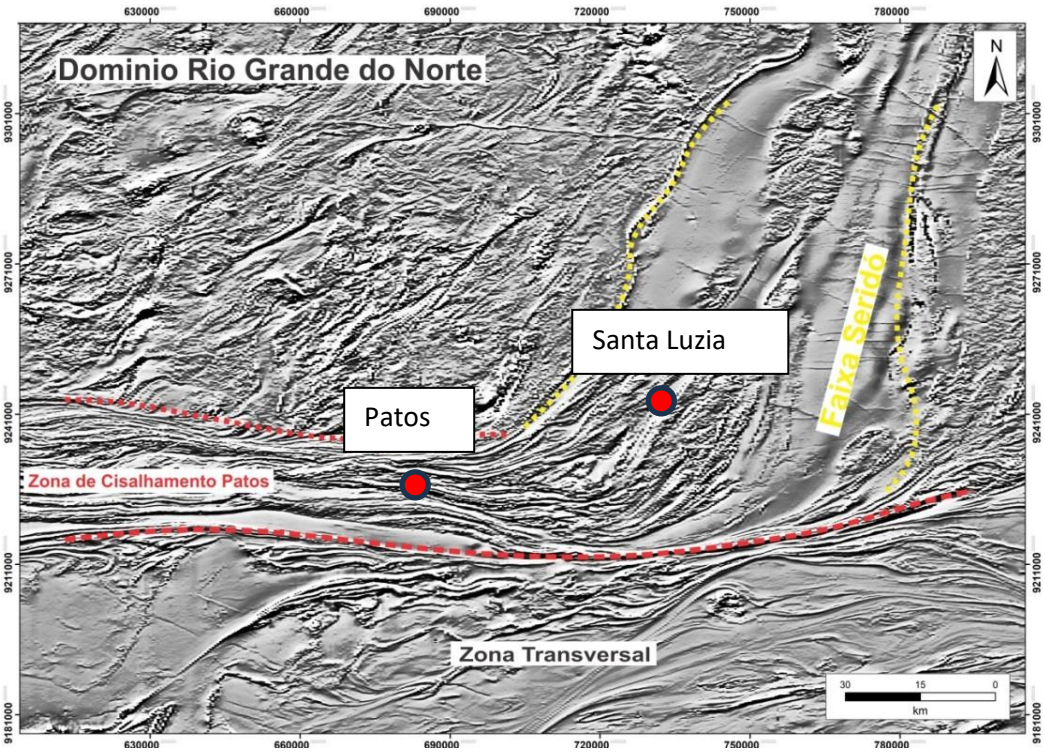

Figura 4. Mapa da primeira derivada vertical de dados magnetométricos, elucidando as estruturas do sistema de cisalhamento na Região de Patos.

Santos et al. (1999) sugerem que os dados isotópicos para esta região apontavam para unidades com idade arqueana – paleoproterozoica. Os núcleos arqueanos dos sistemas de dobramentos agrupam rochas que parecem evoluir a partir de duas fontes diferentes. Um grupo de ortognaisses demonstra ser de

fonte máfica, possivelmente mantélica e outro grupo de ortognaisses mostra Maciço São José do Campestre está localizado características de fonte supracrustal retrabalhada. O conjunto se mostra polideformado e migmatizado em trama complexa com anatexitos (Scheid & Ferreira, 1991). Costa (2002) caracterizou unidades antigas arqueanas próximo a Patos (PB), com gnaisses e migmatitos de natureza cálcio-alcalina, derivados de crosta arqueana, retrabalhada durante as orogenias riaciana e Brasiliana. Trabalhos anteriores (Corsini et al. 1991; Vauchez et al., 1995) demonstram pelo método Ar-Ar que em ca. 500 Ma houve resfriamento crustal. Viegas et al. (2013) mostram que um sistema mecanicamente acoplado em meio a um deslocamento transcorrente é transferido para uma faixa transpressiva, injetando material fundido (anatexitos) com idade de 575 Ma (Viegas et al., 2014).

Núcleos arqueanos semelhantes ao da Zona de Cislhamento Patos são reconhecidos na Borborema, entre eles, o Complexo Granjeiro (2.5 Ga), localizado no extremo oeste do Lineamento Patos, composto por granodioritos e tonalitos e recoberto pela sequência metassedimentar Lavras da Mangabeira (Santos, 1996). Os complexos Mombaça e Cruzeta, localizados no SW da Província, foram datados em torno de 2.6 Ga (Silva, 2002)

O Maciço São José do Campestre está localizado 300 km a norte da área estudada, constituindo segmento muito antigo da Plataforma Sul-Americana (Dantas et al., 2013), formado por TTG's com idades U-Pb em zircão entre 3,41 e 2,69 Ga, de fonte mantélica, com valores εNd positivos (Dantas et al., 2004, 2013).

Também no domínio central do Ceará, ocorrem ortognaisses paleoproterozoicos e metabasaltos com idades modelo Nd entre 2,5 e 2,4 Ga e idades de cristalização entre 2,35 e 2,13 Ga e migmatitos (Fetter et al., 2000; Santos et al., 2008) com fragmentos de crosta arqueana, denominados Maciço Pedra Branca e Tróia (Fetter et al., 2003; Arthaud et al., 2008). O Domínio Ceará Central possui duas sequências paleoproterozoicas. A primeira unidade, chamada Algodões-Choró, ocorre adjacente ao Complexo Cruzeta e compreende rochas supracrustais (metatufos, rochas metassedimentares e metabasaltos com geoquímica característica de platô oceânico). Lentes de anfibolito apresentam

dados isotópicos com idade isocrônica de Sm-Nd e evaporação de zircão de 2.2 Ga e intrusões tonalíticas e quatzo-dioríticas de 2.1 Ga (Martins et al., 2009). A segunda são intrusões com idade de 2.2 Ga de corpos e diques com composição quartzo-diorítica e dioritos com idade modelo Nd de 2.3 Ga (Arthaud et al., 2008). São identificados corpos de ortognaisses paleoproterozoicos com idade U-Pb entre 2.4 e 2.3 Ga no Domínio Rio Grande do Norte (Dantas, 1996) e Ceará Central (Fetter et al., 2000), que são interpretados como remanescente de crosta arqueana retrabalhada e acresção juvenil, respectivamente. A Faixa Seridó abrange uma área comprimida pelo maciço Rio Piranhas a oeste e pelo maciço São José do Campestre a leste e, a sul, inflexiona convergentemente ao Lineamento Patos.

CAPÍTULO 3

Primeiro artigo

Artigo publicado por Gondwana Research:

Paleoarchean to Neoproterozoic crustal formation and migmatization events in the Borborema Province, NE Brazil: implications for the growth and reworking of the continental crust

Frankie J.S. Fachetti [1], Reinhardt A. Fuck [1], Rodrigo S. Marimon [2], Alanielson Ferreira [1], Ana C.D. da Costa [3], Chris J. Hawkesworth [4]

[1]Instituto de Geociências, Universidade de Brasília (UnB), Brasília-DF, Brazil.

[2]Departamento de Geologia e Paleontologia, Museu Nacional, Universidade Federal do Rio de Janeiro (UFRJ), Rio de Janeiro-RJ, Brazil

[3]Faculdade de Geociências, Universidade Federal de Mato Grosso (UFMT), Cuiabá-MT, Brazil.

[4]School of Geosciences, Bristol University, Bristol, United Kingdom

Highlights: crustal reworking, crustal growth, continental collision, crustal evolution, migmatization, Hf-Nd isotopes and disequilibrium

Abstract

The Patos Shear System (PSS) is a 20-40 km wide domain of anastomosing shear zones intercalated with non-mylonitic segments at the core of the Borborema Province, a transpressive Neoproterozoic orogen in NE Brazil, part of the reworked São Francisco Craton. We provide new U-Pb, Lu-Hf and Sm-Nd analyses for non-mylonitic basement migmatitic orthogneisses. Four magmatic events (~3.40, 3.26, 2.68-2.64 and 2.18 Ga), as well as three metamorphic/migmatization ones (~3.0, 2.1-2.0 Ga and 570-575 Ma) were evidenced. Metamorphism and leucosome injection at ~570-575 Ma attest the PSS was subjected to high heat from medium- to high-temperature dextral shearing. A distinct Paleoproterozoic (~2.1-2.0 Ga) migmatization event is probably related to the amalgamation of Neo-Paleoarchean blocks and an older ~3.0 Ga metamorphic event may represent crustal thickening induced by the collision between small Paleoarchean landmasses. Paleoarchean magmatic protoliths obtained here were emplaced concomitant with TTGs and high-K rocks regionally, and our Hf data from these rocks, after filtering for isotopic disequilibrium during anatexis, combined with a large compilation, point to an apparent mixing of magma derived from a CHUR-like reservoir with older crust, better reconciled, although not conclusively, with a stagnant-lid scenario dominated by plume activity. Hf data from 2.68-2.64 Ga old migmatites plot along a conspicuous Meso-Neoproterozoic "reworking array" and our preferred model is that magmatism between 2.9 and 2.6 Ga took place in an accretionary/collisional continental setting, following renewed juvenile additions between ~3.2 to 2.9 Ga. At last, the crystallization age of ~2.18 Ga of an orthogneiss is related to another Wilson Cycle. Our data point to reworking of Archean lithologies during the Paleoproterozoic, as evidenced by inherited Archean zircon grains, but ε_{Hf} and ε_{Nd} close to CHUR suggest involvement of more juvenile

material as well, consistent with regional data, and the preferred scenario is that of subduction followed by collision.

3.1 Introduction

Studies of when and how the continental crust was generated have typically focused on areas where samples of new crust are exposed, relatively little affected by crustal reworking. However, much of the continental crust is made up of polymetamorphic rocks and it remains a priority to evaluate processes of crust generation from these terrains (e.g., Moyen and Laurent, 2018; Hawkesworth et al., 2020; Windley et al., 2021). Establishing the proportion of juvenile versus reworked crust in the magmatic record, and hence the rate at which the continental crust grew through time, is not straightforward and many have attempted to do so by means of Hf and O systematics for instance (e.g., Hawkesworth and Kemp, 2006; Kemp et al., 2009; Belousova et al., 2010; Dhuime et al., 2012). However, mixing between crustal and mantle material, either during magmatic emplacement and ascent through the continental crust (Hildreth and Moorbath, 1988), and Sm/Nd (Bea et al., 2023) and Lu/Hf fractionation (e.g., Xia et al., 2022) during crustal partial melting, may obscure the estimated timing of new crust generation from model Nd and Hf ages. At present, the rate at which the continental crust grew through time, and the rates of crust generation that are recorded in different terrains, remain largely enigmatic, evidenced by the sheer variety of crustal growth models (Hawkesworth et al., 2019).

Detailed field, isotopic and petrographic study of Archean to Paleoproterozoic crust is important to establish the relative roles reworking and juvenile additions played in the ancient magmatic record, not least since old rocks often bear evidence of several successive magmatic and metamorphic events (e.g., Laurent et al., 2014; Valeriano et al., 2022). Whereas most juvenile crustal production in the modern Earth takes place in subduction settings, its preservation is tied to collisional orogens (Hawkesworth et al., 2009) as is most of the deformation, and therefore reworking of ancient crust. A considerable proportion of collisional reworking takes place in crustal-scale shear zones, where partial melting, magma and fluid migration, as well as differentiation, occurs (e.g., Jessup and Wintsch, 2001; Carvalho et al., 2016, 2017; Giraldo et

al., 2019; Vinagre et al., 2020). In addition, large shear zones often develop at weakened sections of the crust, such as old suture zones, and can thus preserve the record of multiple tectono-thermal episodes, that led to extensive changes in the constitution and structure of the continental crust (e.g., Giraldo et al., 2019; Zhong et al., 2023).

As most of the ancient continental crust is composed of rocks subjected to one or more metamorphic episodes, migmatites are abundant and represent the reworking of continental crust during major tectono-metamorphic events (e.g., Sawyer, 2008). The study of zircon grains from crustal melts, such as diatexites, provide information regarding the age of the partial melting event, and of the Hf isotopic composition of the source. Furthermore, the investigation of leucosome-melanosome pairs and/or polymetamorphic migmatites can help clarify whether Hf-Nd isotopic fractionation took place during anatexis, which may distort the calculated model ages (Xia et al., 2022; Beat et al., 2023).

We have investigated, by means of U-Pb, Lu-Hf and Sm-Nd systematics, basement polymetamorphic migmatitic orthogneisses with protoliths of Archean to Paleoproterozoic age, located in the Patos Shear Zone, a large-scale Neoproterozoic transpressive shear zone system at the heart of the Brasiliano Borborema Province (Fig. 1; Archanjo et al., 2021), whose basement is thought to represent the continuation of the São Francisco Craton prior to Neoproterozoic reworking (Neves et al., 2021). The studied migmatites, characterized by moderate (metatexites) to higher degrees of partial melting (diatexites), bear evidence of several reworking and crustal growth episodes. The new data are incorporated into a large compilation of Paleoarchaen to Paleoproterozoic Hf data from igneous/metaigneous basement rocks that constitute the São Francisco Craton, including inliers in adjacent Neoproterozoic orogens. We use both our data and the wider compilation to better constrain regional processes of crustal growth and differentiation and discuss implications for continental formation and recycling during continental collision, and models for Paleoarchean tectonics.

3.2 Regional Geology

The Neoproterozoic Borborema Province (BP) is a mosaic of mobile belts amalgamated by the convergence of the São Luís-West Africa and São Francisco-Congo cratons during the Brasiliano/Pan African Orogeny, as part of the western portion of the Gondwana supercontinent (Fig. 1A; Almeida et al., 1981; Brito Neves et al., 2000). The northern segment of the Borborema Province (BP) comprises dismembered Archean nuclei, surrounded by progressively younger accreted terrains of Paleoproterozoic to Neoproterozoic age, and is cross-cut by extensive regional shear zones (e.g., Dantas et al., 2004, 2013; Viegas et al., 2014; Souza et al., 2016; Hollanda et al., 2015; Costa et al., 2018; Ruiz et al., 2019; Ferreira et al., 2020, 2021; Archanjo et al., 2021). Archean nuclei of the Borborema Province (Fig. 1) range in age from ~3.5 Ga (São José do Campestre) to approximately 2.5 Ga and are dominated by metaigneous rocks, including migmatitic TTG and high-K orthogneisses with distinctive amphibolitic residues and enclaves (Fetter, 1999; Dantas et al., 2004, 2013; Ganade et al., 2017; Santos et al., 2018; Pitarello et al., 2019; Ferreira et al., 2020, 2021). In the oldest rocks of the BP, the ~3.5 Ga São José do Campestre massif, Dantas et al. (2004; 2013) obtained an age of ~2.65 Ga for leucosomes, a possible evidence of a Neoarchean migmatization event.

Archean nuclei of the Borborema Province (Fig. 1) range in age from ~3.5 Ga (São José do Campestre) to approximately 2.5 Ga and are dominated by metaigneous rocks, including migmatitic TTG and high-K orthogneisses with distinctive amphibolitic residues and enclaves (Fetter, 1999; Dantas et al., 2004, 2013; Ganade et al., 2017; Santos et al., 2018; Pitarello et al., 2019; Ferreira et al., 2020, 2021). In the oldest rocks of the BP, the ~3.5 Ga São José do Campestre massif, Dantas et al. (2004; 2013) obtained an age of ~2.65 Ga for leucosomes, a possible evidence of a Neoarchean migmatization event.

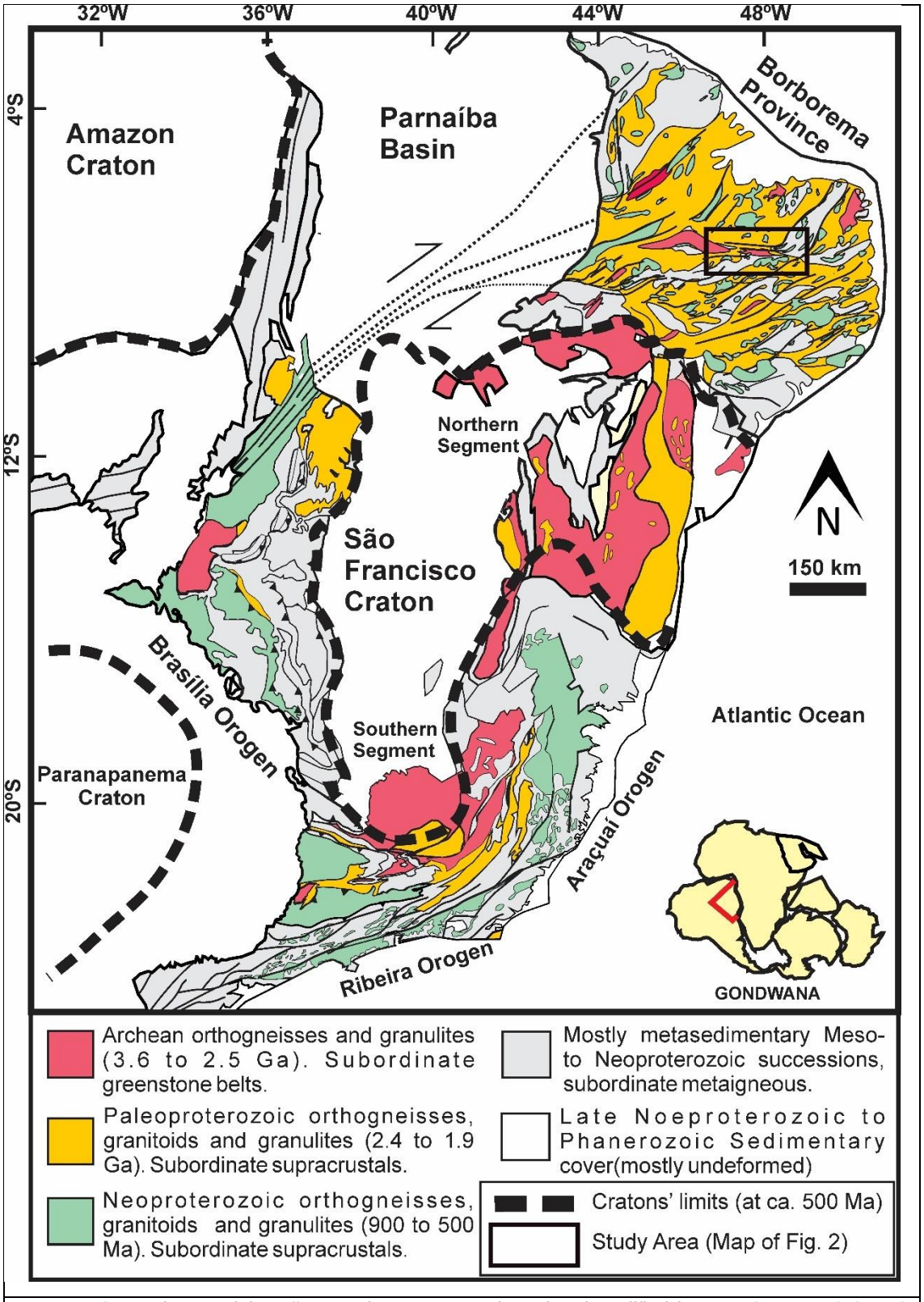

Figure 1) Map of the São Francisco Craton. Adapted and modified from Marimon et al. (2020) and Neves et al. (2021).

The Neoproterozoic Patos Shear Zone System, (PSZS) where the migmatites studied here were collected, is a 700-km long, 20-40 km wide, E-W

structure, characterized by steep-dipping foliations with dextral offset. The PSZS is part of a wider, 2000 km long, shear zone system that marks the suture between the São Francisco-Congo and São Luís-West Africa cratons during Gondwana formation (e.g., Caxito et al., 2020; Fossen et al., 2022). Most of the rocks that crop out along the Patos Shear Zone are migmatitic orthogneiss complexes of Archean to Paleoproterozoic protholith age, with extensive granitic leucosome formation and associated amphibolitic residues, as well as Neoproterozoic metasedimentary cover successions (Fig. 2; Viegas et al., 2013, 2014; Hollanda et al., 2015; Fossen et al., 2022). Cross-cutting all lithological units, anastomosed shear zones (high strain zones) of hundreds of meters wide are characterized by well-developed mylonites, that are separated by larger domains of lower strain (non-mylonitic domains). Orthogneisses that crop out in the Patos system form several dismembered and elongated blocks (Fig. 2) comprising of stromatic metatexites and diatexites with schollen and schlieren structures, as well as extensive leucosome vein injections and leucosome bodies in diatexites (Van Schmus et al., 2011; Viegas et al., 2013, 2014; Archanjo et al., 2021). High-grade mylonites are common at the northern segment of the Patos Shear Zone, whereas subsequent reactivation at lower temperatures during exhumation is evidenced at its southern portion (Viegas et al., 2014).

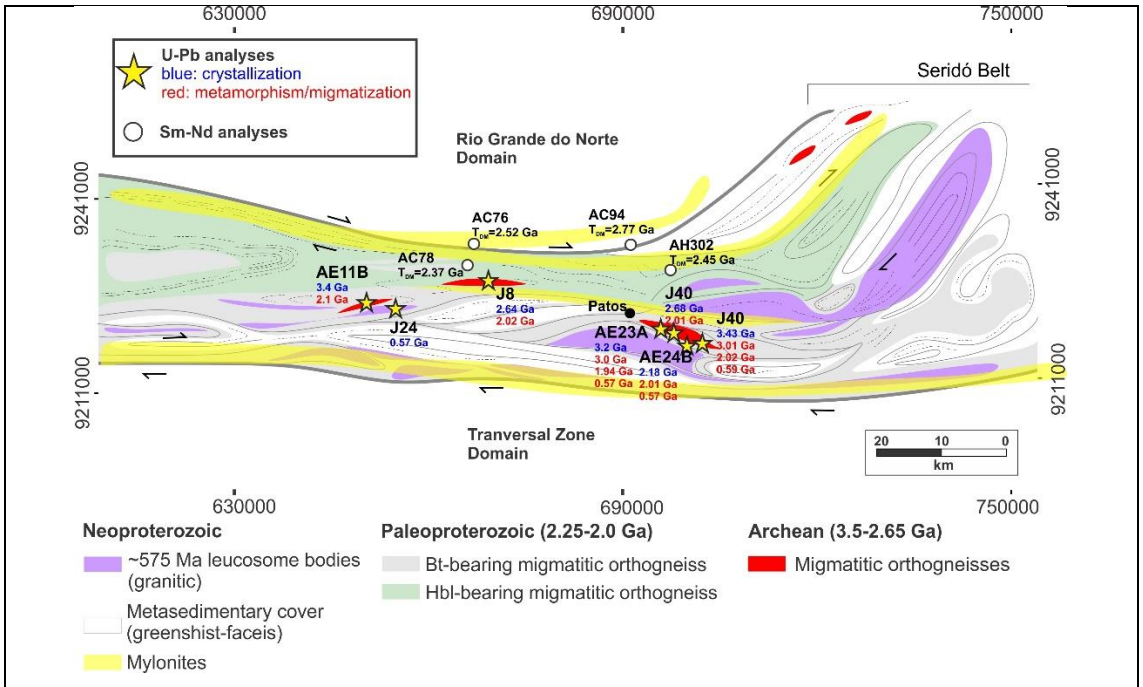

Figure 2) Geological map of the Patos Shear Zone. RGND = Rio Grande do Norte Domain; ZTD – Transversal Zone Domain. Adapted and modified from Viegas et al. (2014).

3.2 Methodology

3.2.1 Zircon U-Pb

Analyses of zircon grains from seven migmatite samples were performed on a Thermo-Fisher Neptune LA-ICP-MS coupled to a Nd:YAG UP213 New Wave laser at the Geochronology Laboratory of the University of Brasília (UnB). The ablation was done with 30µm spots with laser frequency at 10 Hz and energy of 30% for approximately 40 seconds, resulting in laser energy of 1.02 J/cm^2. Between two to five grains from a given sample were analyzed between standard GJ-1 (Jackson et al., 2004) analyses. Raw data were processed off-line and reduced in an Excel spreadsheet. During analyses, a 91500 zircon standard was used to control accuracy (Wiedenbeck et al., 2004). Common lead (^{204}Pb) was monitored using ^{202}Hg and (^{204}Hg + ^{204}Pb), but common lead corrections were not necessary due to low ^{204}Pb counts in most samples. For detailed information on the procedures applied at the Geochronology Laboratory of the University of Brasília, the reader is referred to Bühn et al. (2009).

3.2.2 Zircon Lu-Hf

Following U-Pb dating, zircon grains from four samples were selected for Lu-Hf analyses. Samples were analyzed at the Geochronology Laboratory of the University of Brasília (UnB) in a Neptune LA-ICP-MS. The selected spot size was 50 µm and the ablation time was set for 50 seconds. During analytical sessions, a GJ-1 zircon standard was analyzed and the ^{176}Hf/^{177}Hf value of 0.2820059±15 (2σ) was obtained, in agreement with the literature (Morel et al., 2008). Isotopes ^{171}Yb, ^{173}Yb and ^{175}Lu were used to adjust for the isobaric interference of ^{176}Yb and ^{176}Lu (Chu et al., 2002). Hf isotopic ratios were normalized for ^{179}Hf/^{177}Hf of 0.7325 (Patchett, 1983). εHf(t) values were calculated using the decay constant (λ) of 1.865x10^{-11} (Scherer et al., 2001) and the CHUR values of ^{176}Lu/^{177}Hf= 0.0332 and ^{176}Hf/^{177}Hf=0.282772 (Blichert-Toft and Albarède, 1997). Two-stage model ages (T_{DM}) were calculated from the initial Hf isotopic composition of zircon grains, using the average continental crust ^{176}Lu/^{177}Hf of 0.010 (Pietranik et al., 2008). The ratios of ^{176}Lu/^{177}Hf=0.0384 and ^{176}Hf/^{177}Hf=0.28325 were considered for the depleted mantle (Chauvel and Blichert-Toft, 2001). For detailed information regarding the Lu-Hf methodology applied at the

Geochronology Laboratory of the University of Brasília the reader is referred to Matteini et al. (2010).

3.2.3 Whole-rock Sm-Nd

Eleven samples were selected for whole-rock Sm-Nd analyses at the Geochronology Laboratory of the University of Brasília by means of a TRITON TIMS (multicollector) in static mode. Approximately 50 mg of powdered samples were spiked with a ^{149}Sm-^{150}Nd solution and subsequently dissolved. The determination of Sm and Nd concentration followed conventional chromatography ion exchange techniques, with Teflon columns and LN-Spen resin. The material was put into Re evaporation filaments and measured in the spectrometer. Uncertainties for Sm/Nd and $^{143}Nd/^{144}Nd$ were better than 0.1% (2 σ) and 0.0015 (1σ), respectively, according to repeated analyses of international standard BHVO-1. The obtained $^{143}Nd/^{144}Nd$ values were normalized to $^{146}Nd/^{144}Nd=0.7219$ and the applied decay constant was of (σ) $6{,}54\times10^{-12}$. Model ages (T_{DM}) were calculated using the method of DePaolo (1981). For detailed information regarding the Sm-Nd methodology applied at the Geochronology Laboratory of the University of Brasília the reader is referred to Gioia and Pimentel (2000).

3.3 Results

We use the migmatite nomenclature of Sawyer (2008). The term paleosome is a portion of the rock unaffected by partial melting, retaining all its original characteristics. The polymetamorphic stromatic metatexites studied here, with mostly mm to cm-scale leucosomes, present no portions unaffected by partial melting, as to be called paleosome according to the strict definition above. Since it is hard to separate leucosome from melanosome due to scale, we collected large (>5 kg) representative samples of the neosome from stromatic metatexites which are characterized by limited degrees of partial melting and limited to absent melt migration. The neosome of stromatic metatexites, which dominate the rock, may be texturally different than the protolith, but whole-rock analyses of relatively large samples yield geochemical and isotopic compositions very close to that of the protolith (i.e., paleosome). Sawyer (2008) used the term

paleosome loosely in a few instances to represent rafts in diatexites, which we believe, considering our samples, may not reflect the composition of the protolith due to melt-depletion after high-degrees of partial melting and thus are better described as residue.

3.1 Petrography and field aspects

Migmatitic orthogneisses comprise the basement rocks in the Patos Shear Zone and are the focus of this study. They vary from stromatic metatexites to *schlieren* and *schollen* diatexites, locally with nebulitic texture (Fig. 3; Sawyer, 2008). Gneissic banding is locally cross-cut by coarse-grained leucocratic leucosome veins of metric-scale, as well as granitic leucosome bodies (Figs. 2 and 3). Boudinaged amphibolitic lenses, that likely represent residual rafts or enclaves, are common in diatexites.

Diatexites (samples J41, AE23A, AE11B and AE24B), whose amphibolite residue and leucosome were selected for isotopic analyses, have bulk granodioritic to granitic composition, with syn-anatectic structures. The leucosomes are composed of K-feldspar, plagioclase, quartz, and biotite (Fig. 3). Amphibolite residues (rafts) are composed of hornblende, plagioclase, biotite, and minor quartz, with accessory zircon, apatite, and titanite (Fig. 3).

Associated with some diatexites there are leucocratic metagranites (sample J24), that either crosscut the gneissic banding or form distinct bodies of metric scale (Fig. 4E). These rocks are interpreted to have formed by the migration and accumulation of magma due to migmatization (leucosome veins) in adjacent diatexites and are dominated by K-feldspar and quartz, with minor plagioclase. Accessory minerals include zircon, apatite, and monazite.

Stromatic metatexites (samples J40 and J8) have granodioritic to granitic bulk compositions (Fig. 4). They are represented by in-situ melt production and little or no melt migration, which makes it easier to establish the protolith's composition (paleosome) compared to diatexites. Stromatic metatexites are characterized by K-feldspar, plagioclase and quartz-rich leucosomes and biotite-dominated melanosomes, with subordinate quartz, plagioclase, and rare K-feldspar. Accessory phases in metatexites include zircon, apatite, titanite, allanite and monazite. Locally, metatexites are mylonitic (Fig. 4).

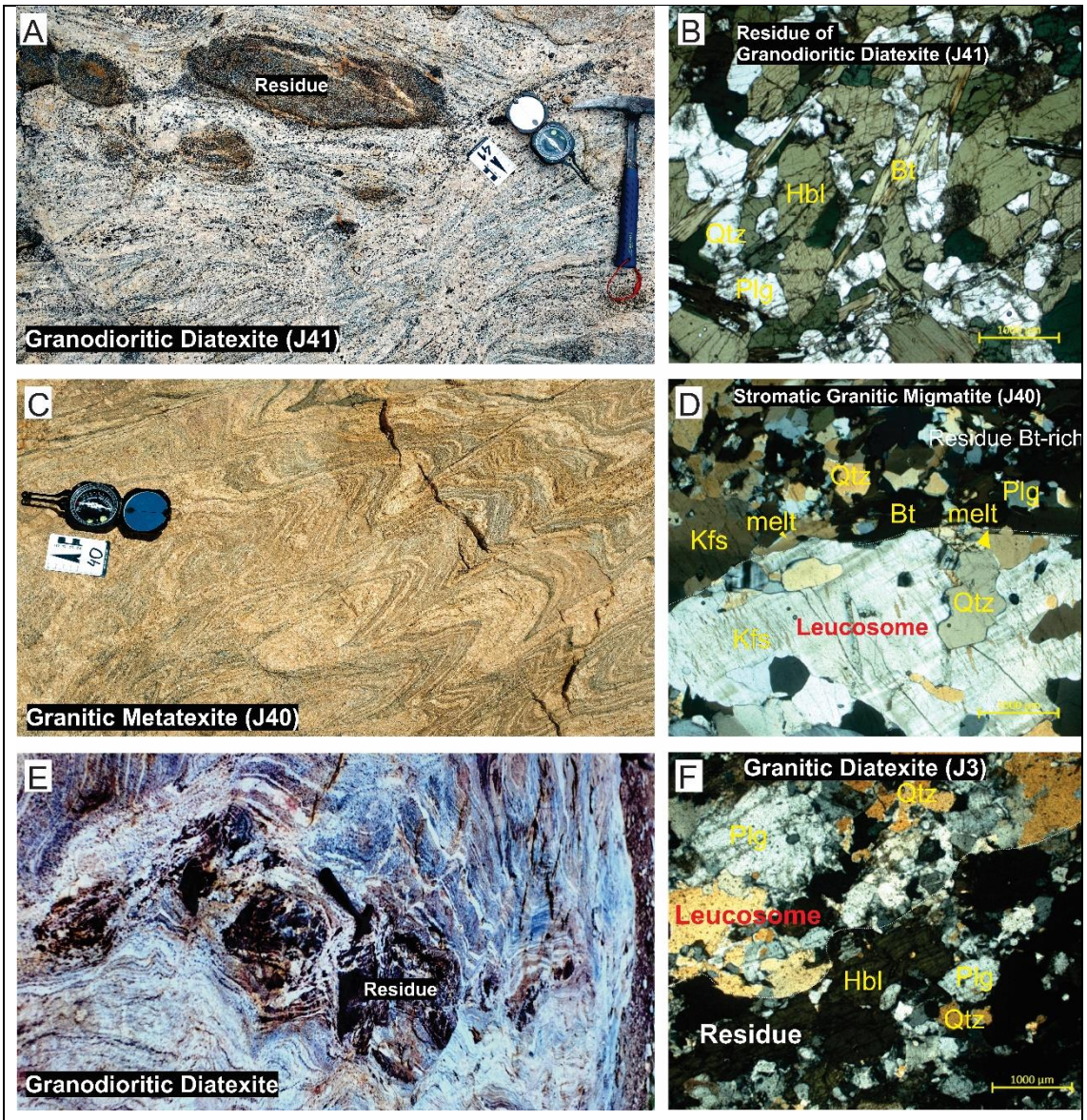

Figure 3) Field and microscopic aspects of migmatites exposed along the Patos Shear Zone. A) Schlieren diatexite with flow structures (J41). Amphibolite residue is cross-cut by anatectic leucosome veins; B) Thin section (crossed polars) of amphibolite residue (J41); C) Stromatic migmatitic orthogneiss of granitic bulk composition (J40); D) Thin section (crossed polars) photo of the limit between melanosome and leucosome in stromatic migmatite (J40); E) Granodioritic diatexite, with residual amphibolite surrounded by a mass of leucosome; F) Thin section of a diatexite (J3), showing the boundary between leucosome and residue.

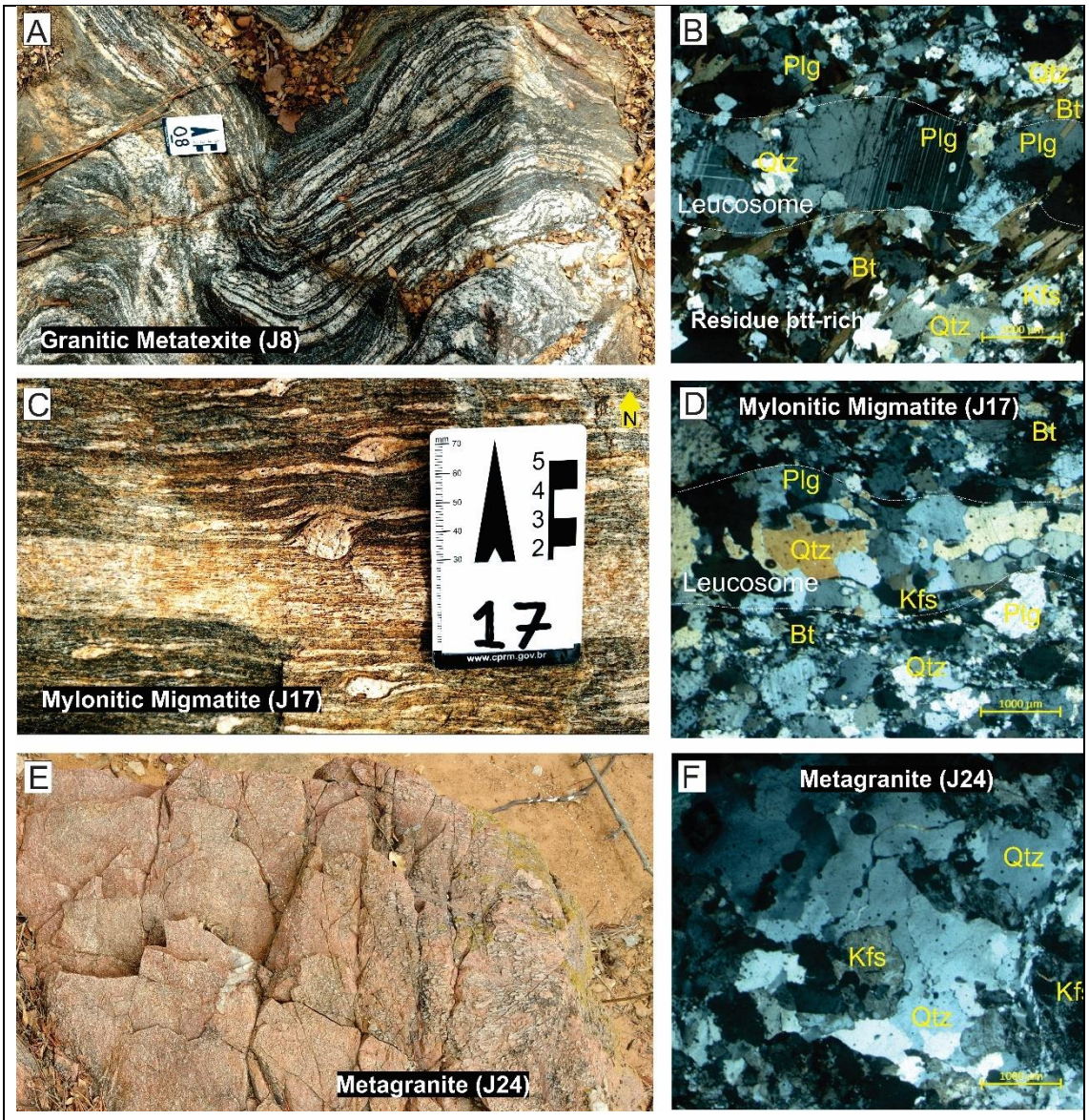

Figure 4) Field and petrographic aspects of studied rocks. A) Metatexitic orthogneiss of granitic composition (J8); B) Leucosome and melanosome in thin section (J8); C) Mylonitized stromatic metatexite; D) Same as C, thin section; E) Foliated metagranite (J24); F) Thin section of J24.

3.2 Isotopic analyses: U-Pb, Lu-Hf and Sm-Nd

Analyses of nuclei and rims of zircon grains were performed for seven migmatite samples, two collected from residual rafts (amphibolitic in composition) diatexites (J41 and AE23A), two from the leucosomes of diatexites (AE11B and AE24B), two from the neosome (i.e., large segments with centimeter-thick intercalations of melanosome and leucosome) of stromatic metatexites (J40 and J8) and one from a granitic injected leucosome vein (J24), that represents melt

migrated from adjacent diatexites. Backscatter scanning electron microscope (SEM) images were obtained at the Geochronology Laboratory of the University of Brasília and were used to guide analyses and interpretations, as discussed in detail below. Complete tables with U-Pb, Lu-Hf and Sm-Nd data are found in Supplementary Material 1, 2 and 3, respectively.

3.2.1 Sample J41 (Residue of granitic diatexite)

Zircon grains from J41 (Figs. 3A and B) are large (200-300 µm) and mostly prismatic. Backscatter SEM images evidence oscillatory-zoned cores surrounded by dark to bright rims, as well as homogenous (bright) grains with small rims (Fig. 5A). Analyses on oscillatory-zoned cores (n=5) yielded a Discordia age of 3437±78 Ma (MSWD=4.8; Fig. 5A). A set of bright overgrowth rims (Fig. 5A) yielded a Discordia age of 3012±36 Ma (n=3; MSWD=0.01; Fig. 5A), whereas grains with homogenous internal structures and overgrowth rims (Fig. 5A) were used to calculate a younger Discordia age of 2018±43 Ma (n=3; MSWD=10; Fig. 5A). Discordant oscillatory-zoned grains that fall between 3.0 and 3.4 Ga were interpreted to represent partial Pb-loss due to the ~3.0 Ga event. At last, two small rims yielded concordant ages of ~637 and 591 Ma (Fig. 5A). The oldest oscillatory zoned cores (~3.43 Ga) were interpreted to represent the crystallization of the protolith, whereas younger homogenous grains and overgrowth rims (~3.0, ~2.0 and ~0.6 Ga) were interpreted to represent successive tectono-thermal (metamorphic) events. This interpretation is mainly based on zircon SEM textures: oscillatory-zoned grains were considered as igneous and homogenous ones, as well as overgrowth rims, metamorphic (Fig. 5A). It is likely, given that zircon grows in temperatures above ~600 ºC, that all these events led to some degree of partial melting and migmatization.

3.2.2 Sample AE11B (Leucosome of granitic diatexite)

Analyses on oscillatory-zoned cores (Fig. 5B) produced two sets of Archean ages, used to calculate Discordias of 3499±22 Ma (MSWD=1.9) and 3405±10 Ma (MSWD=1.8) (Fig. 5B). Zircon grains with homogenous internal structures in SEM images, as well as overgrowth rims, yielded younger

Paleoproterozoic ages, with a set of concordant analyses (n=3) used to calculate a Concordia age of 2110±7 Ma (MSWD=5.5). Based on the zircon SEM structures and on the number of grains in each age population, we interpreted the crystallization age of the protolith to be ~3.4 Ga, following the reworking of older ~3.5 Ga crust (inherited grains). The protolith was later subjected to metamorphism and partial melting/migmatization at ~2.1 Ga, evidenced by zircon overgrowths and grains with homogenous internal structures in SEM images, likely related to recrystallization and obliteration of igneous concentric zoning (Corfu, 2003). Two Paleoarchean grains, characterized by oscillatory zoning, were analyzed for Lu-Hf, as well as one Paleoproterozoic homogenous grain. One ~3.5 Ga grain was analyzed in the core and on its border, and produced consistent results, with $\varepsilon_{Hf(3.5\ Ga)}$ of 0.50 and 0.76, and model ages (T_{DM}) of ~3.62 and 3.64 Ga. Similarly, the oscillatory zoned grain aged ~3.4 Ga yielded a T_{DM} of 3.61 Ga and an $\varepsilon_{Hf(3.4\ Ga)}$ of -1.23 (Fig. 7). On the other hand, two analyses were performed on one grain of homogenous internal structures and an age of ~2.1 Ga, which produced $\varepsilon_{Hf(2.1\ Ga)}$ of 2.04 and 3.92 and model ages of 2.31 and 2.38 Ga (Fig. 7). The latter analyses indicate that at ~2.1 Ga, this rock was either subjected to: i) a mixture with younger, more juvenile melt during migmatization or; ii) isotopic disequilibrium during partial melting. Given that the analyzed rock is a diatexite, characterized by considerable amounts of melt in relation to residue, and that Paleoproterozoic rocks are common in the studied area (Fig. 2), it is not unlikely that magma mixing took place during migmatization. However, to obtain a model age of ~2.3 Ga, for a grain recrystallized at ~2.1 Ga in the leucosome (AE11B) of a ~3.4 Ga protolith, most of the melt in the analyzed leucosome must have come from adjacent relatively juvenile rocks. Based on field relations, it is unlikely that more than ~30% of the melt is allochthonous, and therefore we prefer the isotopic disequilibrium hypothesis. Also a Nd model age (T_{DM}) of 2.97 Ga and an $\varepsilon_{Hf(2.1\ Ga)}$ of -9.44 (Fig. 7) was calculated for leucosome AE11B, and considering that the dominant zircon population and the interpreted protolith of the migmatite (paleosome) is Paleoarchean (~3.4 Ga), a T_{DM} of 2.97 Ga would either indicate melt mixture or disequilibrium for the Sm-Nd system, the latter being more likely.

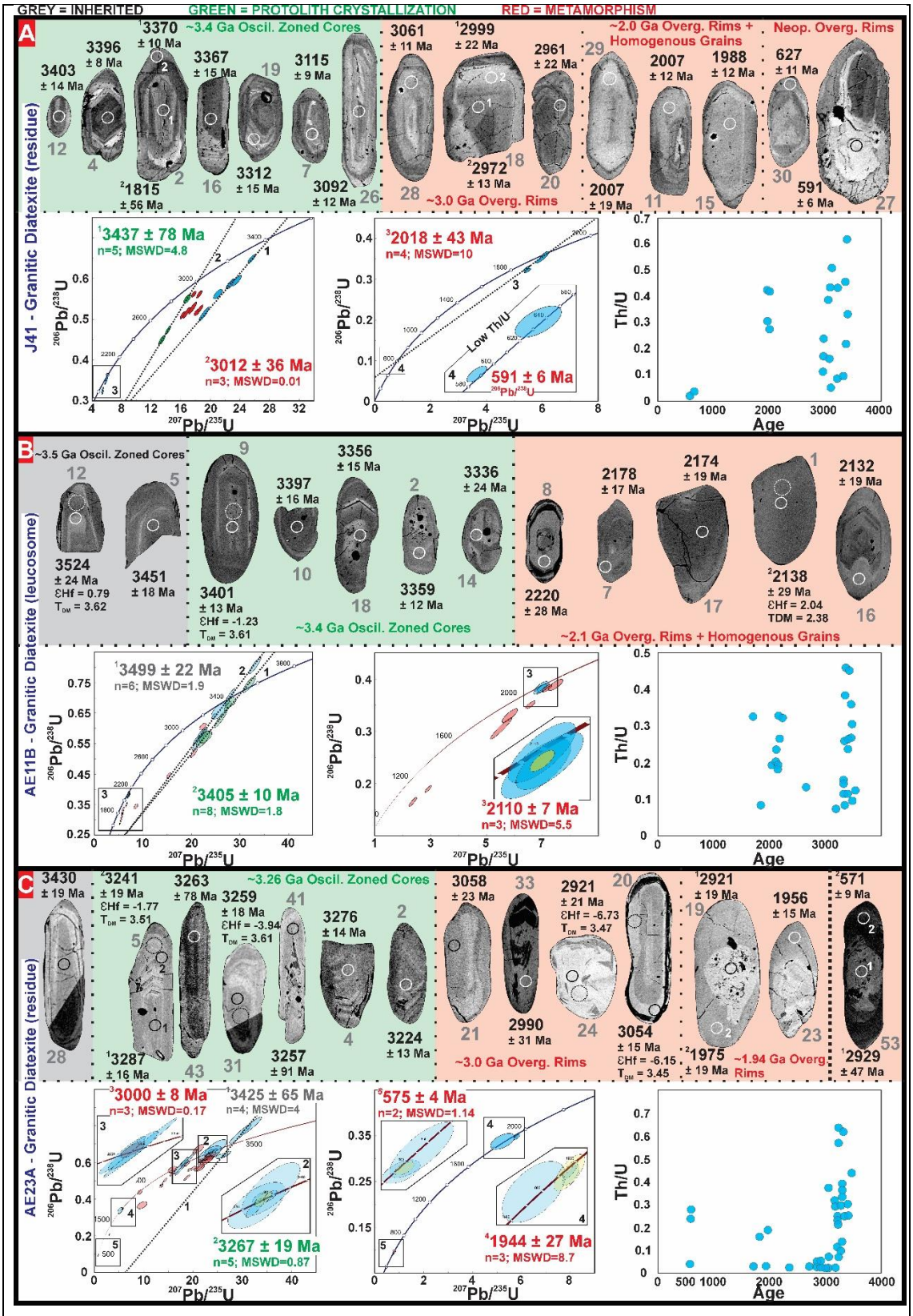

Figure 5) MEV backscatter zircon images and wetherill plots of analyzed samples.

3.2.3 Sample AE23A (Residue of granodioritic diatexite)

Backscatter MEV images of AE23A evidence many complex zircon structures. Grains with preserved oscillatory-zoned cores (Fig. 5C) produced the oldest ages, and two populations stand out. Most analyzed grains rendered a Concordia age of 3267±19 Ma (MSWD=0.87), interpreted as the best estimate for the protolith crystallization. A few analyses aligned to form a Discordia age of 3425±65 Ma (MSWD=4), interpreted to represent inherited grains (Fig. 5C). Bright overgrowth rims that appear to resorb (recrystallize) oscillatory-zoned cores (Fig. 5C), yielded ages around 3.0 Ga, and the three most concordant grains were used to calculate a Concordia age of 3000±8 Ma (MSWD=0.17; Fig. 5C), interpreted to represent a metamorphic event. Similarly, concordant analyses from moderately bright to dark rims and subordinate internally homogenous grains were used to calculate Concordia ages of 1944±19 Ma (MSWD=8.7) and 575±4 (MSWD=1.14; Fig. 5C) interpreted as metamorphic events.

Lu-Hf analyses were performed on nine grains. Three analyses on two grains of ~3.26 Ga, characterized by oscillatory zoning in MEV images, produced clustered $\varepsilon_{Hf\ (3.26\ Ga)}$ from -3.29 to -3.62 (Fig. 7) and calculated Hf model ages (T_{DM}) that vary from 3.57 to 3.59 Ga. This is consistent with reworking of older crust at ~3.26 Ga, as also evidenced by ~3.4-3.5 Ga inherited grains (Fig. 5C). Three different grains with overgrowth rims of ~3.0 Ga yielded $\varepsilon_{Hf\ (3.0\ Ga)}$ of -6.73, -6.15 and 3.02 (Fig. 7) and T_{DM} of 3.47, 3.45 and 3.11 Ga. One of the analyzed ~3.0 Ga overgrowths produced a Hf signature that dissonates from the other two, in that the ε_{Hf} is much more positive (3.02) and is close to DM values (Fig. 7). This is likely the result of either disequilibrium in the Hf isotopic system or mixing due to input of more juvenile material, possibly during partial melting at ~3.0 Ga. However, an increase in more than nine ε_{Hf} units is unlikely, even considering the incorporation of high proportions of juvenile material. We then consider the latter hypothesis less probable. Two analyses on one bright overgrowth rim of ~1.94 Ga produced $\varepsilon_{Hf\ (1.94\ Ga)}$ of -28.05 and -28.8, with T_{DM} of 3.40 and 3.38 Ga, that align well in a reworking array with oscillatory-zoned cores interpreted to represent the crystallization of the protolith (Fig. 7). This indicates crustal reworking at a ~1.94 Ga metamorphic event. On the other hand, one analysis on

another ~1.94 Ga overgrowth yielded a T_{DM} of 1.41 Ga with a very elevated ε_{Hf} of 23.22 (Fig. 7). Given that this analysis is unrealistic, in that it plots well above the DM (Fig. 7), we consider it most likely represents isotopic disequilibrium during partial melting at ~1.94 Ga. At last, a single dark overgrowth rim of ~596 Ma generated an $\varepsilon_{Hf(596\ Ma)}$ of –22.3 and a T_{DM} of 2.0 Ga. Whole rock Sm-Nd analysis on AE23A, the residue, produced an $\varepsilon_{Nd(3.26\ Ga)}$ of 0.6 and a T_{DM} of 3.31 Ga, whereas analysis on the leucosome from the same migmatite (AE23B) produced a T_{DM} of 2.83 Ga and an $\varepsilon Nd_{(3.26\ Ga)}$ of 8.39 (Fig. 7). We take that the deviation in ε_{Nd} and T_{DM} between residue and leucosome is most likely a result of isotopic disequilibrium.

3.2.4 Sample J40 (Neosome of granitic stromatic metatexite)

Zircon grains from J40 (Figs. 3C and D) are mostly small (50-150 μm), rounded to prismatic, and backscatter SEM images evidence distinct core and rim structures (Fig. 6A). Some cores are oscillatory zoned and partly resorbed, whereas rims are homogenous (Fig. 6A). Six core analyses produced a single coherent Discordia age of 2682±48 Ma (MSWD=6.2; Fig. 6A), whereas eleven rims yielded a Discordia age of 2013±39 Ma (MSWD=2.7; Fig. 6A). The first are characterized by high (>0.3) Th/U, whereas the latter have Th/U lower than 0.1 (Fig. 6A). Taken together, these lines of evidence indicate the protolith of AE11B crystallized at ~2.68 Ga and was metamorphosed, at high enough temperatures (i.e., >700 ºC) to induce zircon resorption and subsequent reprecipitation during cooling, at approximately 2.01 Ga. Whole-rock Sm-Nd analysis of J40 produced an ε_{Nd} of -4.49 and T_{DM} of 3.24 Ga, at 2.68 Ga (Fig. 7).

3.2.5 Sample J8 (Neosome of granitic stromatic metatexite)

Sample J8 (Figs. 4A and B) is a granitic stromatic migmatite and two zircon groups were identified based on backscatter MEV imagens. The first group is characterized by oscillatory zoned prismatic grains, a few with homogenous bright rims, whereas the second is formed of rounded to subrounded (soccer-ball) grains with homogenous internal structure, some with sector zoning (Fig.

6B). Oscillatory zoned grains yielded a Discordia of 2644±20 Ma (MSWD=1.5) and some produced older ages, likely inherited, not used for Discordia calculation (Fig. 6B). The second group yielded a Discordia of 2021±29 Ma (MSWD=0.51; Fig. 6B). Based on the zircon textures described above, the age obtained from oscillatory-zoned cores and grains (2644 Ma) is interpreted as the crystallization age of the photolith, whereas subrounded grains, with homogenous to sector-zoned internal structures (SEM; Corfu, 2003), were interpreted as metamorphic and produced a younger age (2021 Ma) that represents the timing of a thermal event. Two oscillatory-zoned Archean cores (~2.64 Ga) were analyzed for Lu-Hf and their $\varepsilon_{Hf(t)}$ are -1.63 and -12.57, with calculated model ages (T_{DM}) of 2.97 and 3.39 Ga (Fig. 7). Whole rock Sm-Nd analysis of J8 produced an $\varepsilon_{Nd(2644\ Ma)}$ of -2.81 and a T_{DM} of 3.1 Ga (Fig. 7).

3.2.6 Sample J24 (Injected metagranitic vein)

Sample J24 (Figs. 4E and F) was collected from a K-feldspar rich small metagranitic injected body regionally associated with a diatexite and is thus interpreted to represent melt accumulation. Zircon grains from this sample are rounded to subrounded and mostly display a homogenous internal structure (indicating recrystallization) in backscatter SEM images, with very few grains presenting very weak oscillatory zoning (Fig. 6C). Some of these cores yielded Paleoproterozoic ages, and the most concordant of those has an age of 2210±54 Ma, likely representing inherited grains. Internally homogenous zircon grains in SEM images are mostly discordant with $^{206}Pb/^{238}U$ Neoproterozoic (700-500 Ma) ages, reinforcing the idea of recrystallization, and the two most concordant analyses were used to calculate a Concordia age of 569±13 Ma, interpreted as the best age estimate for the crystallization of the granitic leucosome vein pocket J24 (MSWD=5.7; Fig. 6C). Younger grains yielded Th/U below 0.1 and inherited Paleoproterozoic grains above 0.4 (Fig. 6C). Whole-rock Sm-Nd analysis of J24 yielded an $\varepsilon_{Nd(569\ Ma)}$ of -20.53 and T_{DM} of 3.07 Ga (Fig. 7).

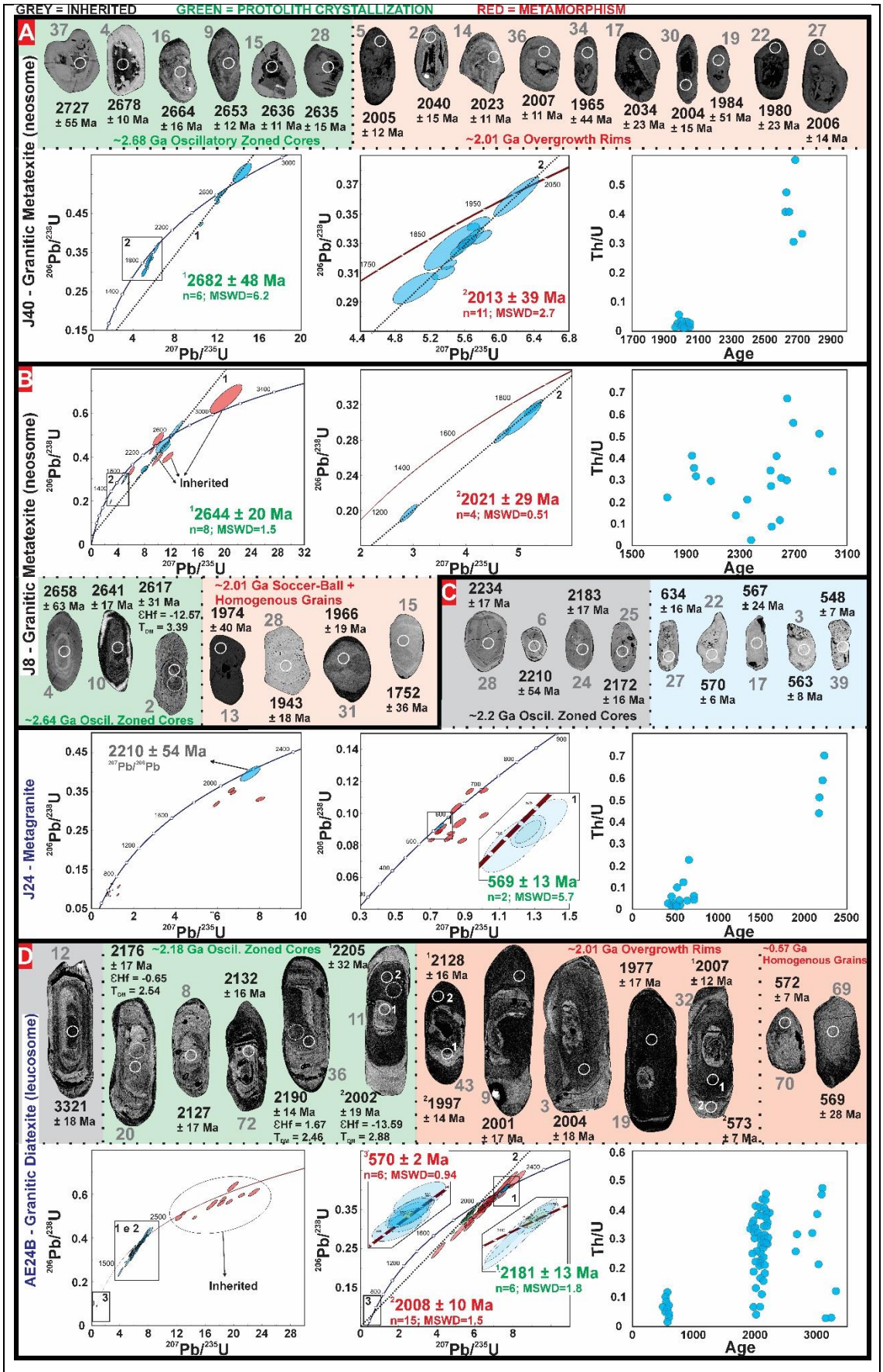

Figure 6) MEV backscatter zircon images and wetherill plots of analyzed samples.

3.2.8 Sample AE24B (Leucosome of granitic diatexite)

In backscatter MEV images, zircon grains of AE24B display oscillatory-zoned cores surrounded by two generations of rims, the inner rim being darker than the outer rim (Fig. 6D). Oscillatory-zoned cores produced older ages and a set of concordant grains from the most abundant age population were used to calculate (n=6) a Concordia age of 2181±13 Ma (MSWD=1.8), interpreted to represent the crystallization age of the protolith (Fig. 6D). Analyses on dark rims were used to calculate a Discordia age of 2008±10 Ma (MSWD=1.5) and the most concordant analyses of bright rims (n=6) yielded a Concordia age of 570±2 (MSWD=0.94; Fig. 6D). The ages of rims are interpreted to represent distinct metamorphic events. Seven Lu-Hf analyses were performed on AE24B zircon grains. An older grain of ~2.69 Ga yielded an $\varepsilon_{Hf(2.69\ Ga)}$ of -11.15 and a T_{DM} of 3.38 Ga. Three grains of ~2.18 Ga produced $\varepsilon_{Hf(2.18\ Ga)}$ between 1.67 and -0.65 and calculated Hf model ages (T_{DM}) cluster between 2.46 and 2.54 Ga (Fig. 7). One dark overgrowth of ~2.0 Ga (Fig. 6D, zircon 11) produced an $\varepsilon_{Hf(2\ Ga)}$ of -13.59 and a T_{DM} of 2.88 Ga, whereas two grains with homogenous internal structures (SEM images) of ~570 Ma yielded $\varepsilon_{Hf(570\ Ma)}$ of -28.98 to -26.25 and T_{DM} of 2.30 and 2.15 Ga. Whole rock Sm-Nd analysis produced an $\varepsilon_{Nd(2.18\ Ga)}$ of -4.05 and a T_{DM} of 2.64 Ga.

3.4 Discussion

In this section we first address the issue of isotopic Hf-Nd fractionation and how it may have affected the isotopic signature of our migmatite samples and their protholith's. We identify incursions towards higher εHf and εNd values that reflect fractionation during partial melting and assess which analyses may best represent the isotopic composition of the source.

We then discuss the timing and tectonic meaning of the metamorphic/migmatization events identified here, in a regional context, by means of cathodoluminescence-supported zircon grain texture interpretations of U-Pb ages. In the following subsection, we discuss magmatic events possibly tied

to intense regional reworking, as evidenced by Hf-Nd systematics and periods of intensified crustal growth, as further discussed below.

Our samples are mostly felsic polymetamorphic migmatitic metagranitoids subjected to several reworking events, and this makes constraining the time these rocks first became part of the continental crust, and hence contributed to its growth, exceedingly difficult. The isotopic information on the ultimate sources and protoliths of our migmatites were obtained through Lu-Hf isotopic analyses of inherited zircon grains, especially those from residual mafic rafts in diatexites, and whole-rock Sm-Nd analyses of *schollen*. Zircons are refractory and grains from the protolith often are preserved during anatexis with virtually unchanged U-Pb and Lu-Hf signatures. Combined with a large regional Hf compilation, we constrain the approximate timing and tectonic significance of major crustal growth events in the São Francisco Craton and the Patos Shear Zone, including a Paleoarchean one, with implications for early Earth geodynamics.

5.1. The anatectic effect on the Lu-Hf and Sm-Nd isotopic systems: implications for isotopic disequilibrium and data interpretation

It is very common that Hf isotopic zircon analyses from a single granitoid sample yield a scatter in ε_{Hf} versus age plots. These variations can even be observed in single zircon crystals, especially those with a complex tectono-metamorphic history (Xia et al., 2022). The reasons for this are debated, but traditionally this is viewed as evidence of magma mixing between a juvenile and a crustal component (e.g., Hawkesworth and Kemp, 2006; Kemp et al., 2007; Santos et al., 2022), Lu/Hf fractionation during partial melting (e.g., Davies and Tommasi, 2000; Tang et al., 2014; Xia et al., 2022; Yang et al., 2022) or inheritance from an already isotopically diverse source (Farina et al., 2014). Lu/Hf of common rock-forming minerals is highly variable, with zircon having the lowest of all (<0.01) and garnet very high values (1 to 11; Chen et al., 2015). This means that different minerals, given enough time, will acquire highly dissonant $^{176}Hf/^{177}Hf$ signatures even if crystallized from the same homogenous magma. During crustal anatexis, pressure, temperature, and composition control which minerals break down and which remain residual and at what proportions (e.g., Marimon et al.,

2022a). Garnet, titanite and ilmenite are common rock forming minerals with high Lu/Hf ratios (amphibole and biotite have moderate to low Lu/Hf), and the preferential melting of these phases, as in a peritectic reaction, could (with time) increase the $^{176}Hf/^{177}Hf$ of the leucosome or migrated melt, and of metamorphic zircon grains crystallized from it, whereas fractional crystallization of the same minerals will have the opposite effect (Cheng et al., 2015; Xia et al., 2022). Of the minerals mentioned above, only garnet has not been observed in thin sections from the studied migmatites.

The behavior of Hf-bearing phases during partial melting also exerts strong influence on isotopic disequilibrium between melt and protolith (e.g., Gao et al., 2021). Zircon is extremely rich in Hf (2-3 wt.%), and the extent of its dissolution during anatexis can affect the $^{176}Hf/^{177}Hf$ isotopic signature of the melt (e.g., Tang et al., 2014; Gao et al., 2021; Xia et al., 2022). On the other hand, the contribution of Hf from the breakdown of other rock forming minerals (e.g., amphibole, biotite, titanite and ilmenite), all with higher Lu/Hf but poorer in Hf (usually <10 ppm to <100 ppm) compared to zircon, may result in higher $^{176}Hf/^{177}Hf$ in the leucosome, especially if only a small proportion of zircon is dissolved into the melt, which is common at lower temperatures and melt fractions (Tang et al., 2014; Chen et al., 2015). As the temperature rises, however, the amount of melt increases and more zircon is dissolved, which diminishes the $^{176}Hf/^{177}Hf$ of the melt and brings it closer to that of the protolith (Tang et al., 2014).

Lu-Hf isotopic disequilibrium is thought to have affected at least some of the studied migmatite samples. For instance, diatexite AE23A (residue) and diatexite AE11B (leucosome), are characterized by heterogenous Hf data from metamorphic zircon rims and grains, which either fall in a well-defined “reworking array” with the protolith’s older oscillatory-zoned grains/cores or are dislocated to much higher ε_{Hf} values, sometimes plotting above DM (Fig. 7), which makes mixing an unlikely possibility given that one of the mixing end-members would have to be unrealistically radiogenic and that no evidence for mixing processes has been observed in the field. It is likely that the highly radiogenic metamorphic zircon grains crystallized during partial melting, under disequilibrium conditions exacerbated by the incomplete dissolution of zircon grains in the melanosome and important contributions from higher Lu/Hf phases (Xia et al., 2022). On the other hand, Hf analyses of metamorphic crystals/domains that plot along a well-

defined “reworking array” with the older grains could be a result of recrystallization of residual protolith grains and retention of the protolith’s Hf isotopic signature.

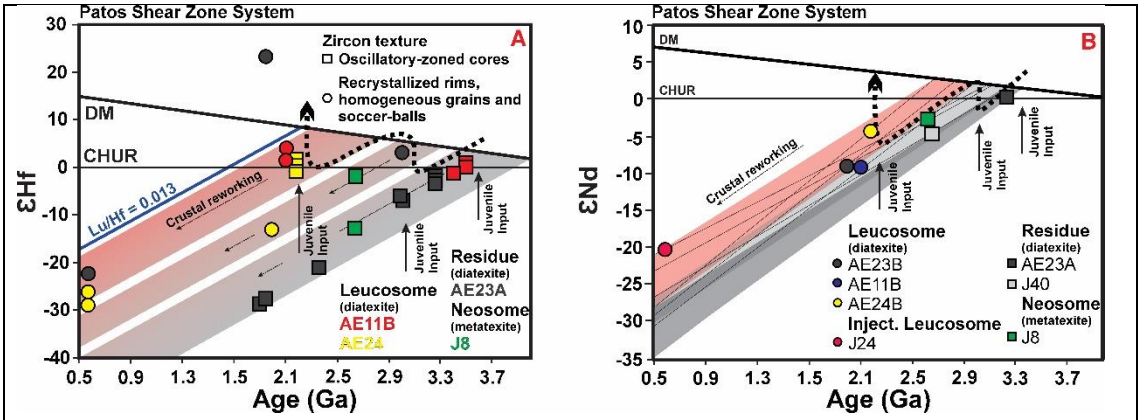

Figure 7) ε_{Hf} versus age and ε_{Nd} versus age for samples analyzed in this study.

Similarly, there is also evidence for Sm/Nd fractionation in both samples, as in diatexite AE23 the leucosome is ~8 ε_{Nd} units higher than the residue, whereas the $T_{DM(Nd)}$ age of leucosome AE11B is younger than the interpreted U-Pb age of the protolith (Fig. 7). Sm/Nd fractionation has been reported for migmatites and the budget of Sm and Nd is mainly controlled by minerals such as apatite, monazite and garnet (e.g., Beat et al., 2023), the preferential dissolution of which may led to imbalances between the $^{143}Nd/^{144}Nd$ of the melt and the protolith (Zeng et al., 2005; Yang et al., 2022). Residual amphibole and titanite, minerals common in residual enclaves of the studied migmatites, may decrease the $^{147}Sm/^{144}Nd$ of the melt, which would then lead to melt T_{DM} ages younger than those of the protolith (Bea et al., 2023). Accordingly, the leucosomes of analyzed samples yielded younger T_{DM} ages than the corresponding melanosomes.

Isotopic disequilibrium is thought to be enhanced in lower temperatures melting and at lower degrees of partial melting during anatexis (Tang et al., 2014; Xia et al., 2022). At these conditions, there is lower solubility of refractory accessory phases that control the Hf-Nd budget, such as zircon (Hf) and monazite (Nd). Our samples are characterized by considerable amounts of inherited zircon, which indicates incomplete dissolution of zircon grains in the protolith and therefore increased potential for isotopic disequilibrium. As temperature increases during partial melting, Sm, Nd, Lu and Hf-bearing phases

continue to break down and the isotopic signature of the melt approximates that of the protolith (Tang et al., 2014; Yang et al., 2022).

Overall, crustal melting processes can substantially change Lu-Hf and Sm-Nd signatures and impart considerable bias when estimating the residence time of sources (Chen et al., 2015; Bea et al., 2023). Interpretations of mixing with juvenile material to explain the variability of ε_{Hf}/ ε_{Nd} and incursions towards higher values may not always be warranted and must be done with caution. To mitigate the effect of anatexis in the Lu-Hf system and draw accurate geotectonic considerations in the following sections we will only use data from magmatic zircon grains (oscillatory-zoned grains), as suggested by Chen et al. (2015), and only consider metamorphic grains (overgrowth rims, soccer-ball grains, etc) that aligned in a "reworking array" with the older grains from the protolith.

5.2. Timing of migmatization events: crustal reworking and implications for regional geology

The analyzed samples were collected in the Patos Shear System (PSS), a 20-40 km wide section of the Neoproterozoic Borborema Province characterized by anastomosing shear zones intercalated with non-mylonitic sections (Fig. 2). The samples analyzed in this study were not mylonitic, however, that doesn't mean they were not subjected to heat from the high- to medium-temperature shearing of adjacent shear zones, which other studies have shown has led to migmatization and diatexite formation (Viegas et al., 2014). Zircon can grow during the prograde metamorphic stage, at temperatures higher than ~600 ºC, either forming new grains or overgrowth rims, or recrystallize resetting its internal clock (Corfu, 2003). Accordingly, our U-Pb analyses on zircon overgrowth rims, soccer-ball grains and metamorphic grains with homogenous internal structure, mostly with low Th/U (< 0.1), produced reliable ages between 570 and 575 Ma (Figs. 5C and 6C and D), establishing the age for the youngest metamorphism in the PSS, which is in accordance with what has been reported in the literature (Archanjo et al., 2012, 2021; Viegas et al., 2014; Cioffi et al., 2021). In addition, we obtained an age of ~570 Ma for a metagranite, spatially associated with a diatexite, thus reinforcing the idea of localized partial melting in the late Neoproterozoic. This granite is likely the result of magma accumulation

during migmatization induced by high- to medium-grade shearing in the PSS (Viegas et al., 2014). Viegas et al. (2014) obtained a similar age for a foliated granite associated with a diatexite and for overgrowths in high temperature mylonites with quartz ribbons recrystallized by grain boundary migration in the PSS.

The Neoproterozoic metamorphic ages obtained in this study are younger than most ages obtained regionally in the Borborema Province, that mostly fall between 630 and 590 Ma (e.g., Ganade et al., 2014a, 2014b, 2021). This indicates transcurrent dextral shearing in the PSS is late related to regional metamorphism, a fact previously observed by other investigators (e.g., Viegas et al., 2014; Archanjo et al., 2021). This is a common characteristic of transpressive orogens, such as the Borborema Province, where tangential thrusting is followed by transcurrent movement in late shear zones and strain partitioning (Vauchez et al., 2014; Egydio-Silva et al., 2018; Archanjo et al., 2021). Another important transpressive Brasiliano orogen is the Ribeira Orogen, in southeastern Brazil (Egydio-Silva et al., 2018), where like in the Borborema Province, a major high-grade dextral transcurrent shear zone is located at its core, the Além Paraíba Shear Zone, which is also slightly late with respect to regional metamorphism with an age of ~590-570 Ma (Giraldo et al., 2019), similar to that of the PSS obtained in this study.

Although half of all analyzed migmatite samples yielded no Neoproterozoic (~570 Ma) metamorphic ages, all analyzed migmatite samples produced Paleoproterozoic (from ~2.1 to 1.95 Ga) metamorphic ages, evidenced by low Th/U zircon overgrowth rims, sector-zoned soccer ball grains and internally homogenous metamorphic zircon crystals in SEM images (Figs. 5, 6). In a few samples (J40 and AE24B), the inner boundary of the Paleoproterozoic overgrowths has an irregular inward curved shape (Fig. 6A, zircon 9 of 6D), indicating that these rims were generated at suprasolidus conditions (Corfu, 2003), during high-grade metamorphism and migmatization at ~2 Ga.

The Paleoproterozoic (2.1-1.94 Ga) metamorphic ages obtained in this study are related to the amalgamation and formation of the São Francisco-Congo Craton by the collision of several Archean blocks following an extended period of arc-related juvenile magmatism (e.g., Ávila et al., 2010, 2014; Peucat et al., 2011; Teixeira et al., 2015; Barbosa et al., 2015, 2019; Cioffi et al., 2016b; Bersan et

al., 2020, 2022; Bruno et al., 2021; Neves et al., 2023). Collisional processes between 2.2 and 1.7 Ga have been reported from several locations worldwide and it is widely believed they eventually led to the formation of the Columbia supercontinent (e.g., Meert and Santosh, 2017). Several investigators, working throughout the São Francisco Craton and inliers in adjacent Neoproterozoic (Brasiliano) orogens, have obtained consistent ages of metamorphism that mostly fall between 2.1 and 1.95 Ga, similar to those obtained here for the Patos Shear System (PSS), as shown in the compilation of Fig. 8 (e.g., Heilbron et al., 2010; Cordeiro et al., 2014; Fuck et al., 2014; Teixeira et al., 2015; Aguilar et al., 2017; Cutts et al., 2018; Degler et al., 2018; Bruno et al., 2020, 2021; Marimon et al., 2020, 2022a). We can infer from the map in Fig. 1 that an Archean block to the west of the Itabuna-Salvador-Curaçá belt (including the Gavião block and the southern São Francisco Craton), that forms the core of the São Francisco Craton today, collided with Archean blocks on all sides, following accretion and arc-magmatism between ~2.4 and 2.1 Ga (e.g., Ávila et al., 2014; Teixeira et al., 2015; Barbosa et al., 2017; Neves et al., 2021). These processes led to the formation of Paleoproterozoic orogens, such as the Minas-Bahia Orogen (Bruno et al., 2020, 2021), that extends from the southern to the northern segments of the craton, including inliers in Brasiliano orogens (e.g., Cordeiro et al., 2014; Heilbron et al., 2010; Cioffi et al., 2016b; Cutts et al., 2018). During continental collision, crustal thickening led to high-grade granulite-facies metamorphism, including UHT conditions in the São Francisco Craton (Barbosa et al., 2017), leading to widespread migmatization. Our PSS migmatites, also affected by high-grade metamorphism during the Paleoproterozoic, are likely part of this broader coeval systems of accretionary and collisional Rhyacian orogenies surrounding Archean blocks in the São Francisco Craton.

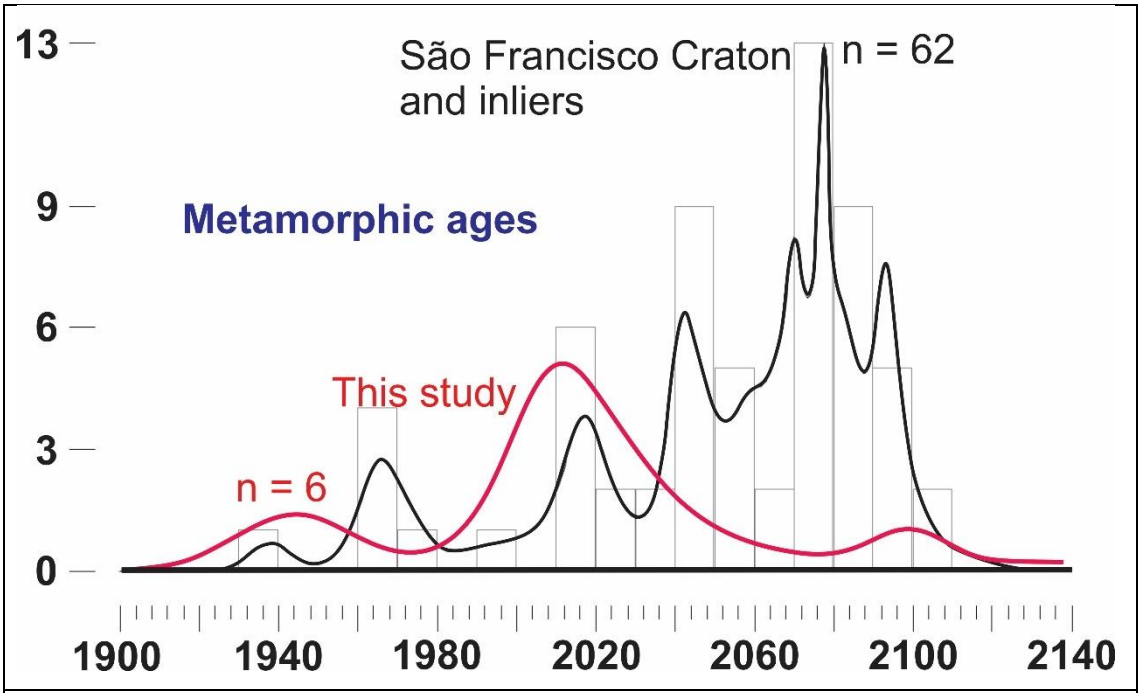

Figure 8) Ages of metamorphism (zircon overgrowths, soccer-ball, etc) for the Paleoproterozoic of the São Francisco Craton, including inliers from adjacent Neoproterozoic orogens. Data from this study were plotted for comparison. Data from the São Francisco Craton and inliers were compiled by Marimon et al. (2020) and references can be found therein.

The earliest metamorphic event identified in migmatitic rocks of this study is of Mesoarchean age. Two migmatite samples (J41 and AE23A) record a ~3.0 Ga metamorphic event, evidenced by the age of metamorphic zircon overgrowth on older oscillatory-zoned cores, internally homogenous metamorphic zircon grains and soccer-balls (Corfu, 2003), some with sector zoning (Figs. 5A and C). However, in the São Francisco Craton and adjacent inliers, the most common Archean metamorphic event is of Neoarchean age, with ages clustering at ~2.7 Ga (see Marimon et al. 2020 for a compilation). Still, ~3.0 Ga orthogranulites of a similar age were recognized in the northernmost segment of the São Francisco Craton, close to the border with the Borborema Province (Uauá terrain; Oliveira et al., 2010 and references therein). Metamorphism at ~3.0 Ga may represent crustal thickening induced by the collision between small Paleoarchean landmasses, which culminated with the amalgamation of several smaller blocks to form the core of the São Francisco Craton at ~2.7 Ga (e.g., Romano et al., 2013; Farina et al., 2015; Albert et al., 2016; Brando-Soares et al., 2020). Close to the studied area, in the São José do Campestre Massif (Borborema Province), dyke-like bodies of metamorphosed gabbros and anorthosites yielded ages of

~3.0 Ga (Dantas et al., 2004, 2013). Underplated high-temperature mantle-derived mafic magmas can induce high-grade metamorphism and this is an alternative explanation for the Mesoarchean metamorphism ages obtained in this contribution. More studies are needed to clarify the geotectonic setting of the ~3.0 Ga metamorphic event.

5.3. Magmatic events: juvenile inputs and/or crustal reworking

Several magmatic episodes can be recognized with the data obtained in this study. The age of magmatic episodes is constrained by the U-Pb dating of oscillatory-zoned grains and cores, either interpreted to represent the crystallization age of the protolith or inherited (Figs. 5 and 6). In this work, based mainly on zircon textures and subordinately on Hf data, we interpreted that the old protoliths of the studied region have crystallization ages of ~3.4 and 3.26 Ga, followed by rocks of 2.64-2.68, 2.18 and 0.57 Ga (Figs. 5 and 6). In addition, one sample yielded an inherited population of ~3.5 Ga.

Zircon U-Pb and Hf data obtained in this study, excluding those analyses that likely represent disequilibrium as discussed above, in conjunction with data from the São Francisco Craton compiled from the literature, are plotted in Figure 9. The obtained Paleoarchean ages (3.5, 3.4 and 3.2 Ga) are similar to the crystallization ages of TTGs and high-K rocks, as well as associated mafic to intermediate rocks, reported in the São José do Campestre Massif, Borborema Province, and in the northern São Francisco Craton (Gavião Block), but their tectonic setting remains enigmatic (Dantas et al., 2004, 2013; Lana et al., 2013; Lopes et al., 2021; Santos et al., 2022). Three age groups of rocks stand out in the Hf compilation of Fig. 9: Paleoarchean, Meso-Neoarchean and Paleoproterozoic. Paleoarchean Hf data, isotopic equilibrium with the source considered, could be interpreted in one of two ways (Fig. 9): i) extraction of magma from a mantle domain with CHUR-like isotopic signature between 3.2 and 3.6 Ga, with variable crustal contamination with older material; or ii) reworking of ancient crust, extracted from the depleted mantle between 3.6 and 4.1 Ga (Fig. 9). Whatever the case may be, the pattern of Hf data from rocks older than ~3.2 Ga is markedly different from those of a younger age (Meso-Neoarchean and

Paleoproterozoic), which form well-defined “reworking arrays”, i.e. the alignment of Hf data along a Lu/Hf (e.g., 0.013) crustal evolution line that evolved from DM to subchondritic Hf signatures (Fig. 9). The mechanisms that lead to the formation of “reworking arrays” are debated, but they are thought to either form through the successive batches of juvenile material mixed with older crust (e.g., Laurent and Zeh, 2015), as in the dilution and refertilization of continental crust in a hot zone according to the modelling of Payne et al., 2016, or through a short period of mostly juvenile magmatism followed by a period of continued and prolonged pure reworking. The absence of reworking arrays for Paleoarchean rocks of the São Francisco Craton and the apparent mixing of magma derived from a CHUR-like reservoir with older crust (Fig. 9) are better reconciled with a stagnant-lid scenario dominated by plume activity.

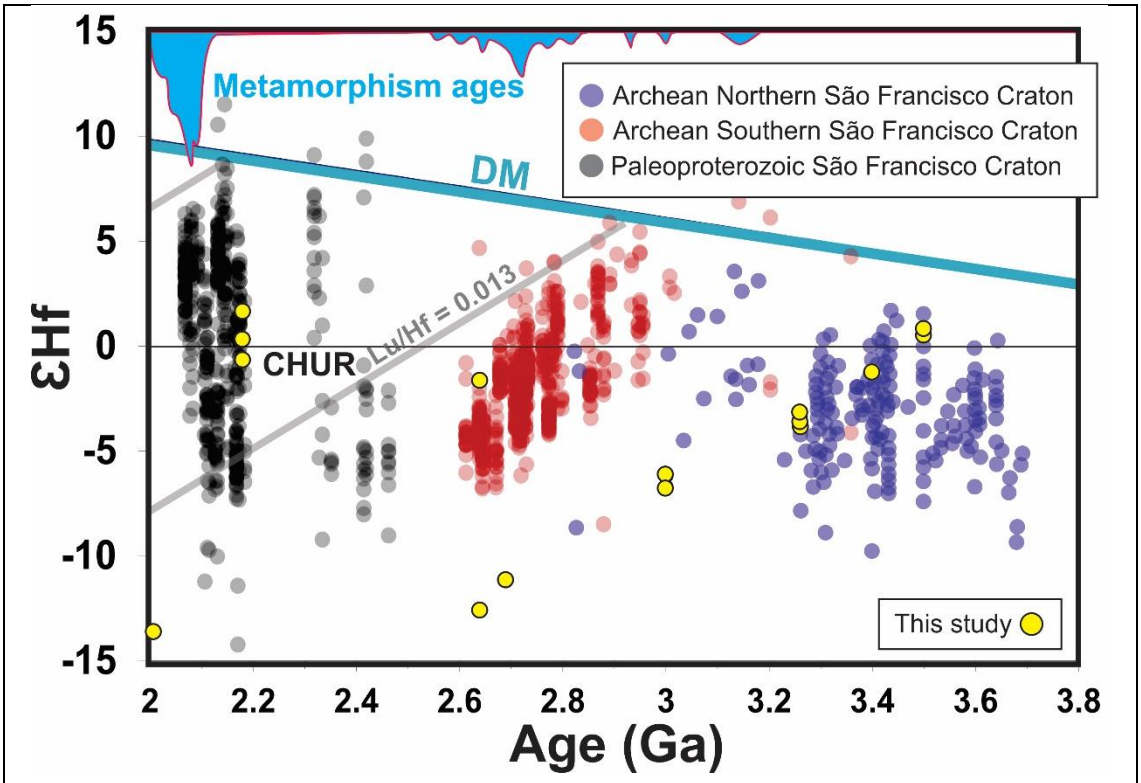

Figure 9) ε_{Hf} versus age data for Archean and Paleoproterozoic rocks of the São Francisco Craton and inliers from adjacent Brasiliano orogens. Data are from the compilations of Marimon et al. (2020) and Santos et al. (2022).

Our Hf compilation and new data indicates that from ~3.1 to 2.9 Ga the São Francisco Craton (including the PSS) experienced an important period of renewed juvenile magmatism, with inputs from older crust, evidenced by the spread of ε_{Hf} data from the depleted mantle evolution line towards subchondritic

values (Fig. 9). Juvenile magmatism between 3.1 and 2.9 Ga in the southern segment of the São Francisco Craton is mostly represented by migmatitic orthogneisses of TTG affinity, likely generated through the partial melting of arc-related basalts (Farina et al., 2015; Albert et al., 2016; Marimon et al., 2022a). This period of initial Meso-Neoarchean magmatic activity, from ~3.1 to 2.9 Ga, is characterized by a spread of data between the DM line and slightly beneath the CHUR line (red in Fig. 9). Therefore, most of these rocks were possibly generated at the initial stage of continental magmatic arc activity, with moderate contributions from preexisting crust and/or continental lithospheric mantle. Samples from ~2.9 to 2.6 Ga align with older juvenile magmas to form linear Hf arrays (Lu/Hf=0.013), as do our samples of 2.64-2.68 Ga (Fig. 9), which presented inherited grains of ~3 Ga and Nd/Hf model ages (T_{DM}) between 2.9 and 3.2 Ga, which is very consistent with the regional scenario of the São Francisco Craton (Fig. 9). This may indicate that the period between 2.9 and 2.6 Ga is characterized by intense reworking, also evidenced by increased high-K crustally derived magmatic activity (e.g., Farina et al., 2015; Albert et al., 2016; Marimon et al., 2022a) as well as regional metamorphism (see blue PDP at the top of Fig. 9), likely induced by crustal thickening (e.g., Cutts et al., 2019). However, sanukitoid and mafic-intermediate rocks emplaced between 2.9 and 2.6 Ga (e.g., Brando-Soares et al., 2020; Valeriano et al., 2022; Marimon et al., 2022a) indicate that mantle inputs also accompanied intensified reworking of older crust. Therefore, the Meso-Neoarchean “reworking array” of the São Francisco Craton (including data from the PSS) was likely formed by a complex association of processes, including juvenile inputs associated with reworking of ancient crust, like the models proposed by Laurent and Zeh (2015) and Payne et al. (2016). The preferred model is that magmatism between 2.9 and 2.6 Ga took place in an accretionary/collisional setting, with older ~3.5 to 2.9 Ga basement (Romano et al., 2013; Albert et al., 2016; Marimon et al., 2022a).

After the waning stages of Archean magmatism at ~2.6 Ga, characterized by A-type orthogneisses (Marimon et al., 2022), a period of quiescence followed in the São Francisco Craton. Juvenile magmatism resumed at ~2.4 Ga (Barbosa et al., 2019), at the beginning of another Wilson Cycle that eventually led to voluminous magmatism, accretion, and continental collision during the Paleoproterozoic (2.2-2.0 Ga; Fig. 9). The pattern of magmatism is very similar

to that described above for the Meso-Neoarchean (Fig. 9). There is a protracted period of juvenile magmatism, associated with crustal reworking, from ~2.4 to 2.15 Ga, followed by intense regional metamorphism (2.1-2.0 Ga), crustal thickening and an excursion towards more negative ε_{Hf} values, following a reworking array along a Lu/Hf=0.013 evolution line (black in Fig. 9). We obtained one Paleoproterozoic crystallization age of ~2.18 Ga, which coincides with the most productive period of juvenile magmatism and reworking in the São Francisco Craton (e.g., Barbosa et al., 2015; Cioffi et al., 2016b; Neves et al., 2023). Indeed, our data indicate there was widespread reworking of Archean rocks during the Paleoproterozoic in the studied area, as evidenced by inherited Archean zircon grains in our Paleoproterozoic sample (Fig. 6D) and ~2.0-2.1 Ga metamorphic grains, related to migmatization, in all our Archean samples (Figs. 5 and 6). For the past 30 years, other studies in the Borborema Province have obtained similar results (e.g., Caby, 1989; 1995; Corsini et al., 1991; Van Schmus et al., 1995; 2011; Dantas et al., 2004, 2013). On the other hand, our Hf data indicate that Paleoproterozoic magmatism may not have been pure reworking of Archean rocks, but there was possibly an involvement of more juvenile material, as in magma mixing, since the ε_{Hf} of our Paleoproterozoic sample's oscillatory-zoned igneous crystallization grains do not form a reworking array with our older Archean rocks, but instead are dislocated to higher values, close to CHUR (Fig. 7). We cannot totally discard that isotopic disequilibrium/fractionation, as discussed in detail above, is not behind this excursion to higher values and detailed future studies, focused on leucosome and residue of migmatites, should address this issue. However, since the analyses were performed on oscillatory-zoned igneous grains and not metamorphic ones (Chen et al., 2015), the grains may not reflect this process. In addition, the compiled results for the São Francisco Craton as a whole are consistent with our interpretation (Fig. 9). Furthermore, on a geochemical perspective, mafic to intermediate magmatism elsewhere in the São Francisco during this period (~2.2-2.1 Ga) indicate juvenile mantle additions to the crust (Cardoso et al., 2019; Neves et al., 2023).

Although there are many migmatitic orthogneiss exposures, most with a sanukitoid high-K affinity (e.g., Cioffi et al., 2016b; Bruno et al., 2020, 2021), with juvenile DM-like isotopic signatures dated between 2.2 and 2.1 Ga, our samples are most likely characterized by a mixture of more juvenile and reworked Paleo-

Mesoarchean components. Our preferred scenario to explain this is subduction beneath the Archean core of the São Francisco Craton during the Paleoproterozoic. The Hf pattern evident in our wider compilation of Fig. 9 (black spheres), i.e. of 2.2-2.1 Ga samples spreading from the DM towards highly negative values, is probably related to a similar accretionary process in a continental environment (e.g., Teixeira et al., 2015; Barbosa et al., 2015). Widespread metamorphism, of a similar and consistent timing throughout the São Francisco Craton (i.e., 2.1 to 2.0 Ga, also obtained in this study), after peak magmatic arc production likely represents continental collision, after consumption of oceanic lithosphere, between large landmasses of Archean cores which led to the formation of the São Francisco Craton (e.g., Heilbron et al., 2017), including the Borborema basement, and eventually of the Columbia supercontinent.

3.5 Conclusion

We report new U-Pb, Lu-Hf and Sm-Nd data for migmatitic Archean-Paleoproterozoic basement rocks of the Patos Shear System, part of a Neoproterozoic orogen: the Borborema Province in NE Brazil. The conclusions of this study are as follows:

- Highly variable ε_{Hf} values for metamorphic zircon grains and a difference between the ε_{Nd} of a paleosome and *in situ* leucosome, point to isotopic disequilibrium/fractionation between source and melt during anatexis. To minimize this effect, only Hf data from magmatic zircon grains and whole-rock Sm-Nd analyses from paleosomes were considered for geotectonic interpretations.
- The magmatic protoliths of six analyzed migmatites yielded Archean to Paleoproterozoic U-Pb ages of ~3.40, 3.26, 2.68-2.64 and 2.18 Ga (Figs. 5 and 6). Three metamorphic events (3.0 Ga, 2.1-2.0 Ga and 570-575 Ma) are evidenced by U-Pb analyses on zircon overgrowth rims, soccer-ball grains, and internally homogenous metamorphic zircon grains in SEM images (Figs. 5 and 6).
- The Patos Shear System (PSS) is a 20-40 km wide section of anastomosing Neoproterozoic shear zones intercalated with non-

mylonitic domains (Fig. 2). This study's migmatites are not mylonitic, but metamorphic ages of ~570-575 Ma and an injected leucosome of ~575 Ma attest they were subjected to high heat from Neoproterozoic medium- to high-temperature shearing.

- The most widespread metamorphic/migmatization event in the analyzed samples is of Paleoproterozoic age (2.1-2.0 Ga). This event is related to the amalgamation and formation of the São Francisco-Congo Craton by the collision of several Archean blocks. Collisional processes between 2.2 and 1.7 Ga are common globally and led to the formation of the Columbia supercontinent (e.g., Meert and Santosh, 2017).
- Two migmatites record a ~3.0 Ga metamorphic event (Figs. 5A and C). This metamorphic event may represent crustal thickening induced by the early stages of collision between small Paleoarchean landmasses, which culminated with the amalgamation of several smaller paleocontinents to form the core of the São Francisco Craton, with metamorphism peaking at ~2.7 Ga (e.g., Farina et al., 2015; Albert et al., 2016; Brando-Soares et al., 2020).
- Palearchean magmatic protoliths (~3.4 and ~3.26 Ga) were emplaced concomitant with TTGs and high-K orthogneisses regionally, albeit their tectonic setting remains enigmatic (Dantas et al., 2004, 2013; Lopes et al., 2021; Santos et al., 2022). Hf data, combined with a large compilation from the São Francisco Craton, indicate that, unlike analyses from younger rocks, Paleoarchean samples lack "reworking arrays", but rather show an apparent mixing of magma derived from a CHUR-like reservoir with older crust (blue in Fig. 9). This is better reconciled, although not conclusively, with a stagnant-lid scenario dominated by plume activity.
- Hf data from 2.68-2.64 Ga migmatites, combined with compiled data, plot along a conspicuous Meso-Neoproterozoic "reworking array" (red in Fig. 9). Considering the whole São Francisco Craton, mantle-derived rocks emplaced between 2.9 and 2.6 Ga suggest juvenile inputs accompanied by reworking (e.g., Brando-Soares et al., 2020), indicating that magmatism between 2.9 and 2.6 Ga took place in an

accretionary/collisional continental setting, following mostly juvenile additions (TTG) between ~3.2 to 2.9 Ga (red in Fig. 9).

- The crystallization age of ~2.18 Ga of the protolith of a migmatite (Fig. 6D) is related to another Wilson Cycle in the São Francisco Craton. Obtained data point to widespread reworking of Archean rocks during the Paleoproterozoic, as evidenced by inherited Archean zircon grains (Fig. 6D) and widespread ~2.0-2.1 Ga metamorphism/migmatization (Figs. 5 and 6). ε_{Hf} and ε_{Nd} values of Paleoproterozoic samples do not form a "reworking array" with older Archean rocks, but instead are dislocated to higher values, close to CHUR (Fig. 7), which suggests involvement of more juvenile material (e.g., mixing), consistent with the regional data (black in Fig. 9). The preferred scenario is that of subduction beneath the São Francisco Craton Archean cores followed by collision during the Paleoproterozoic.

3.6 Acknowledgements

Authors acknowledge support from INCT Estudos Tectônicos (CNPq, CAPES, FAPDF). F.J.S.F is thankful to CAPES for provinding him a PhD scholarship. R.S.M. is thankful to Fundação Carlos Chagas de Amparo à Pesquisa do Estado do Rio de Janeiro (FAPERJ), for providing a post-doctoral fellowship (E-26/202.084/2020 and 2020.03701.1). RAF acknowledges CNPq research fellowships. The authors are very thankful to Elton L. Dantas, for helping with data collection, text review, analyses and for helpful and insightful discussions.

3.7 References

Aguilar, C., Alkmim, F.F., Lana, C., Farina, F., 2017. Palaeoproterozoic assembly of the São Francisco craton, SE Brazil: New insights from U–Pb titanite and monazite dating. Precambrian Res., 289, 95-115.

Albert, C., Farina, F., Lana, C., Stevens, G., Storey, C., Gerdes, A., Dopico, C.M., 2016. Archean crustal evolution in the Southern São Francisco craton, Brazil: Constraints from U-Pb, Lu-Hf and O isotope analyses. Lithos, 266, 64-86.

Almeida, F.F.M., Hasui, Y., Brito Neves, B.B., Fuck, R.A., 1981. Brazilian structural provinces: An introduction. Earth Sci. Rev. 17, 1–29.

Archanjo, C.J., Viegas, L.G., Hollanda, M.H.B.M., 2012. Zircon U-PB (Shrimp) ages of the high-temperature deformation of the Patos mylonite belt (Borborema Province, NE Brazil).

Archanjo, C.J., Hollanda, M.H.B.M., Viegas, L.G.F., 2021. Late Ediacaran lateral-escape tectonics as recorded by the Patos shear zone (Borborema Province, NE Brazil). Brazil. J. Geol., 51.

Ávila, C.A., Teixeira, W., Cordani, U.G., Moura, C.A.V., Pereira, R.M., 2010. Rhyacian (2.23–2.20 Ga) juvenile accretion in the southern São Francisco craton, Brazil: Geochemical and isotopic evidence from the Serrinha magmatic suite, Mineiro belt. Journal of South American Earth Sciences, 29(2), 464-482.

Ávila, C.A., Teixeira, W., Bongiolo, E.M., Dussin, I.A., Vieira, T.A.T., 2014. Rhyacian evolution of subvolcanic and metasedimentary rocks of the southern segment of the Mineiro Belt, São Francisco Craton, Brazil. Precambrian Res., 243, 221–251.

Barbosa, J.S.F., Menezes Leal, A.B., Fuck, R.A., Oliveira, J.S.S., Gonçalves, P.,Leite, C.M.M., 2017. Ultrahigh-temperature metamorphism of 2.0 Ga-Old sapphirine-bearing granulite from the Itabuna-Salvador-Curaçá Block, Bahia, Brazil. USP Série Cient., 17, 89-108.

Barbosa, N.S., Teixeira, W., Ávila, C.A., Montecinos, P.M., Bongiolo, E.M., 2015. 2.17–2.09 Ga crust forming episodes in the Mineiro belt, São Francisco craton, Brazil: U-Pb ages and geochemical constraints. Precambrian Res., 270, 204–225.

Barbosa, N., Teixeira, W., Ávila, C.A., Montecinos, P.M., Bongiolo, E.M., Vasconcelos, F.F., 2019. U-Pb geochronology and coupled Hf-Nd-Sr isotopic-chemical constraints of the Cassiterita Orthogneiss (2.47–2.41-Ga) in the Mineiro belt, São Francisco craton: Geodynamic fingerprints beyond the Archean-Paleoproterozoic Transition. Precambrian Res., 326, 399-416.

Bea, F., Montero, P., Barcos, L., Cambeses, A., Molina, J.F., Morales, I., 2023. Understanding Nd model ages of granite rocks: The effects of the $^{147}Sm/^{144}Nd$ variability during partial melting and crystallization. Lithos, 436, 106940.

Belousova, E. A., Kostitsyn, Y. A., Griffin, W. L., Begg, G. C., O'reilly, S. Y., & Pearson, N. J. (2010). The growth of the continental crust: constraints from zircon Hf-isotope data. Lithos, 119(3-4), 457-466.

Bersan, S.M., Costa, A.F.O., Danderfer, A., Abreu, F.R., Lana, C., Queiroga, G., Storey, C., Moreira, H., 2020. Paleoproterozoic juvenile magmatism within the northeastern sector of the São Francisco paleocontinent: Insights from the shoshonitic high Ba–Sr Montezuma granitoids. Geosci. Front., 11(5), 1821-1840.

Bersan, S.M., Danderfer, A., Storey, C., Bruno, H., Moreira, H., Abreu, F., Lana, C., Gonçalves, L., Nahas, I., 2022. A perspective on potassic and ultrapotassic rocks: Constraints on the Paleoproterozoic late to post-collisional event in the São Francisco paleocontinent. Geosci. Front., 13(5), 101179.

Blichert-Toft, J., Albarède, F., 1997. The Lu-Hf isotope geochemistry of chondrites and the evolution of the mantle-crust system. Earth Planet. Sci. Lett., 148(1-2), 243-258.

Brito Neves, B.B., Santos, E.J., Van Schmus, W.R., 2000. Tectonic history of the Borborema province. In: Cordani, U.G., Milani, E.J., Thomaz Filho, A.,

Campos, D.A. (Eds.), Tectonic Evolution of South America. 31° Int. Geol. Congr. Rio Janeiro 151–182.

Bruno, H., Elizeu, V., Heilbron, M., Valeriano, C.M., Strachan, R., Fowler, M., Bersan, S., Moreira, H., Dussin, I., Eirado Silva, L.G., Tupinambá, M., Almeida, J., Carla, N., Storey, C., 2020. Neoarchean and Rhyacian TTG-Sanukitoid suites in the southern São Francisco Paleocontinent, Brazil: evidence for diachronous change towards modern tectonics. Geosc. Front., 11(5), 1763-1787.

Bruno, H., Heilbron, M., de Morisson Valeriano, C., Strachan, R., Fowler, M., Bersan, S., Moreira, H., Motta, R., Almeida, J., Almeida, R., Carvalho, M., Storey, C., 2021. Evidence for a complex accretionary history preceding the amalgamation of Columbia: the Rhyacian Minas-Bahia Orogen, southern São Francisco Paleocontinent, Brazil. Gondwana Res., 92, 149-171.

Bühn, B., Pimentel, M.M., Matteini, M., Dantas, E.L., 2009. High spatial resolution analysis of Pb and U isotopes for geochronology by laser ablation multi-collector inductively coupled plasma mass spectrometry (LA-MC-ICP-MS). An. Acad. Bras. Cienc. 81, 99-114.

Caby, R., 1989. Precambrian terranes of Benin-Nigeria and northeast Brazil. Terranes in the circum-Atlantic Paleozoic orogens, 230, 145.

Caby, R., Arthaud, M.H., Archanjo, C.J., 1995. Lithostratigraphy and petrostructural characterization of supracrustal units in the Brasiliano Belt of Northeast Brazil: geodynamic implications. J. S. Earth Sci., 8(3-4), 235-246.

Caxito, F.D.A., Santos, L.C.M.L., Ganade, C.E., Bendaoud, A., Fettous, E.H., Bouyo, M.H., 2020. Toward an integrated model of geological evolution for NE Brazil-NW Africa: The Borborema Province and its connections to the Trans-Saharan (Benino-Nigerian and Tuareg shields) and Central African orogens. Brazil. J. Geo., 50.

Carvalho, B.B., Sawyer, E.W., Janasi, V.A., 2016. Crustal reworking in a shear zone: transformation of metagranite to migmatite. J. Met. Geol., 34(3), 237-264.

Chauvel, C., Blichert-Toft, J., 2001. A hafnium isotope and trace element perspective on melting of the depleted mantle. Earth Planet. Sci. Lett. 190, 137–151.

Chen, Y.X., Gao, P., Zheng, Y.F., 2015. The anatectic effect on the zircon Hf isotope composition of migmatites and associated granites. Lithos, 238, 174-184.

Chu, N.C., Taylor, R.N., Chavagnac, V., Nesbitt, R.W., Boella, R.M., Milton, J.A., C.R., German., Bayon, G., Burton, K., 2002. Hf isotope ratio analysis using multi-collector inductively coupled plasma mass spectrometry: an evaluation of isobaric interference corrections. J. An. Atom. Spec. 17, 1567-1574.

Cioffi, C.R., Campos Neto, M.C., Möller, A., Rocha, B.C., 2016a. Tectonic significance of the Meso-to Neoarchean complexes in the basement of the southern Brasília Orogen. Precambrian Res., 287, 91-107.

Cioffi, C.R., Campos Neto, M.C., Möller, A., Rocha, B.C., 2016b. Paleoproterozoic continental crust generation events at 2.15 and 2.08 Ga in the basement of the southern Brasília Orogen, SE Brazil. Precambrian Res., 275, 176-196.

Cioffi, C.R., Meira, V.T., Trindade, R.I., Lanari, P., Ganade, C.E., Gerdes, A., 2021. Long-lived intracontinental deformation associated with high geothermal gradients in the Serido Belt (Borborema Province, Brazil). Precambrian Res., 358, 106141.

Cordeiro, P.F.O., Oliveira, C.G., Della Giustina, M.E.S., Dantas, E.L., Santos, R.V., 2014. The Paleoproterozoic Campinorte arc: tectonic evolution of a Central Brazil pre-Columbia orogeny. Precambrian Res., 251, 49-61.

Corfu, F., Hanchar, J.M., Hoskin, P.W., Kinny, P., 2003. Atlas of zircon textures. Rev. Min. Geoc., 53(1), 469-500.

Corsini, M., Vauchez, A., Archanjo, C., Jardim de Sá, E.F., 1991. Strain transfer at continental scale from a transcurrent shear zone to a transpressional fold belt: the Patos-Seridó system, northeastern Brazil. Geology, 19(6), 586-589.

Costa, F.G., Klein, E.L., Lafon, J.M., Milhomem Neto, J.M., Galarza, M.A., Rodrigues, J.B., Naleto, J.L.C., Corrêa Lima, R.G., 2018. Geochemistry and U–Pb–Hf zircon data for plutonic rocks of the Troia Massif, Borborema Province, NE Brazil: Evidence for reworking of Archean and juvenile Paleoproterozoic crust during Rhyacian accretionary and collisional tectonics. Precambrian Res. 311, 167–194.

Cutts, K., Lana, C., Alkmim, F., Peres, G.G., 2018. Metamorphic imprints on units of the southern Araçuaí belt, SE Brazil: The history of superimposed Transamazonian and Brasiliano orogenesis. Gondwana Res., 58, 211-234.

Cutts, K., Lana, C., Alkmim, F., Farina, F., Moreira, H., Coelho, V., 2019. Metamorphism and exhumation of basement gneiss domes in the Quadrilátero Ferrífero: Two stage dome-and-keel evolution?. Geosci. Front., 10(5), 1765-1787.

Dantas, E.L., Van Schmus, W.R., Hackspacher, P.C., Fetter, A.H., De Brito Neves, B.B., Cordani, U., Nutman, A.P., Williams, I.S., 2004. The 3.4-3.5 Ga São José do Campestre massif, NE Brazil: Remnants of the oldest crust in South America. Precambrian Res. 130, 113–137.

Dantas, E.L., De Souza, Z.S., Wernick, E., Hackspacher, P.C., Martin, H., Xiaodong, D., Li, J.W., 2013. Crustal growth in the 3.4-2.7 Ga São José de Campestre Massif, Borborema Province, NE Brazil. Precambrian Res. 227, 120–156.

Davies, G.R., Tommasini, S., 2000. Isotopic disequilibrium during rapid crustal anatexis: implications for petrogenetic studies of magmatic processes. Chem. Geo., 162(2), 169-191.

Degler, R., Pedrosa-Soares, A., Novo, T., Tedeschi, M., Silva, L.C., Dussin, I., Lana, C., 2018. Rhyacian-Orosirian isotopic records from the basement of the Araçuaí-Ribeira orogenic system (SE Brazil): Links in the Congo-São Francisco palaeocontinent. Precambrian Res., 317, 179-195.

DePaolo, D.J., 1981. A neodymium and strontium isotopic study of the Mesozoic calc-alkaline granitic batholiths of the Sierra Nevada and Peninsular Ranges, California. J. Geophys. Res. Solid Earth 86, 10470–10488.

Dhuime, B., Hawkesworth, C.J., Cawood, P.A., Storey, C.D., 2012. A change in the geodynamics of continental growth 3 billion years ago. Science, 335(6074), 1334-1336.

Egydio-Silva, M., Vauchez, A., Fossen, H., Cavalcante, G.C.G., Xavier, B.C., 2018. Connecting the Araçuaí and Ribeira belts (SE–Brazil): Progressive transition from contractional to transpressive strain regime during the Brasiliano orogeny. J. S. Am. Earth Sci., 86, 127-139.

Farina, F., Stevens, G., Gerdes, A., Frei, D., 2014. Small-scale Hf isotopic variability in the Peninsula pluton (South Africa): the processes that control inheritance of source $^{176}Hf/^{177}Hf$ diversity in S-type granites. Cont. Min. Petro., 168, 1-18.

Farina, F., Albert, C., Lana, C., 2015. The Neoarchean transition between medium-and high-K granitoids: Clues from the Southern São Francisco Craton (Brazil). Precambrian Res., 266, 375-394.

Ferreira, A.C.D., Dantas, E.L., dos Santos, T.J.S., Fuck, R.A., Tedeschi, M., 2020. High-pressure metamorphic rocks in the Borborema Province, Northeast Brazil: Reworking of Archean oceanic crust during proterozoic orogenies. Geosci. Front., 11(6), 2221-2242.

Ferreira, A.C.D., Dantas, E.L., Fuck, R.A., Nedel, I.M., Reimold, W.U., 2021. Multiple stages of migmatite generation during the Archean to Proterozoic crustal evolution in the Borborema Province, Northeast Brazil. Gondwana Res., 90, 314-334.

Fetter, A.H., 1999. U/Pb and Sm/Nd Geocronological Constraints on the Crustal Framework and Geologic History of Ceará State, NW Borborema Province, NE Brazil: Implications for the Assembly of Gondwana. Kansas University, Lawrence.

Fossen, H., Harris, L.B., Cavalcante, C., Archanjo, A.J., Ávila, C.F., 2022. The Patos-Pernambuco shear system of NE Brazil: Partitioned intracontinental transcurrent deformation revealed by enhanced aeromagnetic data. Journal of Structural Geology, 158, 104573.

Fuck, R.A., Dantas, E.L., Pimentel, M.M., Botelho, N.F., Armstrong, R., Laux, J.H., Junges, S.J., Soares, J.E., Praxedes, I.F., 2014. Paleoproterozoic crust-formation and reworking events in the Tocantins Province, central Brazil: A contribution for Atlantica supercontinent reconstruction. Precambrian Res., 244, 53-74.

Ganade, C.E.A., Weinberg, R.F., Cordani, U.G., 2014a. Extruding the Borborema Province (NE-Brazil): a two-stage Neoproterozoic collision process. Terra Nova, 26(2), 157-168.

Ganade, C.E.A., Rubatto, D., Hermann, J., Cordani, U. G., Caby, R., Basei, M.A., 2014b. Ediacaran 2,500-km-long synchronous deep continental subduction in the West Gondwana Orogen. Nature communications, 5(1), 5198.

Ganade, C.E., Basei, M.A.S., Grandjean, F.C., Armstrong, R., Brito, R.S., 2017. Contrasting Archaean (2.85–2.68 Ga) TTGs from the Tróia Massif (NE-Brazil) and their geodynamic implications for flat to steep subduction transition. Precambrian Res. 297, 1–18.

Ganade, C.E., Weinberg, R.F., Caxito, F.A., Lopes, L.B., Tesser, L.R., Costa, I.S., 2021. Decratonization by rifting enables orogenic reworking and transcurrent dispersal of old terranes in NE Brazil. Sci. Reports, 11(1), 5719.

Gao, P., Yakymchuk, C., Zhang, J., Yin, C., Qian, J., Li, Y., 2022. Preferential dissolution of uranium-rich zircon can bias the hafnium isotope compositions of granites. Geology, 50(3), 336-340.

Gardiner, N.J., Mulder, J.A., Kirkland, C.L., Johnson, T.E., Nebel, O., 2021. Palaeoarchaean TTGs of the Pilbara and Kaapvaal cratons compared; an early Vaalbara supercraton evaluated: S. Afri. J. Geo., v. 124, p. 37–52.

Gioia, S.M.C.L., Pimentel, M.M., 2000. The Sm-Nd isotopic method in the Geochronology Laboratory of the University of Brasília. An. Acad. Bras. Cienc. 72, 218–245.

Giraldo, S.J., Trouw, R.A.J., Duffles, P., Costa, R.V., Mejia, M.I., Marimon, R.S., 2019. Structural analysis combined with new geothermobarometric and geochronological results of the Além Paraíba shear zone, between Três Rios and Bananal, Ribeira Orogen, SE Brazil. J. S. Am. Earth Sci., 90, 118-136.

Hawkesworth, C.J., Kemp, A.I.S., 2006. Evolution of the continental crust. Nature, 443(7113), 811-817.

Hawkesworth, C., Cawood, P., Kemp, T., Storey, C., Dhuime, B., 2009. A matter of preservation. Science, 323(5910), 49-50.

Hawkesworth, C., Cawood, P., Dhuime, B., 2013. Continental growth and the crustal record. Tectonophysics, 609, 651-660.

Hawkesworth, C., Cawood, P.A., Dhuime, B., 2019. Rates of generation and growth of the continental crust. Geosci. Front., 10(1), 165-173.

Hawkesworth, C.J., Cawood, P.A., Dhuime, B., 2020. The evolution of the continental crust and the onset of plate tectonics. Front. Earth Sci., 8, 326.

Heilbron, M., Duarte, B.P., Valeriano, C.M., Simonetti, A., Machado, N., Nogueira, J.R., 2010. Evolution of reworked Paleoproterozoic basement rocks within the Ribeira belt (Neoproterozoic), SE-Brazil, based on U–Pb geochronology: Implications for paleogeographic reconstructions of the São Francisco-Congo paleocontinent. Precambrian Res., 178(1-4), 136-148.

Heilbron, M.; Cordani, U.G.; Alkmim, F.F.; Reis, H.L.S. 2017. Tectonic Genealogy of a Miniature Continent. In: Heilbron, M., Cordani, U. & Alkmim, F. (eds.), The São Francisco Craton and its Margins: Tectonic Genealogy of a Miniature Continent. Springer, Reg. Geo. Rev., cap. 17, 321-331.

Hildreth, W., Moorbath, S., 1988. Crustal contributions to arc magmatism in the Andes of central Chile. Cont. Min. Petro., 98, 455-489.

Hollanda, M.H.B.M., Archanjo, C.J., Bautista, J.R., Souza, L.C., 2015. Detrital zircon ages and Nd isotope compositions of the Seridó and Lavras da Mangabeira basins (Borborema Province, NE Brazil): Evidence for exhumation and recycling associated with a major shift in sedimentary provenance. Precambrian Res., 258, 186-207.

Jackson, S.E., Pearson, N.J., Griffin, W.L., Belousova, E.A., 2004. The application of laser ablation-inductively coupled plasma-mass spectrometry to in situ U–Pb zircon geochronology. chemical Geology 211, 47-69.

Jessup, M.J., Wintsch, R.P., 2001. Deformation-induced melting in shear zones. J. Struct. Geol., 23(2-3), 391-400.

Kemp, A.I.S., Hawkesworth, C.J., Foster, G.L., Paterson, B.A., Woodhead, J.D., Hergt, J.M., Gray, C.M., Whitehouse, M.J., 2007. Magmatic and crustal differentiation history of granitic rocks from Hf-O isotopes in zircon. Science, 315(5814), 980-983.

Kemp, A.I.S., Hawkesworth, C.J., Collins, W.J., Gray, C.M., Blevin, P.L., 2009. Isotopic evidence for rapid continental growth in an extensional accretionary orogen: The Tasmanides, eastern Australia. Earth Planet. Sci. Lett., 284(3-4), 455-466.

Lana, C., Alkmim, F.F., Armstrong, R., Scholz, R., Romano, R., Nalini Jr, H.A., 2013. The ancestry and magmatic evolution of Archaean TTG rocks of the Quadrilátero Ferrífero province, southeast Brazil. Precambrian Res., 231, 157-173.

Laurent, O., Martin, H., Moyen, J. F., Doucelance, R., 2014. The diversity and evolution of late-Archean granitoids: Evidence for the onset of “modern-style” plate tectonics between 3.0 and 2.5 Ga. Lithos, 205, 208-235.

Laurent, O., Zeh, A., 2015. A linear Hf isotope-age array despite different granitoid sources and complex Archean geodynamics: Example from the Pietersburg block (South Africa). Earth Planet. Sci. Lett., 430, 326-338.

Lopes, L.B.L., Ganade, C.E., Campos, L.D., Rodrigues, J.B., Oliveira, L.B.T., Larizzatti, J.H., Shen, M., Gao, T., Xu, M., Zhou, Y., Yao, Z., 2021. Crustal

reworking and Archean TTG generation in the south Gavião Block, São Francisco Craton, Brazil. Precambrian Res., 363, 106333.

Marimon, R.S., Trouw, R.A., Dantas, E.L., 2020. Significance of age periodicity in the continental crust record: The São Francisco Craton and adjacent Neoproterozoic orogens as a case study. Gondwana Res., 86, 144-163.

Marimon, R.S., Hawkesworth, C.J., Dantas, E.L., Trouw, R.A.J., Teixeira, W., Hackspacher, P.C., Fetter, A., Ávila, C.A., Volante, S., Corrêa Neto, A.V., Bongiolo, E.M., Vinagre, R., Simon, M., 2022a. The generation and evolution of the Archean continental crust: The granitoid story in southeastern Brazil. Geosci. Front., 13(4), 101402.

Marimon, R.S., Hawkesworth, C.J., Trouw, R.A., Trouw, C., Dantas, E.L., Ribeiro, A., Vinagre, R., Hackspacher, P., Ávila, C., Motta, R., Moraes, R., 2022b. Subduction and continental collision in the Neoproterozoic: Sanukitoid-like magmatism and paired metamorphism in SE Brazil. Precambrian Res., 383, 106888.

Matteini, M., Dantas, E.L., Pimentel, M.M., Bühn, B., 2010. Combined U-Pb and Lu-Hf isotope analyses by laser ablation MC-ICP-MS: methodology and applications. Na. Acad. Bras. Ciênc. 82, 479-491.

Meert, J.G., Santosh, M., 2017. The Columbia supercontinent revisited. Gondwana Res., 50, 67-83.

Morel, M.L.A., Nebel, O., Nebel-Jacobsen, Y.J., Miller, J.S., Vroon, P.Z., 2008. Hafnium isotope characterization of the GJ-1 zircon reference material by solution and laser-ablation MC-ICPMS. Chem. Geol. 255, 231-235.

Moyen, J.F., Laurent, O., 2018. Archaean tectonic systems: A view from igneous rocks. Lithos, 302, 99-125.

Moyen, J.F., Zeh, A., Cuney, M., Dziggel, A., Carrouée, S., 2021, The multiple ways of recycling Archaean crust: A case study from the ca. 3.1 Ga granitoids from the Barberton Greenstone belt, South Africa: Precambrian Res., 353, 105998.

Neves, S.P., 2021. Comparative geological evolution of the Borborema Province and São Francisco Craton (eastern Brazil): Decratonization and crustal reworking during West Gondwana assembly and implications for paleogeographic reconstructions. Precambrian Res., 355, 106119.

Neves, C.V.S., Ávila, C.A., Bongiolo, E.M., Neumann, R., Teixeira, W., Faulstich, F.R.L., Heilbron, M., Valeriano, C.M., 2023. Preserved interactions between acid and intermediate magmas in a 2.15–2.10 Ga Rhyacian continental arc: Insights from petrographic, geochemical and isotopic data of the Macuco de Minas metagranitoid, Mineiro belt, Brazil. Lithos, 440, 107048.

Oliveira, E.P., McNaughton, N.J., Armstrong, R., 2010. Mesoarchaean to Palaeoproterozoic growth of the northern segment of the Itabuna–Salvador–Curaçá orogen, São Francisco craton, Brazil. Geol. Soc., London, Special Publications, 338(1), 263-286.

Payne, J.L., McInerney, D.J., Barovich, K.M., Kirkland, C.L., Pearson, N.J., Hand, M., 2016. Strengths and limitations of zircon Lu-Hf and O isotopes in modelling crustal growth. Lithos, 248, 175-192.

Patchett, P.J., 1983. Importance of the Lu-Hf isotopic system in studies of planetary chronology and chemical evolution. Geoc. et Cosmoc. Acta, 47(1), 81-91.

Peucat, J.J., Barbosa, J.S.F., Araújo Pinho, I.C., Paquette, J.L., Martin, H., Fanning, C.M., Leal, A.B.M., Cruz, S., 2011. Geochronology of granulites from the south Itabuna-Salvador-Curaçá Block, São Francisco Craton (Brazil): Nd isotopes and U–Pb zircon ages. J. S. Am. Earth Sci., 31(4), 397-413.

Pietranik, A.B., Hawkesworth, C.J., Storey, C.D., Kemp, A.I.S., Sircombe, K.N., Whitehouse, M.J., Bleeker, W., 2008. Episodic, mafic crust formation from 4.5 to 2.8 Ga: New evidence from detrital zircons, Slave craton, Canada. Geology 36, 875.

Pitarello, M.Z., Santos, T.J.S., Ancelmi, M.F., 2019. Syn-to post-depositional processes related to high grade metamorphic BIFs: Geochemical

and geochronological evidences from a Paleo to Neoarchean (3.5–2.6 Ga) terrane in NE Brazil. J. S. Am. Earth Sci. 96, 102312.

Romano, R., Lana, C., Alkmim, F.F., Stevens, G., Armstrong, R., 2013. Stabilization of the southern portion of the São Francisco craton, SE Brazil, through a long-lived period of potassic magmatism. Precambrian Res., 224, 143-159.

Ruiz, F.V., Della Giustina, M.E.S., Oliveira, C.G., Dantas, E.L., Hollanda, M.H.B.M., 2019. The 3.5 Ga São Tomé layered mafic-ultramafic intrusion, NE Brazil: Insights into a Paleoarchean Fe-Ti-V oxide mineralization and its reworking during West Gondwana assembly, Precambrian Res. 326, 462-478.

Santos, L.C.M.L., Dantas, E.L., Cawood, P.A., Lages, G.A., Lima, H.M., Santos, E.J., 2018. Accretion Tectonics in Western Gondwana Deduced From Sm-Nd Isotope Mapping of Terranes in the Borborema Province, NE Brazil. Tectonics, 37(8), 2727-2743.

Santos, C., Zincone, S.A., Queiroga, G.N., Bersan, S.M., Lana, C.C., Oliveira, E.P., 2022. Evidence for change in crust formation process during the Paleoarchean in the São Francisco Craton (Gavião Block): Coupled zircon Lu-Hf and U-Pb isotopic analyses and tectonic implications. Precambrian Res., 368, 106472.

Sawyer, E.W., 2008. Atlas of migmatites (Vol. 9). NRC Research press.

Scherer, E., Münker, C., Mezger, K., 2001. Calibration of the lutetium-hafnium clock. Science 293, 683-687.

Souza, Z.S., Kalsbeek, F., Deng, X.D., Frei, R., Kokfelt, T.F., Dantas, E.L., Li, J.W., Pimentel, M.M., Galindo, A.C., 2016. Generation of continental crust in the northern part of the Borborema Province, northeastern Brazil, from Archaean to Neoproterozoic. J. S. Am. Earth Sci. 68, 68–96.

Tang, M., Wang, X.L., Shu, X.J., Wang, D., Yang, T., Gopon, P., 2014. Hafnium isotopic heterogeneity in zircons from granitic rocks: Geochemical evaluation and modeling of “zircon effect” in crustal anatexis. Earth Planet. Sci. Lett., 389, 188-199.

Teixeira, W., Ávila, C.A., Dussin, I.A., Neto, A.C., Bongiolo, E.M., Santos, J.O., Barbosa, N.S., 2015. A juvenile accretion episode (2.35–2.32 Ga) in the Mineiro belt and its role to the Minas accretionary orogeny: Zircon U–Pb–Hf and geochemical evidences. Precambrian Res., 256, 148-169.

Valeriano, C.M., Turbay, C.V.G., Bruno, H., Simonetti, A., Heilbron, M., Bersan, S.M., Strachan, R. 2022. Paleo-and Mesoarchean TTG-sanukitoid to high-K granite cycles in the southern São Francisco craton, SE Brazil. Geosci. Front., 13(5), 101372.

Van Schmus, W.R., Brito Neves, B.B., Hackspacher, P.C., Babinski, M., 1995. UPb and SmNd geochronologic studies of the eastern Borborema Province, Northeastern Brazil: initial conclusions. J. S. Am. Earth Sci., 8(3-4), 267-288.

Van Schmus, W.R., Kozuch, M., de Brito Neves, B.B., 2011. Precambrian history of the Zona Transversal of the Borborema Province, NE Brazil: Insights from Sm-Nd and U-Pb geochronology. J. S. Am. Earth Sci. 31, 227–252.

Vauchez, A., Tommasi, A., Egydio-Silva, M., 1994. Self-indentation of a heterogeneous continental lithosphere. Geology, 22(11), 967-970.

Viegas, L.G.F., Archanjo, C.J., Vauchez, A., 2013. Fabrics of migmatites and the relationships between partial melting and deformation in high-grade transpressional shear zones: the Espinho Branco anatexite (Borborema Province, NE Brazil). J. Stru. Geo., 48, 45-56.

Viegas, L.G.F., Archanjo, C.J., Hollanda, M.H.B.M., Vauchez, A., 2014. Microfabrics and zircon U-Pb (SHRIMP) chronology of mylonites from the Patos shear zone (Borborema Province, NE Brazil). Precambrian Res. 243, 1–17.

Vinagre, R., Trouw, R.A.J., Marimon, R.S., Nepomuceno, F., Mendes, J.C., Dantas, E., 2020. São Bento do Sapucaí Shear Zone: Constraining age and PT conditions of a collisional Neoproterozoic oblique shear zone, Ribeira Orogen, Brazil. J. S. Am. Earth Sci., 98, 102418.

Windley, B.F., Kusky, T., Polat, A., 2021. Onset of plate tectonics by the Eoarchean. Precambrian Res., 352, 105980.

Xia, Q.X., Chen, Y.X., Chen, R.X., Zheng, Y.F., 2022. Elevation of zircon Hf isotope ratios during crustal anatexis: Evidence from migmatites close to the eastern Himalayan syntaxis in southeastern Tibet. Lithos, 412, 106592.

Yang, L., Wang, J.M., Liu, X.C., Khanal, G.P., Wu, F.Y., 2022. Sr-Nd-Hf isotopic disequilibrium during the partial melting of Metasediments: insight from Himalayan Leucosome. Front. in Earth Sci., 10, 891960.

Zeng, L., Saleeby, J.B., Asimow, P., 2005. Nd isotope disequilibrium during crustal anatexis: A record from the Goat Ranch migmatite complex, southern Sierra Nevada batholith, California. Geology, 33(1), 53-56.

Zhong, Y., Kusky, T.M., Wang, L., Wang, C., Peng, Y., Wang, T., Yan, C., 2023. Alpine-style tectonic nappe stacking in an Archean suture zone: Quantitative structural profile places constraints on orogenic architecture. Gondwana Res., 117, 86-116.

CAPÍTULO 4

Segundo artigo

Artigo submetido a Journal of South American Earth Science.

An Andean-type magmatic-arc-to-collision orogenic system of 2.4-1.9 Ga reworked in the Neoproterozoic: The Greater São Francisco Orogen in Brazil.

Frankie J.S. Fachetti[1]; Rodrigo S. Marimon[2]; Reinhardt A. Fuck[1]; Carlos Ribeiro[1]; Ana Cláudia D. da Costa[3]; Chris J. Hawkesworth[4]

[1] Instituto de Geociências, Universidade de Brasília (UnB), Brasília-DF, Brasil.

[2] Instituto de Geociências, Universidade Federal do Rio de Janeiro (UFRJ), Rio de Janeiro-RJ, Brasil

[3] Faculdade de Geociências, Universidade Federal de Mato Grosso (UFMT), Cuiabá-MT, Brasil.

[4] School of Geosciences, Bristol University, Bristol, United Kingdom

Abstract

Magmatic arcs, which extend for thousands of kilometers, represent important sites of magmatic production and volcanism today. The average composition of the continental crust is like that of rocks produced in continental magmatic arcs, which has prompted investigators to suggest most of the continental crust was produced in these settings. Here, we provide new U-Pb, Lu-Hf and Sm-Nd data on felsic basement migmatitic orthogneisses from the Borborema Province, NE Brazil, a Neoproterozoic orogen (630-570 Ma) close to the northern border of the São Francisco Craton, which is by definition only metamorphosed at low grades during the Neoproterozoic (Brasiliano Orogeny). We obtained U-Pb zircon ages of 2.26-2.07 Ga and moderately positive (up to +5) to highly negative (-10) ƐHf and ƐNd values. This, and inherited Archean grains, suggests juvenile input accompanied crustal reworking during magmatism, a common feature of continental magmatic arcs. Evidence from metamorphic zircon grains (e.g., soccer-ball) point to two stages of high-grade metamorphism, one in the Neoproterozoic (~570 Ma) and the other in the Paleoproterozoic (2.1-2.0 Ga), both interpreted as related to continental collisions. Therefore, the migmatitic orthogneisses analyzed in this study are likely part of a Paleoproterozoic (2.26-2.0.7 Ga) magmatic arc system, established on Archean (3.5-2.5 Ga) crust, that evolved to a collisional orogen (2.1-2.0 Ga). Basement rocks of similar crystallization and metamorphism ages, composition, petrography and isotopic signatures are found surrounding the São Francisco Craton's Archean core, and most are overprinted by Neoproterozoic orogenies. These rocks formed a large subduction-to-collision orogenic system in the Paleoproterozoic, that was thousands of kilometers long and today occupies a large segment of the Brazilian territory. We call it the Greater São Francisco Orogen as segments of it are found as inliers in Neoproterozoic belts, interpreted to represent reworked basement inliers. This ultimately led to the formation of the Columbia supercontinent.

Keywords:

Magmatic arc, crustal reworking, continental collision, migmatites, Hf-Nd isotopes

1. Introduction

Magmatic arcs are one of the most remarkable features of plate tectonics. They form ribbon-like structures that extend for thousands of kilometers and represent important sites of magmatic production and volcanism in the modern Earth. The average composition of the continental crust, including its trace element signature, is very similar to the most abundant rocks in continental magmatic arcs (Andean-type): calc-alkaline andesites (Rudnick and Gao, 2003; Ducea et al., 2015). This has been used as support to the idea that most of the present-day continental crust was formed in magmatic arcs (Taylor and McLennan, 1985; Hawkesworth et al., 2013).

Continental magmatic arcs evolve to stable continental crust over time, after crustal-scale magmatic differentiation during a long period of subduction (Jagoutz, 2014) followed by oceanic basin closure and continental collision that shield the arc lithosphere from further tectonic erosion caused by the down-going slab (e.g., Stern, 2011) and preserves the crust in the geological record (Hawkesworth et al., 2009, 2013, 2020). Compared to island arcs, continental magmatic arcs are composed of thicker crust, have a larger compositional magmatic diversity and are dominated by magmatic rocks of higher silica content (Ducea et al., 2015).

The crust of continental magmatic arcs is divided into the upper, middle and lower segments. The upper portions are dominated by volcanic rocks, the middle is composed mostly of intermediate to felsic batholiths and the lower segments, also known as “the root”, are made up of intermediate to mafic and ultramafic rocks, with mafic intrusives (i.e. new additions to the crust), cumulates and partial melting residues that get periodically removed by gravitational foundering associated with mantle convection (Saleeby et al., 2003; Jagoutz, 2014; Ducea et al., 2015; Jagoutz and Kelemen, 2015). The continental arc’s lower crust is dominated by high-grade migmatitic rocks that can also encompass the basement of the upper plate. This is where juvenile magmas, constantly

replenished from the mantle wedge, interact with the preexisting continental upper plate, and if it is old compared to the arc magmatism, this interaction will generate more evolved melts (both isotopically and chemically), in a process akin to MASH, that will eventually rise and dominate the batholithic segments (felsic) of the upper arc crust (Hildreth and Moorbath, 1988; Dufek and Bergantz, 2005; Ducea et al., 2015).

In modern continental arcs, migmatization is mostly restricted to the lower crust (Ducea et al., 2015), but ancient magmatic arcs may have all its crustal segments migmatized, considering old arcs have been subjected to multiple tectono-metamorphic events (e.g., continental collisions) throughout their long histories. Migmatites are generated by partial melting processes during crustal thickening that can take place at the core of collisional orogens (Sawyer, 2008; Brown, 2010). Despite the complexity of migmatites, their detailed isotopic, geochronological and compositional study is necessary to produce a complete picture regarding the genesis and evolution of the continental crust throughout Earth's history, and to estimate the amount of juvenile addition and crustal reworking through time.

Given that modern continental magmatic arcs stretch for thousands of kilometers, by analogy older arcs must have also formed regional structures. Still, after several superimposed orogenies, multiple tectono-thermal events and/or sedimentary basin development, the true geometry of ancient magmatic arcs tends to become obscured. In this contribution, we investigate basement migmatitic felsic orthogneisses from the Borborema Province, NE Brazil (Patos Shear Zone System), a Neoproterozoic orogen (630-570 Ma) at the northern border of the São Francisco Craton, and provided new geochronological and isotopic evidence for continental arc magmatism, with assimilation of older Archean crust, between 2.4 and 2.1 Ga, followed by continental collision and post-collisional lithospheric relaxation. We then draw regional comparisons with rocks of similar age, lithotype, isotopic signature and composition to try and partially reconstruct this 2.4-1.9 Ga subduction-to-collision system, that spans a large portion of the Brazilian territory and surrounds the Archean core of the São Francisco Craton. We named this orogen the Greater São Francisco Orogen.

4.2. Regional setting

4.2.1 The Borborema Province

The Borborema Province (BP; Fig. 1) is an orogen formed during the Neoproterozoic Brasiliano/Pan-African Orogeny, through the successive collision of the São Francisco-Congo, São Luís-West Africa and Amazonian Cratons that formed a portion of West Gondwana (Van Schmus et al., 1995). The BP is subdivided into three subprovinces, the North subprovince, Central subprovince and South subprovince, separated by relatively wide shear zone systems oriented E-W (Van Schumus et al., 1995; Costa et al., 2018). The BP is considered a transpressive orogen, and one of its most conspicuous characteristics is a dense anastomosing network of mostly dextral shear-zones that crosscut the whole orogen and follow partial melting and granitoid formation (Hackspacher et al., 1997; Neves et al., 2000; Archanjo et al., 2021; Fossen et al., 2022).

The oldest nuclei of the Borborema Province (BP; Fig. 1) vary in age from ~3.5 Ga (São José do Campestre Massif) to approximately 2.5 Ga and are usually dominated by felsic migmatitic orthogneisses, locally with amphibolite residual boudins, and with a composition varying from sodic (TTG) to potassic (granites and sanukitoids) (Dantas et al., 1998, 2004, 2013; Ganade et al., 2017; Costa et al., 2018; Santos et al., 2018; Pitarello et al., 2019; Ferreira et al., 2021).

The North subprovince of the BP is made up mostly of migmatitic orthogneisses of Paleoproterozoic age (dominantly 2.2 to 2.1 Ga) and restricted Archean fragments (Dantas et al., 2004, 2013 ; Viegas et al., 2014; Souza et al., 2016; Hollanda et al., 2015; Costa et al., 2018; Ruiz et al., 2019; Ferreira et al., 2021), overlain by metamorphosed volcano-sedimentary successions, possibly of varying age and tectonic setting, as well as syn- to late-tectonic granitic bodies (Hollanda et al., 2011, 2015; Archanjo et al., 2013; Basto et al., 2019).

The basement of the Central subprovince, which is separated from the Northern subprovince by the Patos Shear Zone System (PSZS), is made up of Paleoproterozoic-Archean migmatitic orthogneisses of varying bulk composition, but dominantly felsic (Brito Neves et al., 2022), Mesoproterozoic alkaline granites (~1.6 Ga) and Tonian rocks are juxtaposed by accretionary events from ~1.0 to

0.92 Ga, known as the Cariris Velhos Orogeny (e.g., Santos et al., 2018; Van Schmus et al., 2011; Caxito et al., 2020a). It is worth noting that there is no evidence of the Cariris Velhos Orogeny in the Northern segment of the Borborema Province, which suggests the Patos Shear Zone System, described in detail below, constitutes a tectonic boundary that limits blocks of distinct crustal evolutionary histories (Vauchez et al., 1995; Van Schmus et al., 2008, Archanjo et al., 2021).

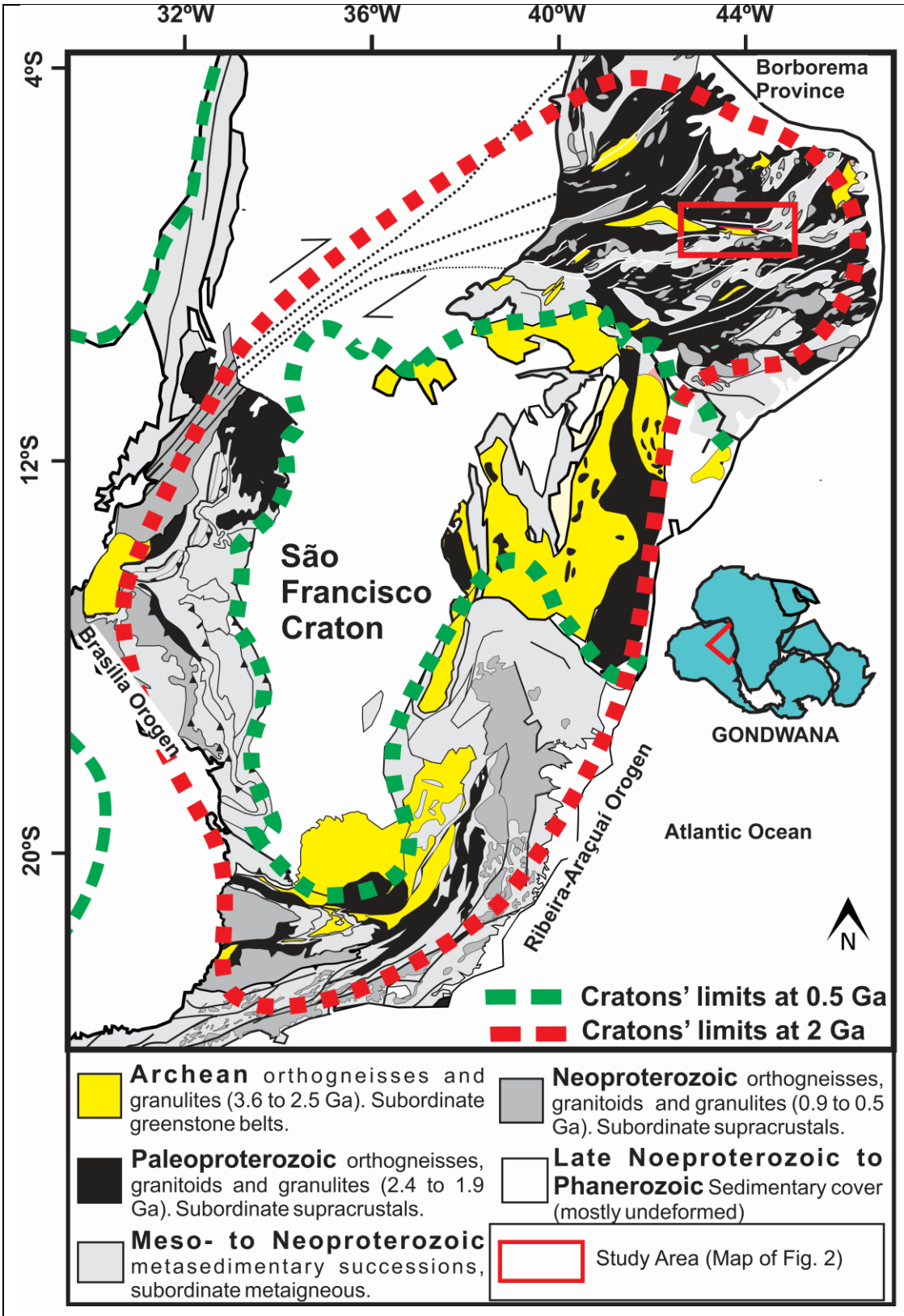

Figure 1) Schematic map of the Borborema Province. Adapted and modified from Fachetti et al. 2024.

2.2 The Patos Shear Zone System

The Patos Shear Zone System (PSZS), where the migmatities were collected, is approximately 400 km long and 20-40 km wide, characterized by a dense network of anastomosing shear zones, where high temperature mylonites dominate, separated from lower strain domains dominated by migmatites with Paleoproterozoic or Archean protoliths (e.g., Viegas et al., 2013, 2014; Archanjo et al., 2021; Fossen et al., 2022). The Patos Shear Zone System (PSZS) extends to west Africa as the Garoua Lineament south of lake Chad and extends towards the south of Libia (Caxito et al., 2020b).

Beneath the Neoproterozoic metasedimentary cover, most of the rocks that crop out in the central segment of the PSZS are orthogneiss migmatitic complexes that locally grade into high- to medium-temperature mylonites, and are characterized by widespread partial melting and the formation of large leucosome bodies in diatexites, as well as boudinaged amphibolitic residual rafts (Fig. 2; Viegas et al., 2013,was 2014; Hollanda et al., 2015). In the northern segment of the PSZS, mylonitization took place at granulite facies conditions, whereas medium temperature mylonitization is reported in the south, possibly related to exhumation (Viegas et al., 2014).

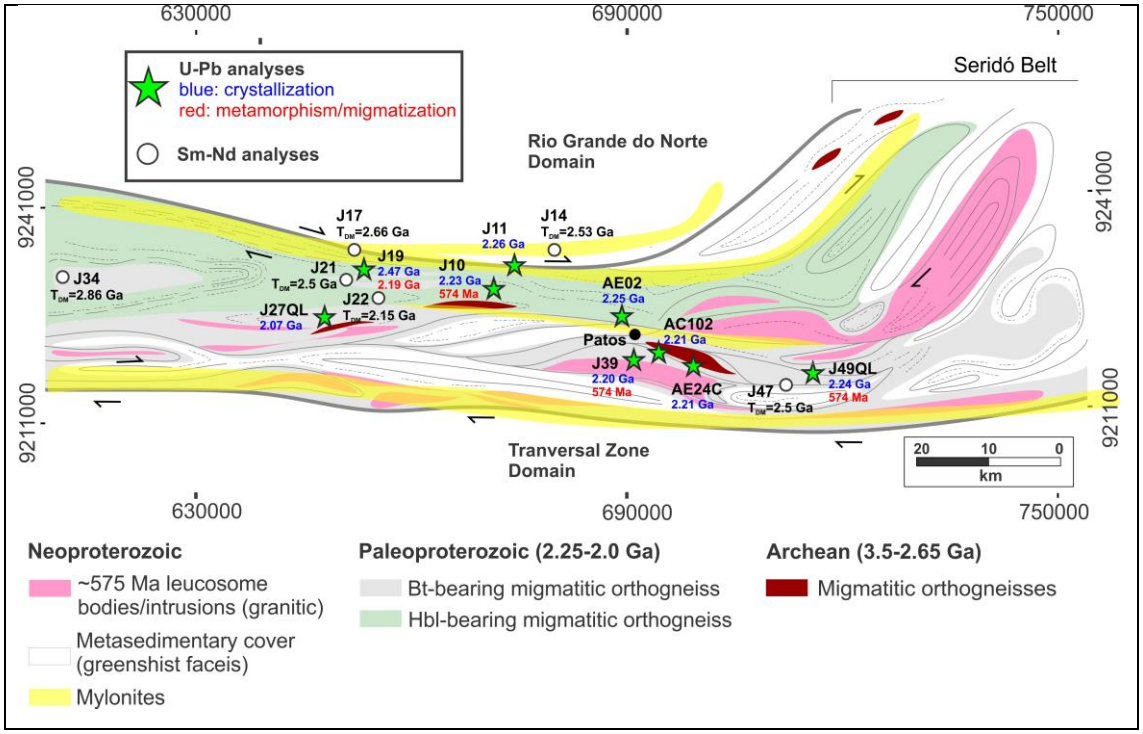

Figure 2) Geological map of the Patos Shear Zone System. Adapted and modified from Viegas et al. (2014).

In the western segment of the PSZS, there is the Granjeiro Complex, dominated by orthogneisses of Archean age (3.0 to 2.5 Ga) tectonically intercalated with Paleoproterozoic orthogneisses and supracrustals (2.5-2.0 Ga), as well as Neoproterozoic cover (Hollanda et al., 2015).

4.3. Methodology

4.3.1 Zircon U-Pb

Zircon grains from twelve rock samples were analyzed on a Thermo-Fisher Neptune LA-ICP-MS coupled to a Nd:YAG UP213 New Wave laser at the Geochronology Laboratory of the University of Brasília (UnB). Thirty micrometer ablation spots were used with a laser frequency at 10 Hz. Sample analyses were bracketed between standard GJ-1 (Jackson et al., 2004) and blank analyses. A 91500 zircon standard was used to control accuracy and raw data were reduced in an Excel spreadsheet. Common lead corrections were not necessary due to low ^{204}Pb counts in most samples. For more information on the methodology applied at the Geochronology Laboratory of the University of Brasília, the reader is referred to Bühn et al. (2009).

4.3.2 Zircon Lu-Hf

Seven samples were selected for Lu-Hf analyses at the Geochronology Laboratory of the University of Brasília (UnB) in a Neptune LA-ICP-MS coupled to a Nd:YAG UP213. Spot sizes of 50 μm were selected with 50 second ablation time. Concomitant with the analyses of the selected samples, a GJ-1 zircon standard yielded a $^{176}Hf/^{177}Hf$ value of 0.2820052±15 (2σ), similar to the average value reported by Morel et al (2008). Isobaric interference of ^{176}Yb and ^{176}Lu were adjusted based on measured ^{171}Yb, ^{173}Yb and ^{175}Lu (Chu et al., 2002). Hf isotopic ratios were normalized for $^{179}Hf/^{177}Hf$ of 0.7325 (Patchett, 1983) and the decay constant (λ) of $1.865x10^{-11}$ (Scherer et al., 2001) and CHUR values of

$^{176}Lu/^{177}Hf$ = 0.0332 and $^{176}Hf/^{177}Hf$=0.282772 (Blichert-Toft and Albarède, 1997), were used to calculate εHf(t). Model ages (T_{DM}) were calculated from the initial Hf isotopic composition of analyzed grains, the average continental crust $^{176}Lu/^{177}Hf$ ratio of 0.010 (Pietranik et al., 2008) and the depleted mantle (DM) ratios of $^{176}Lu/^{177}Hf$=0.0384 and $^{176}Hf/^{177}Hf$=0.28325 (Chauvel and Blichert-Toft, 2001). For more information on the Lu-Hf procedures adopted at the Geochronology Laboratory of the University of Brasília can be found in Matteini et al. (2010).

4.3.3 Whole-rock Sm-Nd

Whole-rock Sm-Nd analyses were performed on a TRITON TIMS multicollector at the University of Brasília (UnB). Pulverized samples were spiked with a ^{149}Sm-^{150}Nd solution and subsequently dissolved. Conventional chromatography ion exchange techniques were followed to determine the concentration of Sm and Nd, with Teflon columns and LN-Spen resin. Based on repeated analyses of international standard BHVO-1, uncertainties for Sm/Nd and $^{143}Nd/^{144}Nd$ were better than 0.1% (2 σ) and 0.0015 (1σ), respectively. The obtained $^{143}Nd/^{144}Nd$ values were normalized to $^{146}Nd/^{144}Nd$=0.7219 and the applied decay constant was of (σ) $6{,}54\times10^{-12}$. Model ages (T_{DM}) were calculated using the method of DePaolo (1981). For more information on the Sm-Nd methodology applied at the Geochronology Laboratory of the University of Brasília the reader is referred to Gioia and Pimentel (2000).

4.4. Results

4.4.1 Petrography and field aspects

Migmatitic orthogneisses are the most abundant lithotype in the Patos Shear Zone System (PSZS) and the focus of this contribution (Fig. 3). They occur tectonically intercalated with subordinate mylonitic orthogneisses, with leucosomes characterized by K-feldspar porphyroclasts (Fig. 3D), garnet-biotite

paragneisses, metric marble and calc-silicate rock lenses and banded iron formations. The dominant migmatitic orthogneisses exhibit a complex framework (Fig. 4), with metaxite (Fig. 4A, C, F) and stromatic migmites (Figs. 3 E, F and 4F, G).

The stromatic metatexites (analyzed samples AE02, J10, J11, J19, AC102B and AE24C; Fig. 3) locally present peritectic hornblende (Fig 4F) and boudinaged layers with leucosome injected perpendicular to the gneissic banding at low-pressure zones (Fig. 4G). At the terminal stages of the metatexite-diatexite transition, leucosomes become interconnected and form relatively large pegmatite pockets (Fig. 4D). The melanosome of metatexites varies in composition from biotite-bearing tonalitic (Fig. 5F) to amphibolitic, whereas leucosomes are mostly granitic in composition, locally with peritectic hornblende (Fig. 5D), and with accessory biotite, titanite, allanite, epidote, zircon, apatite, ilmenite and muscovite.

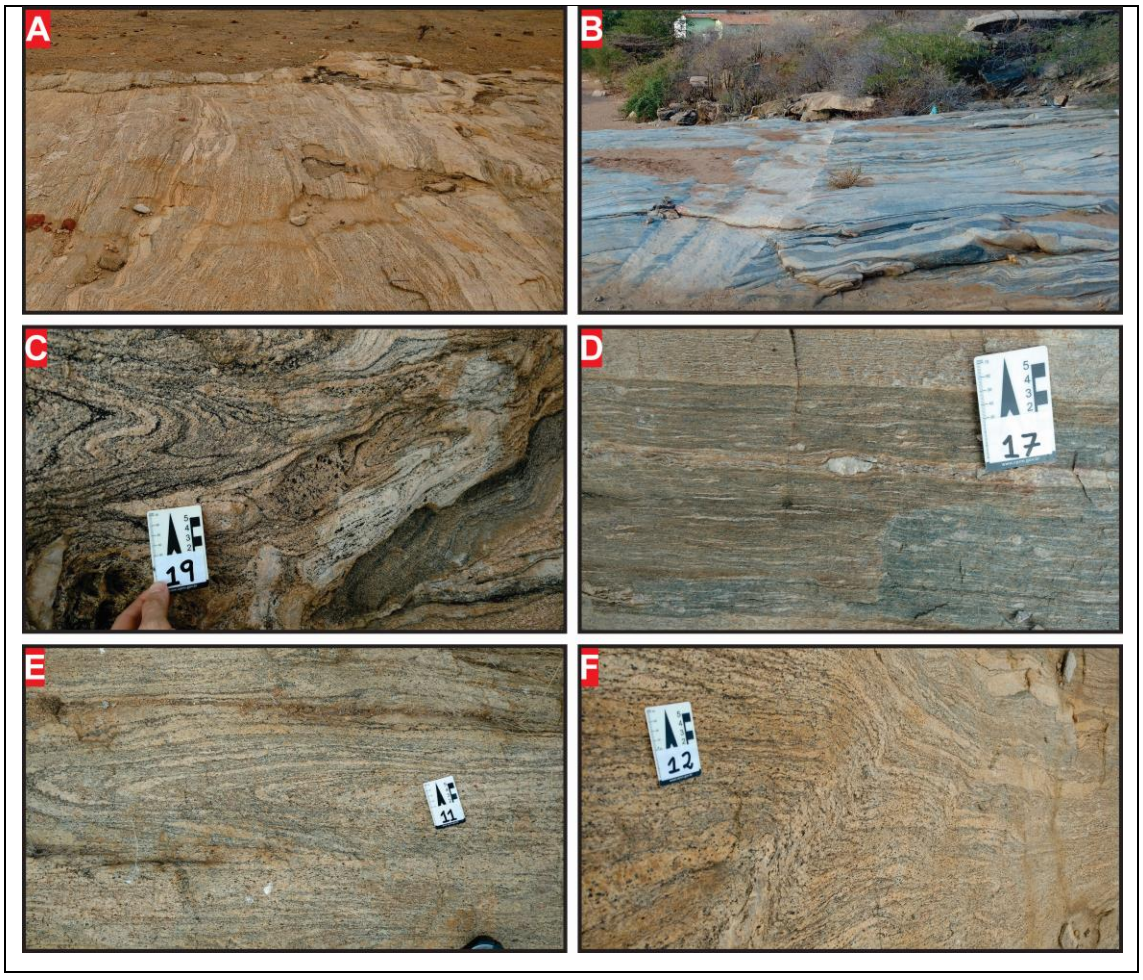

Figure 3) Field aspects of migmatites from the Patos Shear Zone System (PSZS). A) stromatic migmites; B) alkaline dick cutting the main foliation; E) Diatexite D) mylonitic orthogneisses, with leucosomes characterized by K-feldspar porphyroclasts; E) folded stromatic migmites; F) Hornblende rich stromatic migmites

Diatexites (analyzed sample J39) commonly present residual amphibolite rafts (Fig. 5B), *schlieren* or melanosome bands rich in hornblende and biotite, whereas locally tonalitic gneiss enclaves are present (Fig. 4C). The melanosome of diatexites is rich in hornblende, biotite and plagioclase, and little-to-absent K-feldspar and quartz, with accessory zircon, apatite, allanite, epidote and titanite. Leucosomes are mostly granitic in composition and present accessory hornblende (locally peritectic), titanite, ilmenite, apatite, allanite, epidote and zircon. K-feldspar can occur as thin, small lenses between grain boundaries (Fig. 5C). Titanite may occur as reaction rims mantling ilmenite crystals (Fig. 5C) and epidote coronae surround allanite crystals (Fig. 5E).

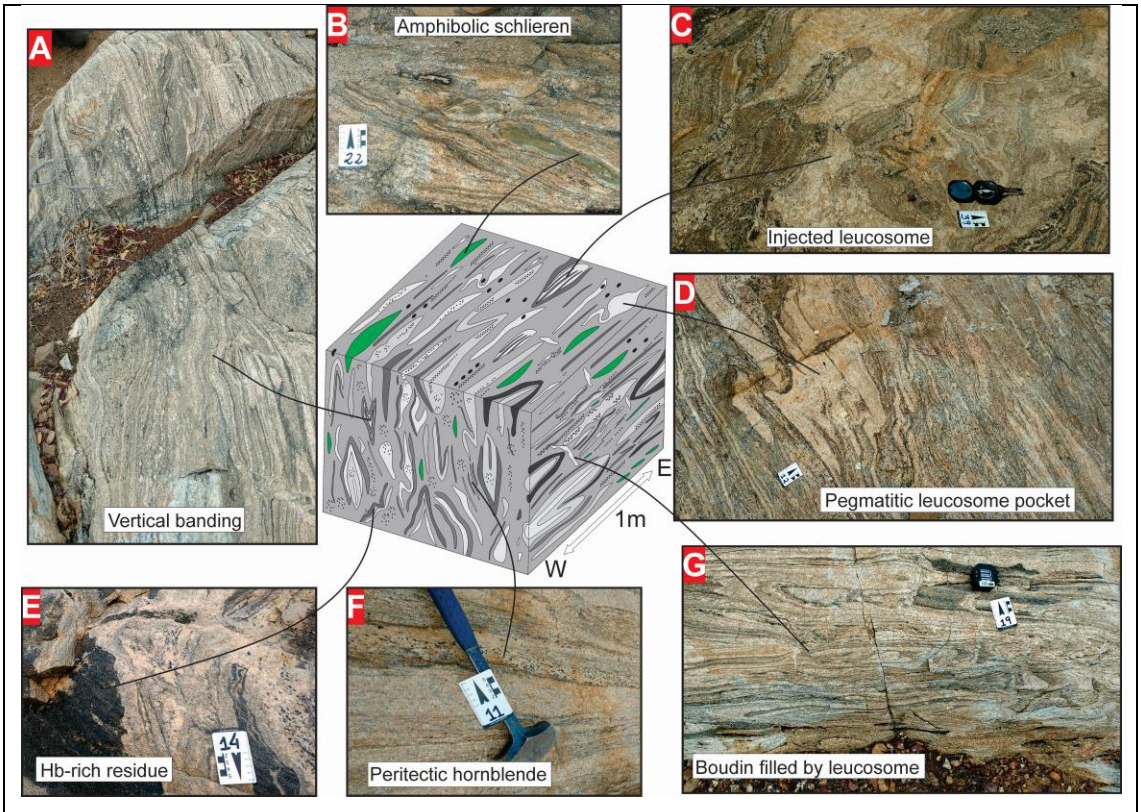

Figure 4) Mesoscopic aspects of migmatites from the PSZS. A) Metatexite with vertical banding. B) Amphibolitic schlieren in metatexite-diatexite transition. C) Injected pegmatitic leucosome in diatexite. D) Pegmatitic leucosome pockets formed by melt migration. E) Hornblende-rich melanosome (residue) in diatexite. F) Peritectic hornblende in leucosome of metatexite. G) Boudins filled with leucosome.

4.4.2 Isotopic analyses: U-Pb, Lu-Hf and Sm-Nd

Analyses of nuclei and rims of zircon grains were performed in twelve samples, eleven of migmatitic orthogneisses (AE02, J10B, J11B, J39B e AE24C, J19A, J10A, J11A, J29, J39A, AC102B) and one of a calc-silicate rock (J49) associated with a marble lense.

Backscatter scanning electron microscope (SEM) images were obtained at the Geochronology Laboratory of the University of Brasília and were used to locate the spots of LA-ICP-MS analyses and aid geochronological interpretations. Complete U-Pb, Lu-Hf and Sm-Nd tables can be found in Supplementary Material 1.

4.4.2.1 Metatexite J19A (melanosome)

Zircon crystals of metatexite J19A are large (200-300 µm), mostly prismatic. Two distinct groups of zircon grains were separated based on SEM backscatter images. The first group is characterized by prismatic grains with oscillatory zoning in SEM images, some with irregular corroded boundaries, that yielded a Discordia age of 2477 ± 15 Ma (MSWD = 0.15; n = 6), interpreted to represent an inherited population. The second group is composed of prismatic to rounded grains, with oscillatory-zoned or homogenous internal structures (Corfu, 2003; Fig. 6A), that were used to calculate a Discordia age of 2193 ± 8 Ma (MSWD = 0.97; n = 21; Fig. 6A), interpreted to represent the crystallization age of the protolith. Whole-rock Sm-Nd analysis yielded an $\varepsilon Nd_{(2193\ Ma)}$ of 2.19 and a T_{DM} of 2.45 Ga (Fig. 8B).

4.4.2.2 Metatexite AE02 (leucosome)

Zircon crystals of metatexite AE02 have between 150 and 300 µm, and yielded oscillatory zoned grains in SEM images (Fig. 6B) with a calculated Discordia age of 2259 ± 22 Ma (MSWD = 0.81; n = 22; Fig. 6B). One zircon grain was analyzed for Lu-Hf and its $\varepsilon Hf_{(t)}$ is of -1.02 (Fig. 8A) with a calculated T_{DM} of

2.65 Ga. The whole-rock Sm-Nd analysis of AE02 yielded an $\varepsilon Nd_{(t)}$ of -1.02 (Fig. 8B) and a T_{DM} of 2.53 Ga.

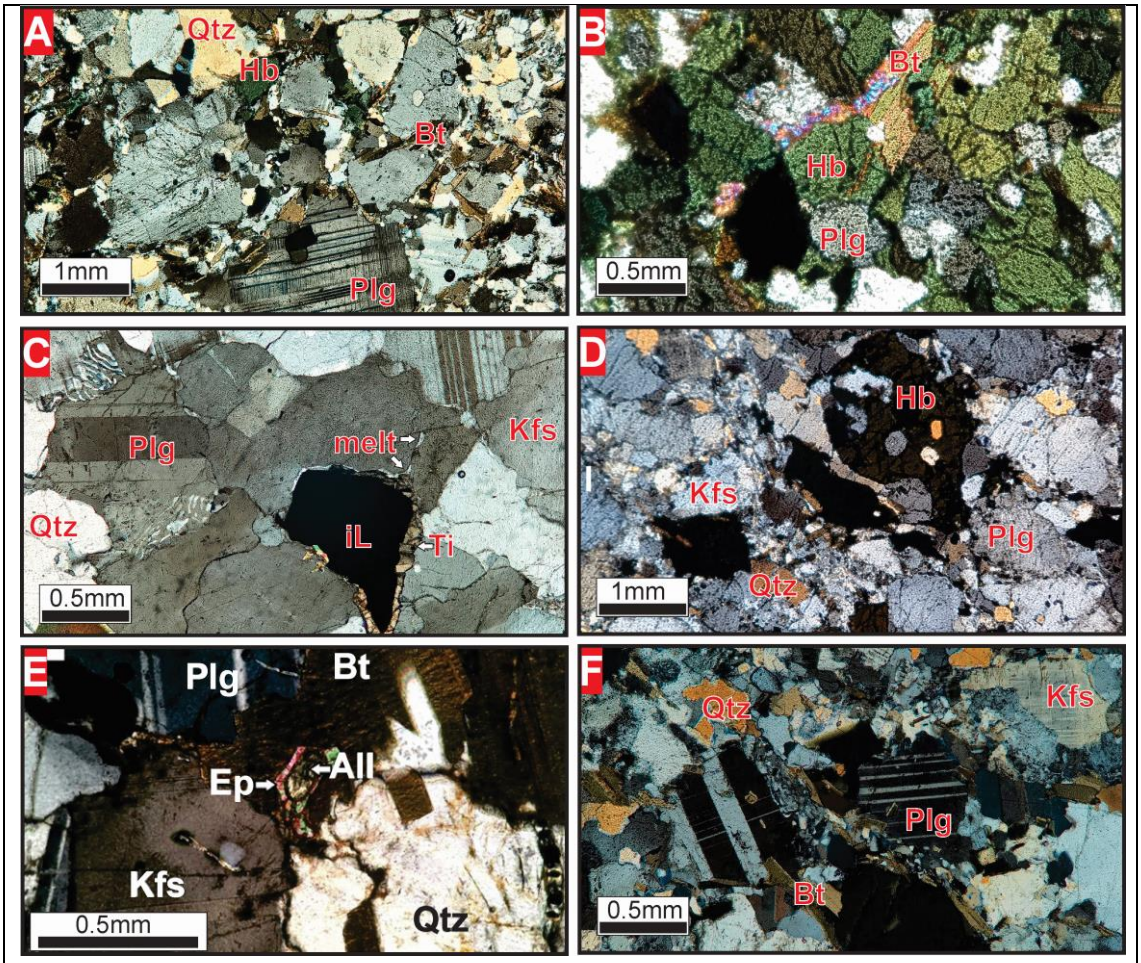

Figure 5) Microscopic aspects of migmatites from the PSZS. A) Tonalitic residue of sample J19A. B) Amphibolitic residue of sample J10A. C) Titanite coronae surrounding ilmenite; plagioclase crystals with subrounded corners and thin melt pockets made up of plagioclase and K-feldspar (J39B). D) Peritectic hornblende from leucosome of sample J11B. E) Epidote corona around allanite in a granitic leucosome. F) Granitic leucosome with myrmekitic K-feldspar crystals. Abbreviations: All = allanite; Bt = biotite; Ep = epidote; Hb = hornblende; Kfs = K-feldspar; Plg = plagioclase; Qtz = quartz.

4.4.2.3 Metatexite J10B (leucosome)

Zircon crystals of metatexite J10B can be divided into two populations based on size and morphology in SEM images (Fig. 6C). One population is composed of large grains with oscillatory-zoned cores and yielded a Discordia age of 2231 ± 25 Ma (MSWD = 2.0; n = 11; Fig. 6C), interpreted to represent the crystallization age of the protolith. One zircon crystal belonging to this population

was analyzed for Lu-Hf and its $\varepsilon Hf_{(t)}$ is of 0.52 and its calculated T_{DM} is of 2.64 Ga (Fig. 8A). The zircon population is composed of smaller rounded crystals, with homogenous internal structure in SEM images (Fig. 6C). These grains were used to calculate a Concordia age of 574 ± 3 Ma (MSWD = 0.13; n = 2) and based on their morphology and low Th/U (Rubatto, 2002) were interpreted to represent a metamorphic event. These younger crystals were analyzed for Lu-Hf and yielded $\varepsilon Hf_{(t)}$ values of -33.89 and -30.15 and T_{DM} of 2.29 and 2.45 Ga (Fig. 8A).

4.4.2.4 Metatexite J10A (melanosome)

Similar to J10B, two popuations of zircon crystals were identified for J10A (Fig. 6D). The larger, prismatic crystals yielded a Discordia age of 2197 ± 7 Ma (MSWD = 1.4; n = 22; Fig. 6D), interpreted to represent the crystallization age of protolith. Two crystals from this Paleoproterozoic population were analyzed for Lu-Hf and produced $\varepsilon Hf_{(t)}$ values of 1.75 and -7.34, as well as T_{DM} ages of 2.45 and 2.81 Ga (Fig. 8A). The other zircon grain population is composed of smaller sub-rounded grains (soccer ball), and one of these grains yielded a $^{207}Pb/^{206}Pb$ age of 572±16 Ma, as well as an $\varepsilon Hf_{(t)}$ of -41.27 and a T_{DM} of 2.7 Ga (Fig. 8A). Based on the zircon morphology and low Th/U, this was interpreted to represent the age of metamorphism.

4.4.2.5 Metatexite J11B (leucosome)

Zircon crystals of metatexite J11B are prismatic and dark to homogenous in backscatter SEM images, some with faint oscillatory zoning (Fig. 6E). Analyses on the nuclei of grains produced a Discordia age of 2262 ± 8 Ma (MSWD = 0.82; n = 28; Fig. 6E). Whole-rock Sm-Nd analysis of J11B produced an $\varepsilon Nd_{(t)}$ of -9.36 (Fig. 8B) and a T_{DM} of 3.43 Ga.

4.4.2.6 Metatexite J11A (melanosome)

Zircon crystals of metatexite J11A are prismatic and characterized by oscillatory and complex zoning in backscatter SEM images (Fig. 6F). Analyzed grains produced a Discordia age of 2246 ± 9 Ma (MSWD = 0.56; n = 32; Fig. 6F). Whole-rock Sm-Nd analysis yielded an $\varepsilon Nd_{(t)}$ of 0.04 and a T_{DM} of 2.37 Ga (Fig. 8B).

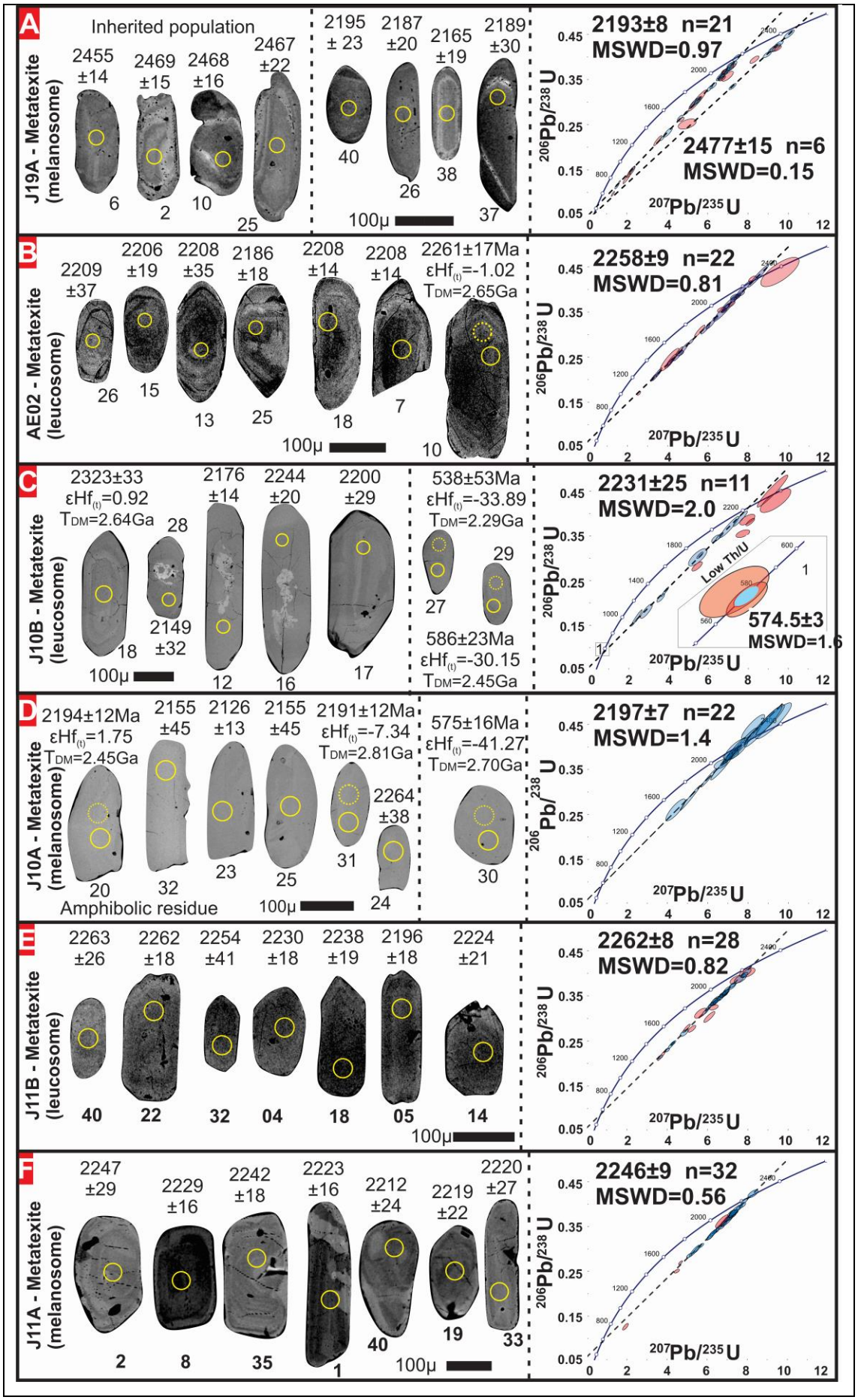
A
J19A - Metatexite (melanosome)
Inherited population
2455 ±14
2469 ±15
2468 ±16
2467 ±22
2195 ± 23
2187 ±20
2165 ±19
2189 ±30
6
2
10
25
40
26
38
37
100µ
2193±8 n=21
MSWD=0.97
2477±15 n=6
MSWD=0.15
B
AE02 - Metatexite (leucosome)
2209 ±37
2206 ±19
2208 ±35
2186 ±18
2208 ±14
2208 ±14
2261±17Ma
εHf(t)=-1.02
TDM=2.65Ga
26
15
13
25
18
7
10
100µ
2258±9 n=22
MSWD=0.81
C
J10B - Metatexite (leucosome)
2323±33
εHf(t)=0.92
TDM=2.64Ga
28
2149 ±32
18
2176 ±14
2244 ±20
2200 ±29
12
16
17
538±53Ma
εHf(t)=-33.89
TDM=2.29Ga
29
27
586±23Ma
εHf(t)=-30.15
TDM=2.45Ga
100µ
2231±25 n=11
MSWD=2.0
Low Th/U
574.5±3
MSWD=1.6
D
J10A - Metatexite (melanosome)
2194±12Ma
εHf(t)=1.75
TDM=2.45Ga
2155 ±45
2126 ±13
2155 ±45
2191±12Ma
εHf(t)=-7.34
TDM=2.81Ga
2264 ±38
20
32
23
25
31
24
575±16Ma
εHf(t)=-41.27
TDM=2.70Ga
30
Amphibolic residue
100µ
2197±7 n=22
MSWD=1.4
E
J11B - Metatexite (leucosome)
2263 ±26
2262 ±18
2254 ±41
2230 ±18
2238 ±19
2196 ±18
2224 ±21
40
22
32
04
18
05
14
100µ
2262±8 n=28
MSWD=0.82
F
J11A - Metatexite (melanosome)
2247 ±29
2229 ±16
2242 ±18
2223 ±16
2212 ±24
2219 ±22
2220 ±27
2
8
35
1
40
19
33
100µ
2246±9 n=32
MSWD=0.56
206Pb/238U
207Pb/235U

Figure 6) SEM backscatter zircon images and Wetherill plots of analyzed samples. Ages are in millions of years (Ma). Errors are 2σ.

4.4.2.7 Diatexite J39B (leucosome)

Zircon grains of diatexite J39A are prismatic, large (400 to 100 µm) and show oscillatory zoning in backscatter SEM images (Fig. 7A). Analyzed nuclei yielded a Discordia age of 2200 ± 8 Ma (MSWD = 0,94; n = 30; Fig. 7A), interpreted to represent the crystallization age of the protolith, and two crystals were analyzed for Lu-Hf, which produced $\varepsilon Hf_{(t)}$ of -2.36 and -5.54 and model ages (T_{DM}) of 2.59 and 2.67 Ga (Fig. 8A). Whole-rock Sm-Nd analyses produced an $\varepsilon Nd_{(t)}$ of -3.26 and a T_{DM} of 2.55 Ga (Fig. 8B).

4.4.2.8 Diatexite J39A (melanosome)

Zircon grains of the melanosome of diatexite J39A, of tonalitic composition, are prismatic with oscillatory-zoned cores in SEM images and a subordinate population of smaller grains with homogenous internal structure in backscatter images (Fig. 7B). The first population produced a Discordia age of 2217 ± 11 Ma (MSWD = 1,7; n = 23), interpreted to represent the crystallization age of the protolith, and one grain from the latter population was analyzed and yielded a $^{207}Pb/^{206}Pb$ age of 573 ± 18Ma (Fig. 7B), interpreted to be the result of metamorphic overprint. Whole-rock Sm-Nd analyses produced an $\varepsilon Nd_{(t)}$ of -3.12 (Fig. 8B) and a T_{DM} of 2.59 Ga.

4.4.2.9 Metatexite AC102B (melanosome)

Zircon crystals from this amphibolitic residue (melanosome) are characterized by oscillatory zoning in SEM images (Fig. 7C). Analyses on the nuclei of the oscillatory-zoned grains yielded a Discordia age of 2211 ± 27 Ma (MSWD = 1.9; n = 27; Fig. 7C), interpreted to represent the crystallization age of the protolith. Two grains were anlyzed for Lu-Hf and produced $\varepsilon Hf_{(t)}$ of -5.22 and -5.17 (Fig. 8A) and T_{DM} of 2.66 and 2.69 Ga. Conversely, whole-rock Sm-Nd analysis yielded an $\varepsilon Nd_{(t)}$ of -14.65 and a model age (T_{DM}) of 3.99 Ga (Fig. 8B).

4.4.2.10 Metatexite AE24C (leucosome)

Zircon crystals from metatexite AE24C have oscillatory-zoned grains (500-300 µm) in SEM backscatter images (Fig. 7D). Analyses on grain cores yielded a Discordia age of 2170 ± 8 Ma (MSWD = 1.9; n = 24; Fig. 7D), interpreted to represent the crystallization age of the protolith. Three zircon grains were analyzed for Lu-Hf and produced $\varepsilon Hf_{(t)}$ of -1.61, 0.05 and 3.13, as well as T_{DM} ages of 2.58, 2.52 and 2.38 Ga, respectively (Fig. 8A).

4.4.2.11 Calc-silicate paragneiss J49QL

Zircon grains from calc-silicate paragneiss J49QL (marl protolith), associated in the field with marbles, are characterized by oscillatory zoned cores surrounded by bright homogenous rims in SEM backscatter images (Fig. 7E). Analyses from cores and rims yielded indistinguishable results that form a single population and were used together to calculate a Discordia age of 2246 ± 25 Ma (MSWD = 1.7; n = 16; Fig. 7E), considered as the maximum depositional age for this metasedimentary rock. Analyses on two crystals, with homogenous internal structures in SEM images, were used to calculate a Concordia age of 574 ± 2 (MSWD = 0.24), interpreted to represent the age of metamorphism. One of these younger grains was analyzed for Lu-Hf and generated an $\varepsilon Hf_{(t)}$ of -43.1 and a T_{DM} of 2.81 Ga (Fig. 8A).

4.4.2.12 Mylonitic orthogneiss J27QL

In the field, mylonitic orthogneiss J27QL is in tectonic contact with marbles and calc-silicate rocks. In backscatter SEM imagens, zircon grains from J27QL exhibit varying sizes and morphologies, as well as no distinguishable internal structures (homogenous; Fig. 7F). Zircon analyses were used to calculate a Discordia age of 2071 ± 15 (MSWD = 2.4; n = 24; Fig. 7F), interpreted to represent the crystallization age of the protolith.

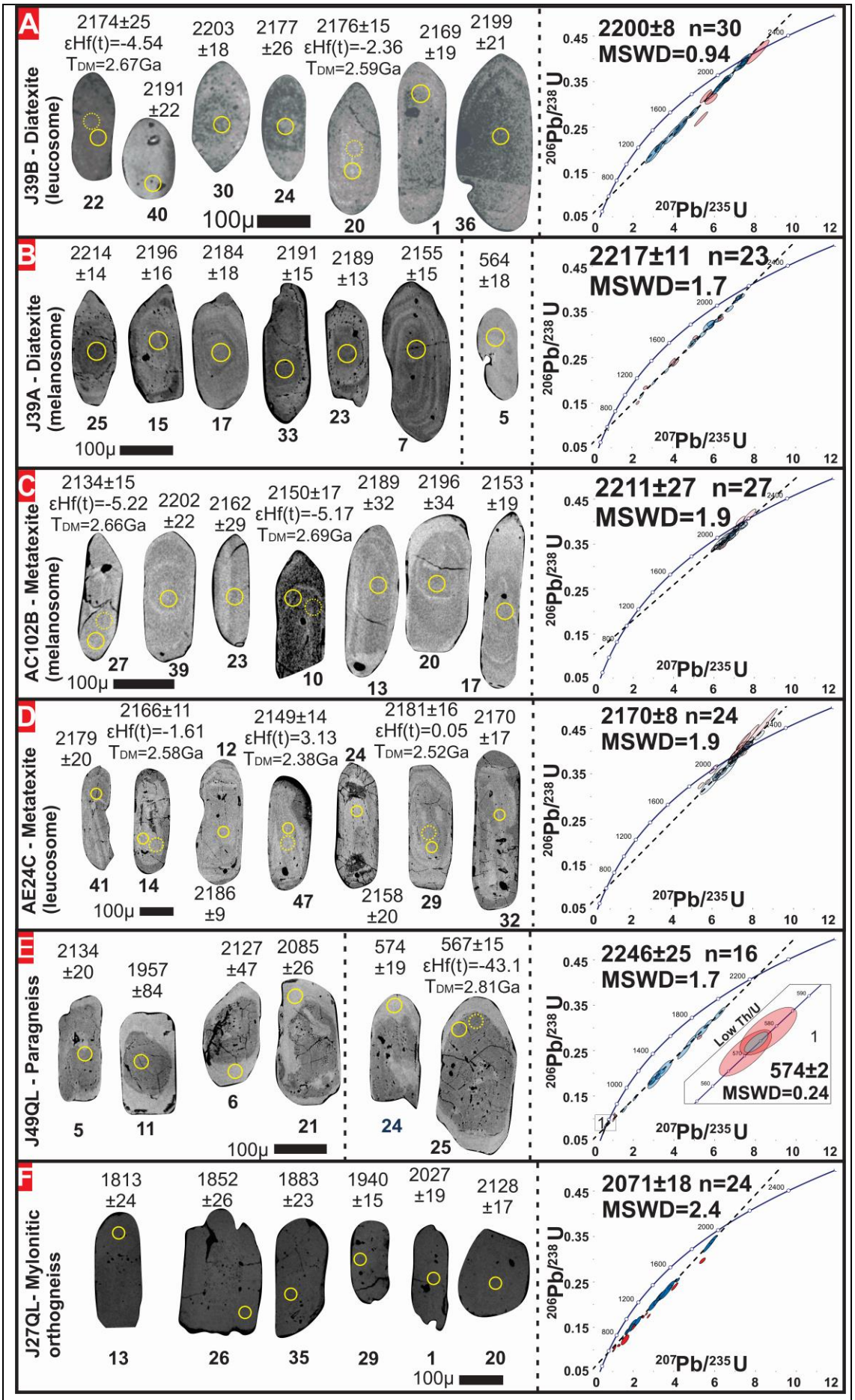
A
J39B - Diatexite (leucosome)
2174±25
εHf(t)=-4.54
TDM=2.67Ga
2191 ±22
2203 ±18
2177 ±26
2176±15
εHf(t)=-2.36
TDM=2.59Ga
2169 ±19
2199 ±21
22
40
30
24
20
1
36
100µ
2200±8 n=30
MSWD=0.94
B
J39A - Diatexite (melanosome)
2214 ±14
2196 ±16
2184 ±18
2191 ±15
2189 ±13
2155 ±15
564 ±18
25
15
17
33
23
7
5
100µ
2217±11 n=23
MSWD=1.7
C
AC102B - Metatexite (melanosome)
2134±15
εHf(t)=-5.22
TDM=2.66Ga
2202 ±22
2162 ±29
2150±17
εHf(t)=-5.17
TDM=2.69Ga
2189 ±32
2196 ±34
2153 ±19
27
39
23
10
13
20
17
100µ
2211±27 n=27
MSWD=1.9
D
AE24C - Metatexite (leucosome)
2179 ±20
2166±11
εHf(t)=-1.61
TDM=2.58Ga
2149±14
εHf(t)=3.13
TDM=2.38Ga
2181±16
εHf(t)=0.05
TDM=2.52Ga
2170 ±17
41
14
12
2186 ±9
47
24
2158 ±20
29
32
100µ
2170±8 n=24
MSWD=1.9
E
J49QL - Paragneiss
2134 ±20
1957 ±84
2127 ±47
2085 ±26
574 ±19
567±15
εHf(t)=-43.1
TDM=2.81Ga
5
11
6
21
24
25
100µ
2246±25 n=16
MSWD=1.7
Low Th/U
574±2
MSWD=0.24
F
J27QL- Mylonitic orthogneiss
1813 ±24
1852 ±26
1883 ±23
1940 ±15
2027 ±19
2128 ±17
13
26
35
29
1
20
100µ
2071±18 n=24
MSWD=2.4
206Pb/238U
207Pb/235U

Figure 7) SEM backscatter zircon images and Wetherill plots of analyzed samples. Ages are in millions of years (Ma). Errors are 2σ.

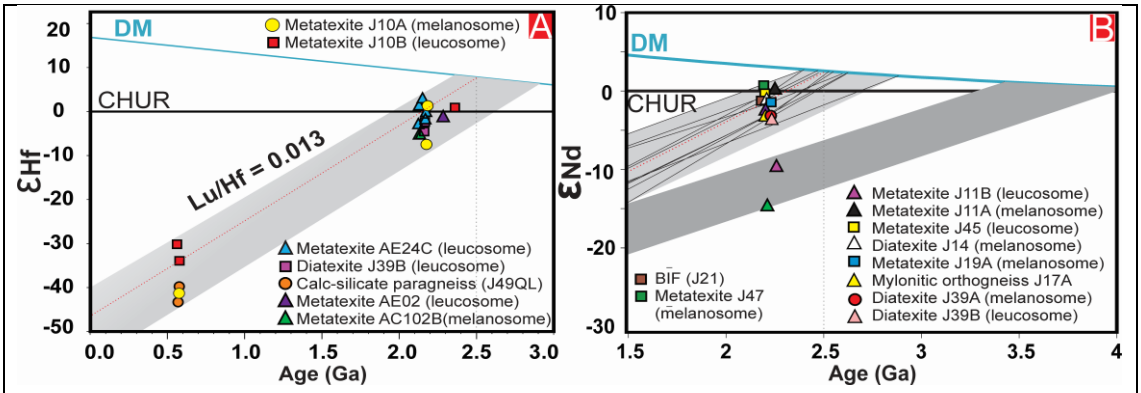

Figure 8) A) ƐHf (t) versus age and B) ƐNd (t) versus age.

4.5. Discussion

4.5.1 A Rhyacian (2.26-2.07 Ga) continental magmatic arc in the Neoproterozoic Patos Shear Zone System (PSZS)

The Borborema Province, including the Patos Shear Zone System (PSZS), is characterized by basement rocks composed mainly of polymetamorphic migmatitc orthogneisses of Archean (~3.5-2.5 Ga) to Paleoproterozoic age (2.3-2.0 Ga), that were deformed, metamorphosed and underwent partial melting associated with granitoid intrusions during successive regional tectono-thermal events (Souza et. al., 2007, 2023; Hollanda et al., 2011; Dantas et. al., 2004, 2013, Ferreira et al. 2021; Neves, 2021).

Locally in the studied area, Archean rocks were emplaced between 3.5 and 2.5 Ga (Archanjo et al., 2021; Fachetti et al., 2024) and are intruded by migmatitic orthogneisses of felsic protolith, mostly of Rhyacian age (2.3-2.05 Ga). Paleoproterozoic migmatitic orthogneisses analyzed here yielded U-Pb crystallization ages between 2.26 and 2.07 Ga, and most samples produced Archean Nd-Hf model ages (T_{DM}) and moderately to highly negative ƐHf and ƐNd values (Figs. 8 and 9B), thus providing evidence for pervasive reworking of preexisting Archean rocks between 2.26 and 2.07 Ga. In support of this interpretation, inherited Archean grains have been reported from 2.1 Ga old rocks

in the PSZS, as well as soccer-ball zircon grains in Archean samples that evidence high-grade migmatization during the Paleoproterozoic (Fachetti et al., 2024), as was similarly reported elsewhere in the Borborema province (e.g., Hollanda et al., 2011; Costa et al., 2018; Ferreira et al., 2021).

On the other hand, some Paleoproterozoic (2.26-2.07 Ga) rocks yielded Hf-Nd model ages (T_{DM}) below 2.5 Ga, the age of the youngest Archean rocks in the PSZS (Archanjo et al., 2021), and close to their crystallization age (e.g., 2.29 Ga), associated with moderately positive ƐHf and ƐNd values (Figs. 8 and 9B), that point to juvenile input during the 2.26-2.07 Ga magmatism, in addition to concomitant reworking discussed in the paragraph above (this study; see also Fachetti et al., 2024).

In summary, Paleoproterozoic rocks of the PSZS are dominated by migmatitic orthogneisses of felsic protoliths that are the result of reworking of older Archean rocks concomitant with juvenile magmatic inputs. These characteristics are typical of Andean-type continental magmatic arc systems. The predominance of Hf-Nd unradiogenic signatures in continental arcs (Xia and Li, 2019), similar to those reported here, may be either due to contamination in the mantle source following subduction erosion (e.g., Stern, 2011) or in the thick continental crust during emplacement (Hildreth and Moorbath, 1988). The latter is preferred for the Paleoproterozoic orthogneisses of the PSZS, given that inherited Archean grains have been reported for these rocks (Fachetti et al., 2024). Therefore, we propose that the migmatitic orthogneisses studied here represent the root of a Paleoproterozoic (2.26-2.0.7 Ga) magmatic arc system, established on Archean continental crust (3.5-2.5 Ga), that may have evolved from an early Paleoproterozoic (2.5-2.4 Ga) arc stage evidenced in this study by inherited grains (Fig. 6A), likely related to the early stages of magmatic arc formation, similar to what has been proposed for the Southern São Francisco Craton (Barbosa et al., 2019).

In addition, in tectonic contact with the Paleoproterozoic orthogneisses there were metasedimentary rocks, namely biotite schists, banded iron formations (BIFs), calc-silicate paragneisses and marbles. One sample of a calc-silicate paragneiss was analyzed for U-Pb and yielded mostly Rhyacian ages, with a dominant peak at 2.1 Ga (Fig. 7E), whereas one BIF was analyzed for Sm-Nd and yielded a Paleoproterozoic model age (Fig. 8B). At first, this might lead

to the interpretation that the mapped metasedimentary unit is part of a Paleoproterozoic sequence, established in a shallow sea and metamorphosed during the Brasiliano Orogeny. However, given the high variability of zircon age patterns in metasedimentary successions (Cawood et al., 2012; Marimon et al., 2023), especially in Neoproterozoic metamorphosed passive margin sequences that surround the São Francisco Craton, where many samples yield dominant Paleoproterozoic age peaks with absent younger grains (Marimon et al., 2020a; 2021), we cannot therefore discard that the studied metasedimentary is of Neoproterozoic age. However, BIFs are less common in younger sequences and there have been reports of marbles and calc-silicate rocks of Paleoproterozoic age affected by a late Paleoproterozoic (~2.0 Ga) orogenic event elsewhere in the Borborema Province (Santos et al., 2013). Therefore, we prefer the preliminary interpretation that the metasedimentary sequence studied here is of Paleoproterozoic age, but more data are needed to accurately unravel the age and tectonic setting of the succession studied here. Long-lived continental magmatic arcs tend to be cyclic, with distinct extensional and compressional phases, and sedimentary basins are established in continental arcs usually during an extensional phase (Ducea et al., 2015)

4.5.2 A long Rhyacian continental magmatic arc surrounding an Archean nucleus: the Greater São Francisco Orogen

Felsic-to-intermediate migmatitic orthogneisses and igneous/metaigneous rocks, with similar age (2.4-2.0 Ga), composition and isotopic signatures to those studied here have been reported throughout the São Francisco Craton and its borders reworked during the Neoproterozoic (Brasiliano Orogeny), including basement inliers in the Araçuaí, Ribeira and Brasília orogens (black in Fig. 1; Ávila et al., 2010; Heilbron et al., 2010; Seixas et al., 2013; Teixeira et al., 2015; Cioffi et al., 2016; Cruz et al., 2016; Barbosa et al., 2017; Nascimento et al., 2017; Degler et al., 2018; Pinheiro et al., 2019; Marimon et al., 2020b; Bruno et al., 2020, 2021; Neves, 2021; Bersan et al., 2022). It is important to point out that the São Francisco Craton is, by definition, a crustal segment, with Archean to Paleoproterozoic basement, that was only affected by low-grade (greenschist

facies or lower) regional metamorphism during the Neoproterozoic (660-590 Ma) Brasiliano Orogeny (green dashed line in Fig. 1). Still, there are basement rocks from Brasiliano Orogens (e.g., Ribeira, Araçuaí, Brasília and Borborema) that are thought to have been part of the São Francisco Craton before the Neoproterozoic, representing reworked cratonic borders and are hereafter called “basement inliers”. We employ the term São Francisco Paleocontinent to refer to the São Francisco Craton plus surrounding basement inliers in Neoproterozoic orogens, in other words the configuration of the São Francisco prior to the Neoproterozoic orogeny, which is widespread in the South American Platform.

The Paleoproterozoic (2.4-1.9 Ga) crust of the São Francisco Paleocontinent is interpreted to have been formed in subduction to continental collision and post-collision environments. The main lines of evidence that support a subduction scenario from 2.4 to 2.1 Ga around the Archean core of the São Francisco Paleocontinent, in other words a magmatic arc, are (Fig. 1; Giustina et al., 2009; Ávila et al., 2010; Heilbron et al., 2010; Teixeira et al., 2015; Moreira et al., 2018; Bruno et al., 2021; Ferreira et al., 2021; Araújo et al., 2021; Neves et al., 2023; Fachetti et al., 2024): 1) highly positive (close to DM) to negative Hf-Nd isotopic signatures (e.g., Fig. 9), which suggest juvenile input together with crustal assimilation (reworking) of older Archean crust (country rock); 2) a large magmatic compositional diversity during the period, mostly composed of TTGs, sanukitoids, biotite- two-mica granites and diorites, all common products of subduction environments; 3) trace element geochemical signatures typical of arc magmatism, such as high Th/Nb and Nb-Ta-Ti anomalies, including in less differentiated diorites. In addition, Hf cyclic variations from negative to positive (dashed white line in Fig. 9A) through time may indicate varying contributions from the upper continental crust of Archean age along the arc’s history, as is typical for younger continental magmatic arcs (Ducea et al., 2015).

Subduction systems, as the consumption of intervening oceanic lithosphere progresses, tend to develop into continental collisional belts. In the Paleoproterozoic basement rocks of the São Francisco Paleocontinent there is widespread evidence for continental collision, that include high-grade metamorphism, shear zone development, granulitization and migmatization between ~2.1 to 2.0 Ga, as evidenced by U-Pb dating of soccer-ball zircon grains (collected from high-grade migmatites and granulites, constrained by

geothermobarometry), zircon overgrowths and monazite from medium- to high-grade metamorphic rocks (e.g., Leite et al., 2009; Cordeiro and Oliveira, 2014; Barbosa et al., 2017; Aguilar et al., 2017; Carvalho et al., 2017; Cutts et al., 2018; Bruno et al., 2021; Fachetti et al., 2024). High-grade metamorphism is accompanied by syn-collisional magmatism (biotite- two-mica granites), resulting from the anatexis of the continental crust (Bruno et al., 2021). The late- to post-collisional stage (younger than 1.93 Ga) is characterized by bimodal magmatism in an extensional setting (e.g., Bersan et al., 2022). The Paleoproterozoic tectonic evolution of the São Francisco Paleocontinent is summarized in Figure 9C.

The abundance of Rhyacian magmatic rocks in the eastern segment of the São Francisco Paleocontinent (Fig. 1), combined with their similarity in age, Nd-Hf isotopic signature, petrography and geochemistry, prompted investigators to propose they belonged to a single orogenic system, called the Minas-Bahia Orogen, characterized by arc magmatism (2.4-2.1 Ga) succeeded by continental collision between 2.1 and 2.0 Ga (Fig. 1; e.g., Bruno et al., 2021; Araújo et al., 2021; Grochowski et al., 2021; Almeida et al., 2022; Mauri et al., 2023). However, the rocks that make up the Minas-Bahia Orogen are also largely similar to those located to the northeast, such as the migmatites investigated here (Fig. 9; Fachetti et al., 2024) and form most of the basement rocks in the Neoproterozoic Borborema Province (Fig. 1; Souza et al., 2007; Hollanda et al., 2011; Ferreira et al., 2021; Neves, 2021), which are considered inliers related to the São Francisco Craton (Fig. 9A and B), as previously recognized (e.g., Neves, 2021; Ganade et al., 2021).

It follows that the Paleoproterozoic basement of the Borborema Province likely represents the continuation of the Paleoproterozoic (2.4-1.9 Ga) Minas-Bahia Orogen towards the northeast, as shown in Fig. 1 (black). Furthermore, Paleoproterozoic rocks from the eastern and northeastern São Francisco Paleocontinent (Minas-Bahia Orogen and Borborema Province) are also strikingly similar to rocks from its western segment, represented by basement inliers from the Brasília Orogen (Fig. 1, including southern and northern Brasília Orogen), in that they are also characterized by a spread of ℇHf and ℇNd values, from highly positive (juvenile additions) to negative (reworking of Archean crust; Fig. 9), identical crystallization and metamorphic U-Pb ages, as well as similar granitoid composition (Giustina et al., 2009; Fuck et al., 2014; Cordeiro et al.,

2014; Sousa et al., 2016; Cioffi et al., 2016; Cuadros et al., 2017; Cordeiro and Oliveira, 2017; Sabóia et al., 2020; Filgueiras et al., 2020; Oliveira et al., 2019; Pinheiro et al., 2019, 2022; Martins-Ferreira et al., 2020; Fontainha et al., 2021; Moura and Campos, 2022).

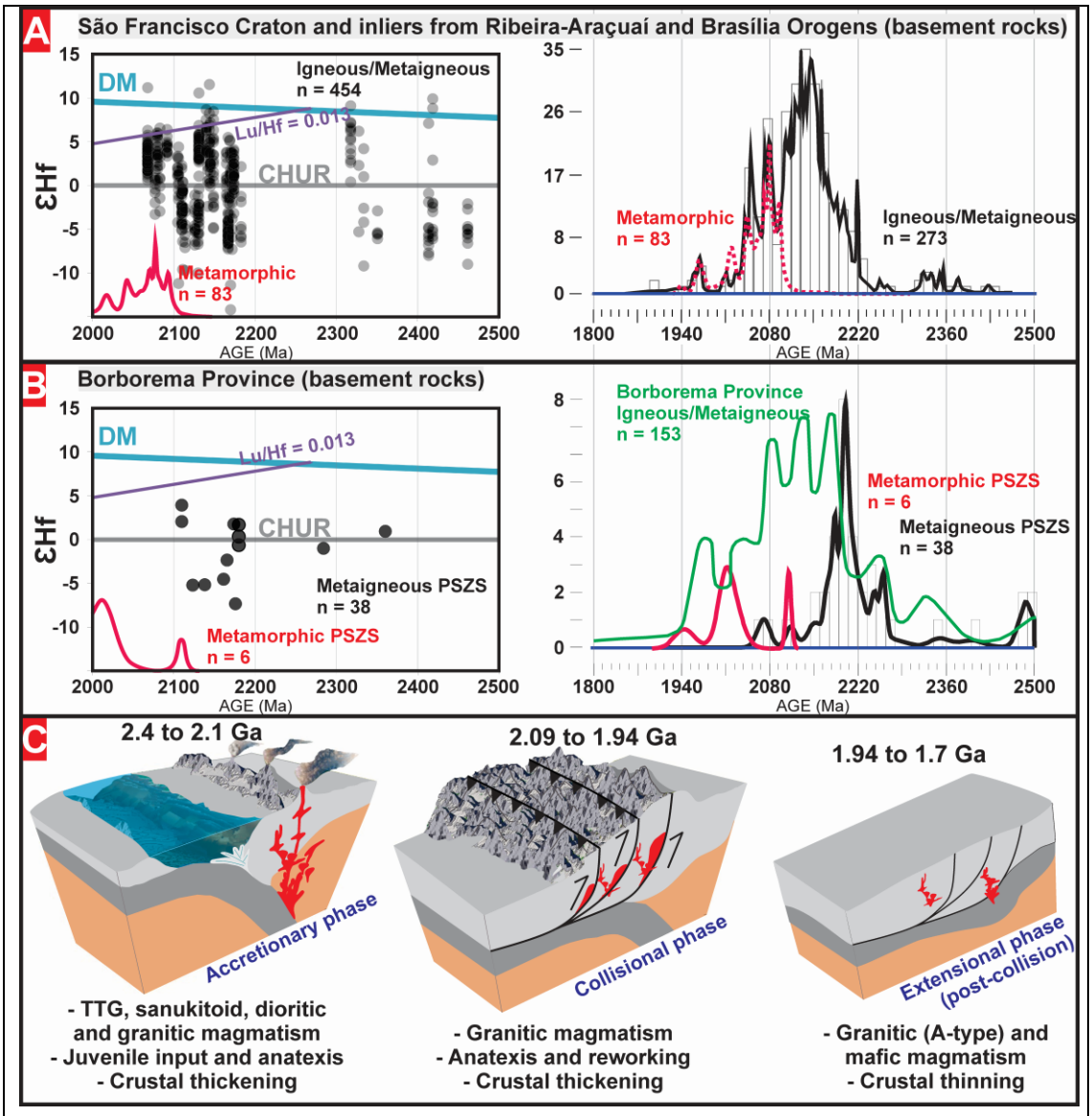

Figure 9) A) Compilation of Paleoproterozoic igneous/metaigneous basement rocks from the São Francisco Craton and inliers from the Araçuaí-Ribeira and Brasília Orogens (data compiled by Marimon et al., 2020b). B) Compilation of Paleoproterozoic igneous/metaigneous rocks from the basement of the Borborema Province (from Ganade et al., 2021), including a compilation from the Patos Shear Zone System (Hollanda et al., 2011, 2015; Archanjo et al., 2021; Fachetti et al., 2024; this study). C) A schematic figure representing the tectonic evolution of the Greater São Francisco Orogen.

Therefore, given the striking similarity between Paleoproterozoic basement rocks that surround the Archean core (e.g., Marimon et al., 2022) of

the São Francisco Paleocontinent (black in Fig. 1 and Fig. 9), we propose these rocks were part of a coeval subduction-to-collision orogenic system, dated between 2.4 and 1.9 Ga (Fig. 9), and possibly continuous at the time of formation. However, the exact geometry of this Paleoproterozoic orogenic system is hard to precisely constrain, given Neoproterozoic overprint and Phanerozoic sedimentation (Fig. 1). Following these considerations, we propose the Paleoproterozoic crust of the São Francisco Paleocontinent, that shares a similar history and tectonic setting (Fig. 9), be collectively called the Greater São Francisco Orogen (2.4 to 1.9 Ga; black in Fig. 1). Although the term Minas-Bahia Orogen is widespread in the literature, we cannot just expand the original definition and keep the terminology given the geographic constraints of the term, as Minas and Bahia are two Brazilian states, and by no means the Paleoproterozoic orogenic system here discussed is restricted to these states, hence the need for a more comprehensive nomenclature. This orogenesis is thought to represent the beginning of the Columbia supercontinent formation (Meert, 2012; Meert and Santosh, 2017).

4.5.3 Timing of partial melting events and the assembly of Gondwana

In previous studies focused on the PSZS, investigators have obtained both Paleoproterozoic (2.1-2.0 Ga) and Neoproterozoic (580-560 Ma) metamorphic/migmatization ages, based on the dating of zircon overgrowth rims and soccer ball grains, with homogenous internal structures in SEM images (Viegas et al., 2014; Archanjo et al., 2021; Fachetti et al., 2024). In this study, we obtained metamorphic zircon ages of 574 Ma (Fig. 6C, 7E), similar to those obtained in other studies for the PSZS (Viegas et al., 2014; Fachetti et al., 2024). Data from the literature (Viegas et al., 2014; Fachetti et al., 2024), combined with data from this study, underpin the notion that the PSZS is a major Neoproterozoic (Brasiliano) structure, related to the formation of West Gondwana, that reactivated structures formed during a previous high-grade tectono-metamoprhic Paleoproterozoic episode. Both events resulted in widespread crustal reworking, migmatization and granitogenesis. The protolith of sample J27 (Fig. 7L) crystallized at ~2.07 Ga, which overlaps the period of high-grade metamorphism

obtained for the Paleoproterozoic tectonic cycle, both in the PSZS (Fachetti et al., 2024) and in the wider São Francisco Craton (Marimon et al., 2020b), which evidences granitogenesis accompanied metamorphism and migmatization between 2.1-2.0 Ga.

Neoproterozoic rifting and subsequent orogenesis roughly coincided with previous Paleoproterozoic orogens (compare thick dashed red and green lines in Fig. 1). This was likely because suture zones represent weakened planes in the continental crust and therefore preferred locations for rifting and later continental collision. This is the reason many cratons (e.g., Amazonian and North American shield) have grown concentrically, along older orogenic belts, and preserved Archean nuclei.

4.6. Conclusions

After an extensive isotopic investigation of Paleoproterozoic basement migmatitc orthogneisses (metatexites and diatexites) from the Neoproterozoic Patos Shear Zone System (PSZS), Borborema Province (NE Brazil), the conclusions of this study are as follows:

- Many Paleoproterozoic migmatitic orthogneisses analyzed here, that intrude Archean crust (e.g., Fachetti et al., 2024) and have U-Pb zircon ages of 2.26-2.07 Ga, yielded Archean Nd-Hf model ages (T_{DM}) and moderately to highly negative ƐHf and ƐNd values (Figs. 8 and 9B), as well as inherited Archean zircon grains (Fachetti et al., 2024). This clearly evidences pervasive reworking of Archean basement rocks between 2.26 and 2.07 Ga. Conversely, other Paleoproterozoic (2.26-2.07 Ga) migmatitic orthogneisses produced Hf-Nd model ages (T_{DM}) below 2.5 Ga (youngest Archean rock in the region) and close to their crystallization age (e.g., 2.29 Ga). This, together with moderately positive ƐHf and ƐNd values (Figs. 8 and 9B), point to juvenile inputs during the 2.26-2.07 Ga magmatism. Juvenile addition combined with reworking of older crust is a typical feature of Andean-type continental magmatic arcs, therefore the migmatitic orthogneisses analyzed in this study likely form a Paleoproterozoic (2.26-2.0.7 Ga) magmatic arc system, established on Archean (3.5-2.5 Ga) crust.

- Felsic-to-intermediate migmatitic orthogneisses and igneous/metaigneous rocks with similar age (2.4-2.0 Ga) and Hf-Nd isotopic composition (radiogenic to unradiogenic) to those studied here have been found throughout the São Francisco Craton, by definition only affected by the Neoproterozoic (660-580 Ma) regional metamorphism (Brasiliano) at greenschist facies conditions or lower, and in adjacent basement inliers in Neoproterozoic orogens, thought to represent the reworked cratonic margin (e.g., Ávila et al., 2010; Heilbron et al., 2010; Nascimento et al., 2017). This Paleoproterozoic crust (2.4-1.9 Ga) is thought to have been formed in subduction to continental collision and post-collision settings. The main lines of evidence that support subduction from 2.4 to 2.1 Ga in the São Francisco Paleocontinent are the magmatic assemblage, mainly formed of rocks found in subduction environments, such as TTGs, sanukitoids and diorites, with subordinate biotite- two-mica granites related to crustal anatexis (e.g., Bruno et al., 2021; Araújo et al., 2021). In addition, these rocks have positive (close to DM) to negative Hf isotopic signatures (Fig. 9), which suggest juvenile input together with crustal assimilation (reworking) of older Archean crust (country rock) in a continental magmatic arc. This magmatic arc environment developed into a continental collision orogen, from ~2.1 to 2.0 Ga, as evidenced by high-grade regional metamorphism, granulitization, migmatization and crustal anatexis (e.g., Leite et al., 2009; Barbosa et al., 2017; Cutts et al., 2018; Fachetti et al., 2024), followed by post-collision (< 1.9 Ga) relaxation and bimodal magmatism (Bersan et al., 2021). We propose that the Paleoproterozoic crust of the São Francisco Craton and adjacent basement inliers, that carries a similar tectonic history, be regarded as a coeval orogenic system, that was possibly continuous at its formation, and be known as the Greater São Francisco Orogen (black in Fig. 1). This orogenic system surrounds the Archean nucleus of the São Francisco Craton (black in Fig. 1).

- In this study, we obtained metamorphic zircon ages of 574 Ma (Fig. 6C and 7E) for some orthogneisses of the Patos Shear Zone System (PSZS), Borborema Province. Considering that Fachetti et al. (2024) have obtained several metamorphic ages between 2.1 and 2.0 Ga in the same region, we suggest that the PSZS is composed of Paleoproterozoic structures, likely formed

in a continental collision environment, reactivated during the formation of West Gondwana in the Neoproterozoic.

4.7. References

Aguilar, C., Alkmim, F.F., Lana, C., Farina, F., 2017. Palaeoproterozoic assembly of the São Francisco craton, SE Brazil: New insights from U–Pb titanite and monazite dating. Precambrian Research, 289, 95-115.

Almeida, R., Elizeu, V., Bruno, H., Bersan, S.M., Araujo, L.E.A.B., Dussin, I., Valeriano, C.M., Neto, C., Heilbron, M. 2022. Rhyacian-Orosirian tectonic history of the Juiz de Fora Complex: Evidence for an Archean crustal reservoir within an island-arc system. Geoscience Frontiers, 13(5), 101292.

Araujo, L.E.A.B., Heilbron, M., Teixeira, W., Dussin, I.A., Valeriano, C.M., Bruno, H., Sato, K., Paravidini, G, Castro, M. 2021. Siderian to Rhyacian evolution of the Juiz de Fora Complex: arc fingerprints and correlations within the Minas-Bahia Orogen and the Western Central Africa Belt. Precambrian Research, 359, 106118.

Archanjo, C.J., Viegas, L.G.F., Hollanda, M.H.B.M., Souza, L.C., Liu, D. 2013. Timing of the HT/LP transpression in the Neoproterozoic Seridó Belt (Borborema Province, Brazil): constraints from UPb (SHRIMP) geochronology and implications for the connections between NE Brazil and West Africa. Gondwana Research, 23(2), 701-714.

Archanjo, C.J., Hollanda, M.H.B.M., Viegas, L.G.F. 2021. Late Ediacaran lateral-escape tectonics as recorded by the Patos shear zone (Borborema Province, NE Brazil). Brazilian Journal of Geology, 51.

Ávila, C.A., Teixeira, W., Cordani, U.G., Moura, C.A.V., Pereira, R.M. 2010. Rhyacian (2.23–2.20 Ga) juvenile accretion in the southern São Francisco craton, Brazil: Geochemical and isotopic evidence from the Serrinha magmatic suite, Mineiro belt. Journal of South American Earth Sciences, 29(2), 464-482.

Barbosa, N., Teixeira, W., Ávila, C.A., Montecinos, P.M., Bongiolo, E.M., Vasconcelos, F.F. 2019. U-Pb geochronology and coupled Hf-Nd-Sr isotopic-chemical constraints of the Cassiterita Orthogneiss (2.47–2.41-Ga) in the Mineiro belt, São Francisco craton: Geodynamic fingerprints beyond the Archean-Paleoproterozoic Transition. Precambrian Research, 326, 399-416.

Barbosa, J.S.F., Menezes Leal, A.B., Fuck, R.A., Oliveira, J.S.S., Gonçalves, P., Leite, C.M.M. 2017. Ultrahigh-temperature metamorphism of 2.0 Ga-Old sapphirine-bearing granulite from the Itabuna-Salvador-Curaçá Block, Bahia, Brazil. USP Série Científica, 17, 89-108.

Basto, C.F., Caxito, F.A., Vale, J.A.R., Silveira, D.A., Rodrigues, J.B., Alkmim, A.R., Valeriano, C.M., Santos, E.J. 2019. An Ediacaran back-arc basin preserved in the Transversal Zone of the Borborema Province: Evidence from geochemistry, geochronology and isotope systematics of the Ipueirinha Group, NE Brazil. Precambrian Research, 320, 213-231.

Bersan, S.M., Danderfer, A., Storey, C., Bruno, H., Moreira, H., Abreu, F., Lana, C., Gonçalves, L., Nahas, I. 2022. A perspective on potassic and ultrapotassic rocks: Constraints on the Paleoproterozoic late to post-collisional event in the São Francisco paleocontinent. Geoscience Frontiers, 13(5), 101179.

Blichert-Toft, J., Albarède, F., 1997. The Lu-Hf isotope geochemistry of chondrites and the evolution of the mantle-crust system. Earth Planet. Sci. Lett., 148(1-2), 243-258.

Brito Neves, B.B., Santos, T.J.S., Dantas, E.L., 2022. The São Pedro tectonostratigraphic terrane: West of the Transversal Zone-Borborema Province. Geologia USP: Serie Cientifica (Online), 22(4), 44-69.

Bruno, H., Elizeu, V., Heilbron, M., Valeriano, C.M., Strachan, R., Fowler, M., Bersan, S., Moreira, H., Dussin, I., Eirado Silva, L.G., Tupinambá, M., Almeida, J., Neto, C., Storey, C. 2020. Neoarchean and Rhyacian TTG-Sanukitoid suites in the southern São Francisco Paleocontinent, Brazil: evidence for diachronous change towards modern tectonics. Geoscience Frontiers, 11(5), 1763-1787.

Bruno, H., Heilbron, M., Valeriano, C.M., Strachan, R., Fowler, M., Bersan, S., Moreira, H., Motta, R., Almeida, J., Almeida, R., Carvalho, M., Storey, C. 2021. Evidence for a complex accretionary history preceding the amalgamation of Columbia: the Rhyacian Minas-Bahia Orogen, southern São Francisco Paleocontinent, Brazil. Gondwana Research, 92, 149-171.

Bühn, B., Pimentel, M.M., Matteini, M., Dantas, E.L., 2009. High spatial resolution analysis of Pb and U isotopes for geochronology by laser ablation multi-collector inductively coupled plasma mass spectrometry (LA-MC-ICP-MS). An. Acad. Bras. Cienc. 81, 99-114.

Carvalho, B.B., Janasi, V.A., Sawyer, E.W. 2017. Evidence for Paleoproterozoic anatexis and crustal reworking of Archean crust in the São Francisco Craton, Brazil: a dating and isotopic study of the Kinawa migmatite. Precambrian Research, 291, 98-118.

Caxito, F.A., Santos, L.C.M.L., Uhlein, A., Dantas, E.L., Alkmim, A.R., Lana, C. 2020a. New U-Pb (SHRIMP) and first Hf isotope constraints on the Tonian (1000-920 Ma) Cariris Velhos event, Borborema Province, NE Brazil. Brazilian Journal of Geology, 50.

Caxito, F.A., Santos, L.C.M.L., Ganade, C.E., Bendaoud, A., Fettous, E.H., Bouyo, M.H. 2020b. Toward an integrated model of geological evolution for NE Brazil-NW Africa: The Borborema Province and its connections to the Trans-Saharan (Benino-Nigerian and Tuareg shields) and Central African orogens. Brazilian Journal of Geology, 50.

Cawood, P.A., Hawkesworth, C.J., Dhuime, B. 2012. Detrital zircon record and tectonic setting. Geology, 40(10), 875-878.

Chauvel, C., Blichert-Toft, J., 2001. A hafnium isotope and trace element perspective on melting of the depleted mantle. Earth Planet. Sci. Lett. 190, 137–151.

Chu, N.C., Taylor, R.N., Chavagnac, V., Nesbitt, R.W., Boella, R.M., Milton, J.A., C.R., German., Bayon, G., Burton, K., 2002. Hf isotope ratio analysis

using multi-collector inductively coupled plasma mass spectrometry: an evaluation of isobaric interference corrections. J. An. Atom. Spec. 17, 1567-1574.

Cioffi, C.R., Campos Neto, M.C., Moeller, A., Rocha, B.C. 2016. Paleoproterozoic continental crust generation events at 2.15 and 2.08 Ga in the basement of the southern Brasília Orogen, SE Brazil. Precambrian Research, 275, 176-196.

Corfu, F., Hanchar, J.M., Hoskin, P.W., Kinny, P. 2003. Atlas of zircon textures. Reviews in mineralogy and geochemistry, 53(1), 469-500.

Costa, F.G., Klein, E.L., Lafon, J.M., Neto, J.M.M., Galarza, M.A., Rodrigues, J.B., Naleto, J.L.C., Lima, R.G.C. 2018. Geochemistry and U–Pb–Hf zircon data for plutonic rocks of the Troia Massif, Borborema Province, NE Brazil: Evidence for reworking of Archean and juvenile Paleoproterozoic crust during Rhyacian accretionary and collisional tectonics. Precambrian Research, 311, 167-194.

Cuadros, F.A., Botelho, N.F., Fuck, R.A., Dantas, E.L. 2017. The peraluminous Aurumina granite suite in central Brazil: An example of mantle-continental crust interaction in a Paleoproterozoic cordilleran hinterland setting?. Precambrian Research, 299, 75-100.

Cordeiro, P.F.O., Oliveira, C.G., Della Giustina, M.E.S., Dantas, E.L., Santos, R.V. 2014. The Paleoproterozoic Campinorte arc: tectonic evolution of a Central Brazil pre-Columbia orogeny. Precambrian Research, 251, 49-61.

Cordeiro, P.F.O., Oliveira, C.G. 2017. The Goiás Massif: Implications for a pre-Columbia 2.2–2.0 Ga continent-wide amalgamation cycle in central Brazil. Precambrian Research, 298, 403-420.

Cruz, S.C.P., Barbosa, J.S.F., Pinto, M.S., Peucat, J.J., Paquette, J.L., Souza, J.S., Martins, V.S., Chemale, F., Carneiro, M.A. 2016. The Siderian-Orosirian magmatism in the Gavião Paleoplate, Brazil: U–Pb geochronology, geochemistry and tectonic implications. Journal of South American Earth Sciences, 69, 43-79.

Cutts, K., Lana, C., Alkmim, F., Peres, G.G. 2018. Metamorphic imprints on units of the southern Araçuaí Belt, SE Brazil: The history of superimposed Transamazonian and Brasiliano orogenesis. Gondwana Research, 58, 211-234.

Dantas, E.L., Hackspacher, P.C., Van Schmus, W.R., Brito Neves, B.B. 1998. Archean accretion in the São José do Campestre massif, Borborema province, northeast Brazil. Revista Brasileira de Geociências, 28(2), 221-228.

Dantas, E.L., Van Schmus, W.R., Hackspacher, P.C., Fetter, A.H., Brito Neves, B.B., Cordani, U., Nutman, A.P., Williams, I.S., 2004. The 3.4–3.5 Ga São José do Campestre massif, NE Brazil: remnants of the oldest crust in South America. Precambrian Research, 130(1-4), 113-137.

Dantas, E.L., Souza, Z.S., Wernick, E., Hackspacher, P.C., Martin, H., Xiaodong, D., Li, J.W., 2013. Crustal growth in the 3.4–2.7 Ga São José de Campestre Massif, Borborema Province, NE Brazil. Precambrian Research, 227, 120-156.

Degler, R., Pedrosa-Soares, A., Novo, T., Tedeschi, M., Silva, L.C., Dussin, I., Lana, C. 2018. Rhyacian-Orosirian isotopic records from the basement of the Araçuaí-Ribeira orogenic system (SE Brazil): Links in the Congo-São Francisco palaeocontinent. Precambrian Research, 317, 179-195.

DePaolo, D.J., 1981. A neodymium and strontium isotopic study of the Mesozoic calc-alkaline granitic batholiths of the Sierra Nevada and Peninsular Ranges, California. J. Geophys. Res. Solid Earth 86, 10470–10488.

Fachetti, F.J.S., Fuck, R.A., Marimon R.S., Ferreira, A., Costa, A.C.D., Hawkesworth, C.J. 2024. Paleoarchean to Neoproterozoic crustal formation and migmatization events in the Borborema Province, NE Brazil: implications for the growth and reworking of the continental crust. Gondwana Research, 129, 75-90. https://doi.org/10.1016/j.gr.2023.12.005.

Ferreira, A.C., Dantas, E.L., Fuck, R.A., Nedel, I.M., Reimold, W.U., 2021. Multiple stages of migmatite generation during the Archean to Proterozoic crustal evolution in the Borborema Province, Northeast Brazil. Gondwana Research, 90, 314-334.

Filgueiras, B., Oliveira, C.G., de Sousa, I.M.C., Cordeiro, P. 2020. Further evidence of Rhyacian arc magmatism in the basement of the Brasília Belt, western São Francisco pericraton. Journal of South American Earth Sciences, 103, 102739.

Fontainha, M.V., Trouw, R.A., Dantas, E.L., Polo, H.J., Furtado, P.C., Marimon, R.S., Telles, R.C.M., Peternel, R. 2021. Provenance and tectonic evolution of the Andrelândia Group in the region between the Socorro and Guaxupé nappes, Southern Brasília and Ribeira orogens, Brazil. Journal of South American Earth Sciences, 109, 103060.

Fossen, H., Harris, L.B., Cavalcante, C., Archanjo, C.J., Ávila, C.F., 2022. The Patos-Pernambuco shear system of NE Brazil: Partitioned intracontinental transcurrent deformation revealed by enhanced aeromagnetic data. Journal of Structural Geology, 158, 104573.

Fuck, R.A., Dantas, E.L., Pimentel, M.M., Botelho, N.F., Armstrong, R., Laux, J.H., Junges, S.L., Soares, J.E., Praxedes, I.F. 2014. Paleoproterozoic crust-formation and reworking events in the Tocantins Province, central Brazil: A contribution for Atlantica supercontinent reconstruction. Precambrian Research, 244, 53-74.

Ganade, C.E., Basei, M.A., Grandjean, F.C., Armstrong, R., Brito, R.S., 2017. Contrasting Archaean (2.85–2.68 Ga) TTGs from the Tróia Massif (NE-Brazil) and their geodynamic implications for flat to steep subduction transition. Precambrian Research, 297, 1-18.

Ganade, C.E., Weinberg, R.F., Caxito, F.A., Lopes, L.B., Tesser, L.R., Costa, I.S., 2021. Decratonization by rifting enables orogenic reworking and transcurrent dispersal of old terranes in NE Brazil. Scientific Reports, 11(1), 5719.

Gioia, S.M.C.L., Pimentel, M.M., 2000. The Sm-Nd isotopic method in the Geochronology Laboratory of the University of Brasília. An. Acad. Bras. Cienc. 72, 218–245.

Giustina, M.E.S., Oliveira, C.G., Pimentel, M.M., Melo, L.V., Fuck, R.A., Dantas, E.L., Bühn, B.M. 2009. U–Pb and Sm–Nd constraints on the nature and

evolu-tion of Paleoproterozoic juvenile crust in the Tocantins Province, central Brazil. Geological Society, London Special Publication, 323, 255-269.

Grochowski, J., Kuchenbecker, M., Barbuena, D., Novo, T., 2021. Disclosing Rhyacian/Orosirian orogenic magmatism within the Guanhães basement inlier, Araçuaí Orogen, Brazil: A new piece on the assembly of the São Francisco-Congo paleocontinent. Precambrian Research, 363, 106329.

Hackspacher, P.C., Dantas, E.L., Brito Neves, B.B., Legrand, J.M., 1997. Northwestern overthrusting and related lateral escape during the Brasiliano orogeny north of the Patos Lineament, Borborema Province, Northeast Brazil. International Geology Review, 39(7), 609-620.

Heilbron, M., Duarte, B.P., Valeriano, C.M., Simonetti, A., Machado, N., Nogueira, J.R. 2010. Evolution of reworked Paleoproterozoic basement rocks within the Ribeira belt (Neoproterozoic), SE-Brazil, based on U–Pb geochronology: Implications for paleogeographic reconstructions of the São Francisco-Congo paleocontinent. Precambrian Research, 178(1-4), 136-148.

Hildreth, W., Moorbath, S. 1988. Crustal contributions to arc magmatism in the Andes of Central Chile. Contributions to mineralogy and petrology, 98, 455-489.

Hollanda, M.H.B.M., Archanjo, C.J., Souza, L.C., Dunyi, L., Armstrong, R., 2011. Long-lived paleoproterozoic granitic magmatism in the Seridó-Jaguaribe domain, Borborema Province–NE Brazil. Journal of South American Earth Sciences, 32(4), 287-300.

Hollanda, M.H.B.M., Archanjo, C.J., Bautista, J.R., Souza, L.C., 2015. Detrital zircon ages and Nd isotope compositions of the Seridó and Lavras da Mangabeira basins (Borborema Province, NE Brazil): evidence for exhumation and recycling associated with a major shift in sedimentary provenance. Precambrian Research, 258, 186-207.

Jackson, S.E., Pearson, N.J., Griffin, W.L., Belousova, E.A., 2004. The application of laser ablation-inductively coupled plasma-mass spectrometry to in situ U–Pb zircon geochronology. chemical Geology 211, 47-69.

Leite, C.M.M, Barbosa, J.S.F., Goncalves, P., Nicollet, C., Sabaté, P., 2009. Petrological evolution of silica-undersaturated sapphirine-bearing granulite in the Paleoproterozoic Salvador–Curaçá Belt, Bahia, Brazil. Gondwana Research, 15(1), 49-70.

Marimon, R.S., Trouw, R.A.J., Dantas, E.L., Ribeiro, A. 2020a. U-Pb and Lu-Hf isotope systematics on detrital zircon from the southern São Francisco Craton's Neoproterozoic passive margin: Tectonic implications. Journal of South American Earth Sciences, 100, 102539.

Marimon, R.S., Trouw, R.A., Dantas, E.L. 2020b. Significance of age periodicity in the continental crust record: The São Francisco Craton and adjacent Neoproterozoic orogens as a case study. Gondwana Research, 86, 144-163.

Marimon, R.S., Trouw, R.A.J., Dantas, E.L., Ribeiro, A., Santos, P., Kuster, K., Vinagre, R. 2021. Provenance of passive-margin and syn-collisional units: Implications for the geodynamic evolution of the Southern Brasília Orogen, West Gondwana. Sedimentary Geology, 413, 105823.

Marimon, R.S., Hawkesworth, C.J., Dantas, E.L., Trouw, R.A.J., Teixeira, W., Hackspacher, P.C., Fetter, A., Ávila, C.A., Volante, S., Corrêa Neto, A.V., Bongiolo, E.M., Vinagre, R., Simon, M. 2022. The generation and evolution of the Archean continental crust: The granitoid story in southeastern Brazil. Geoscience Frontiers, 13(4), 101402.

Marimon, R.S., Trouw, R.A.J., Hawkesworth, C.J., Waterkemper, J., Ribeiro, A., Vinagre, R., Dantas, E.L. 2023. Challenges of dating metasedimentary successions in collisional orogens: A case study of a Neoproterozoic passive margin in West Gondwana. Gondwana Research, 113, 1-13.

Martins-Ferreira, M.A.C., Dias, A.N.C., Chemale Jr, F., Campos, J.E.G., Seraine, M., Novais-Rodrigues, E. 2020. Multi-stage crustal accretion by magmatic flare-up and quiescence intervals in the western margin of the São Francisco Craton: U-Pb-Hf and geochemical constraints from the Almas Terrane. Gondwana Research, 85, 32-54.

Matteini, M., Dantas, E.L., Pimentel, M.M., Bühn, B., 2010. Combined U-Pb and Lu-Hf isotope analyses by laser ablation MC-ICP-MS: methodology and applications. Na. Acad. Bras. Ciênc. 82, 479-491.

Mauri, S., Heilbron, M., Bruno, H., Marques, R.A., Neto, C., Valeriano, C.M., Bersan, S., Romero, L.F., Geraldes, M.C. 2023. Rhyacian magmatic arc rocks with sanukitoid geochemical signature from the Juiz de Fora Complex, Minas-Bahia Orogenic System (SE-Brazil). Brazilian Journal of Geology, 52.

Meert, J.G. 2012. What's in a name? The Columbia (Paleopangaea/Nuna) supercontinent. Gondwana Research, 21(4), 987-993.

Meert, J.G., Santosh, M. 2017. The Columbia supercontinent revisited. Gondwana Research, 50, 67-83.

Moreira, H., Seixas, L., Storey, C., Fowler, M., Lasalle, S., Stevenson, R., Lana, C. 2018. Evolution of Siderian juvenile crust to rhyacian high Ba-Sr magmatism in the Mineiro Belt, southern São Francisco Craton. Geoscience Frontiers, 9(4), 977-995.

Morel, M.L.A., Nebel, O., Nebel-Jacobsen, Y.J., Miller, J.S., Vroon, P.Z., 2008. Hafnium isotope characterization of the GJ-1 zircon reference material by solution and laser-ablation MC-ICPMS. Chem. Geol. 255, 231-235.

Moura, F.G., Campos, J.E.G. 2022. Characterization and Geological Meaning of the Crystalline Basement Occurrence in the Unaí Region, Minas Gerais State (Central Brasilia Belt). Anuário do Instituto de Geociências, 46.

Nascimento, H.S., Nédélec, A., Bouchez, J.L., 2017. Petrology of Teofilândia granitoids: an example of 2.1 Ga crustal accretion in the São Francisco Craton (Bahia, Brazil). Journal of South American Earth Sciences, 76, 137-151.

Neves, S.P., Vauchez, A., Feraud, G., 2000. Tectono-thermal evolution, magma emplacement, and shear zone development in the Caruaru area (Borborema Province, NE Brazil). Precam. Res., 99(1-2), 1-32.

Neves, S.P., 2021. Comparative geological evolution of the Borborema Province and São Francisco Craton (eastern Brazil): Decratonization and crustal reworking during West Gondwana assembly and implications for paleogeographic reconstructions. Precambrian Research, 355, 106119.

Neves, C.V.S., Ávila, C.A., Bongiolo, E.M., Neumann, R., Teixeira, W., Faulstich, F.R.L., Heilbron, M., Geraldes, M.C., Valeriano, C.M. 2023. Preserved interactions between acid and intermediate magmas in a 2.15–2.10 Ga Rhyacian continental arc: Insights from petrographic, geochemical and isotopic data of the Macuco de Minas metagranitoid, Mineiro belt, Brazil. Lithos, 440, 107048.

Oliveira, M.A.F., Negri, F.A., Zanardo, A., Morales, N. 2019. Archean and paleoproterozoic crust generation events, Amparo complex and Serra Negra orthogneiss in southern Brasília Orogen, SE Brazil. Journal of South American Earth Sciences, 90, 137-154.

Patchett, P.J., 1983. Importance of the Lu-Hf isotopic system in studies of planetary chronology and chemical evolution. Geoc. et Cosmoc. Acta, 47(1), 81-91.

Pietranik, A.B., Hawkesworth, C.J., Storey, C.D., Kemp, A.I.S., Sircombe, K.N., Whitehouse, M.J., Bleeker, W., 2008. Episodic, mafic crust formation from 4.5 to 2.8 Ga: New evidence from detrital zircons, Slave craton, Canada. Geology 36, 875.

Pinheiro, M.A.P., Suita, M.T.F., Lesnov, F. P., Tedeschi, M., Silva, L.C., Medvedev, N.S., Korolyuk, V.N., Pinto, C.P., Sergeev, S.A. 2019. Timing and petrogenesis of metamafic-ultramafic rocks in the Southern Brasília orogen: Insights for a Rhyacian multi-system suprasubduction zone in the São Francisco paleocontinent (SE-Brazil). Precambrian Research, 321, 328-348.

Pinheiro, M.A.P., Guice, G.L., Magalhães, J.R., 2022. Archean–Ediacaran evolution of the Campos Gerais Domain—A reworked margin of the São Francisco paleocontinent (SE Brazil): Constraints from metamafic–ultramafic rocks. Geoscience Frontiers, 13(5), 101201.

Pitarello, M.Z., Santos, T.J., Ancelmi, M.F., 2019. Syn-to post-depositional processes related to high grade metamorphic BIFs: Geochemical and geochronological evidences from a Paleo to Neoarchean (3.5–2.6 Ga) terrane in NE Brazil. Journal of South American Earth Sciences, 96, 102312.

Rubatto, D. 2002. Zircon trace element geochemistry: partitioning with garnet and the link between U–Pb ages and metamorphism. Chemical geology, 184(1-2), 123-138.

Ruiz, F.V., Della Giustina, M.E.S., Oliveira, C.G., Dantas, E.L., Hollanda, M.H.B., 2019. The 3.5 Ga São Tomé layered mafic-ultramafic intrusion, NE Brazil: Insights into a Paleoarchean Fe-Ti-V oxide mineralization and its reworking during West Gondwana assembly. Precambrian Research, 326, 462-478.

Saboia, A.M., Oliveira, C.G., Dantas, E.L., Scandolara, J.E., Cordeiro, P., Rodrigues, J. B., Sousa, I.M.C. 2020. The 2.26 to 2.18 Ga Arc-Related Magmatism of the Almas-Conceição do Tocantins Domain: An Early Stage of the São Francisco Paleocontinent Assembly in Central Brazil. Journal of South American Earth Sciences, 104, 102757.

Santos, R.V., Santos, E.J., Souza Neto, J.A., Carmona, L.C.M., Sial, A.N., Mancini, L.H., Santos, L.C.M.L., Nascimento, G.H., Mendes, L.U.S., Anastácio, E.M.F. 2013. Isotope geochemistry of Paleoproterozoic metacarbonates from Itatuba, Borborema Province, Northeastern Brazil: Evidence of marble melting within a collisional suture. Gondwana Research, 23(1), 380-389.

Santos, L.C.M.L., Dantas, E.L., Cawood, P.A., Lages, G.A., Lima, H.M., Santos, E.J. 2018. Accretion Tectonics in Western Gondwana Deduced from Sm-Nd Isotope Mapping of Terranes in the Borborema Province, NE Brazil. Tectonics, 37(8), 2727-2743.

Sawyer, E.W., 2008. Atlas of migmatites (Vol. 9). NRC Research press.

Scherer, E., Münker, C., Mezger, K., 2001. Calibration of the lutetium-hafnium clock. Science 293, 683-687.

Seixas, L.A.R., Bardintzeff, J.M., Stevenson, R., Bonin, B. 2013. Petrology of the high-Mg tonalites and dioritic enclaves of the ca. 2130 Ma Alto Maranhão suite: evidence for a major juvenile crustal addition event during the Rhyacian orogenesis, Mineiro Belt, southeast Brazil. Precambrian Research, 238, 18-41.

Sousa, I.M.C., Della Giustina, M.E.S., Oliveira, C.G. 2016. Crustal evolution of the northern Brasília Belt basement, central Brazil: a Rhyacian orogeny coeval with a pre-Rodinia supercontinent assembly. Precambrian Research, 273, 129-150.

Souza, Z.S., Martin, H., Peucat, J.J., Jardim De Sá, E.F., Macedo, M.H.F., 2007. Calc-alkaline magmatism at the Archean–Proterozoic transition: the Caicó Complex basement (NE Brazil). Journal of Petrology, 48(11), 2149-2185.

Souza, Z.S., Dantas, E.L., Oliveira, E.P., Vilalva, F.C.J., Motta, R.G.D., Martin, H., Valcácio, S.N. 2023. Zircon U-Pb dating and petrogenesis of the São José do Campestre Granite Complex, NE Brazil: an example of Neoarchean mantle-derived post-collisional magmatism. Brazilian Journal of Geology, 53, e20220079.

Stern, C.R. 2011. Subduction erosion: rates, mechanisms, and its role in arc magmatism and the evolution of the continental crust and mantle. Gondwana Research, 20(2-3), 284-308.

Teixeira, W., Ávila, C.A., Dussin, I.A., Neto, A.C., Bongiolo, E.M., Santos, J.O., Barbosa, N.S., 2015. A juvenile accretion episode (2.35–2.32 Ga) in the Mineiro belt and its role to the Minas accretionary orogeny: Zircon U–Pb–Hf and geochemical evidences. Precambrian Research, 256, 148-169.

Van Schmus, W.R., Brito Neves, B.B., Hackspacher, P.C., Babinski, M. 1995. U-Pb and Sm-Nd geochronologic studies of the eastern Borborema Province, Northeastern Brazil: initial conclusions. Journal of South American Earth Sciences, 8(3-4), 267-288.

Van Schmus, W.R., Oliveira, E.P., Silva Filho, A.F., Toteu, S.F., Penaye, J., Guimarães, I.P. 2008. Proterozoic links between the Borborema province, NE

Brazil, and the central African fold belt. Geological Society, London, Special Publications, 294(1), 69-99.

Van Schmus, W.R., Kozuch, M., Brito Neves, B.B. 2011. Precambrian history of the Zona Transversal of the Borborema Province, NE Brazil: insights from Sm–Nd and U–Pb geochronology. Journal of South American Earth Sciences, 31(2-3), 227-252.

Vauchez, A., Neves, S., Caby, R., Corsini, M., Egydio-Silva, M., Arthaud, M., Amaro, V. 1995. The Borborema shear zone system, NE Brazil. Journal of South American Earth Sciences, 8(3-4), 247-266.

Viegas, L.G.F., Archanjo, C.J., Vauchez, A. 2013. Fabrics of migmatites and the relationships between partial melting and deformation in high-grade transpressional shear zones: the Espinho Branco anatexite (Borborema Province, NE Brazil). Journal of Structural Geology, 48, 45-56.

Viegas, L.G.F., Archanjo, C.J., Hollanda, M.H.B., Vauchez, A., 2014. Microfabrics and zircon U–Pb (SHRIMP) chronology of mylonites from the Patos shear zone (Borborema Province, NE Brazil). Precambrian Research, 243, 1-17.

Xia, L., Li, X., 2019. Basalt geochemistry as a diagnostic indicator of tectonic setting. Gondwana Research, 65, 43-67.

CAPÍTULO 5

Considerações Finais

A Zona de Cisalhamento Patos é uma extensa estrutura de sutura com orientação W-E, que separa dois domínios com histórias evolutivas distintas, sendo a sul a sub-província da Zona Transversal e ao Norte o Domínio Rio Grande do Norte, e guarda fragmentos crustais arqueanos e proterozóicos

As rochas de idade paleoarqueana localizam-se em dois núcleos, um mais antigo (Migmatito AE 11B de 3,5 Ga), localizado próximo ao distrito de Itajubatiba, pertencente ao município de Catingueira, e outro mais jovem (Migmatito AE 23A de 3,3 Ga) no município de Patos. Esses núcleos foram submetidos a diversos eventos tectonometamórficos, que geraram crescimento e retrabalhamento crustal. As estruturas desses eventos foram obliteradas pelo evento posterior, A Orogenia Brasiliana. As idades de 3,45 Ga (núcleo Bom Jesus), 2,15 Ga (embasamento da Provincia Borborema) e 2,0 Ga (faixas paleoproterozoicas do Cráton do São Francisco), evidenciam que essas rochas podem ter participado da colagem que formou o Supercontinente Atlântica.

As rochas de idade paleoproterozoica do Complexo Patos são migmatitos, gnaisses e anfibolitos com assinatura geoquímica isotópica de arco magmático. Os migmatitos paleoproterozoicos possuem idade de cristalização em aproximadamente 2,2 Ga, com valores εNd entre 0,17 e -5,46, εHf positivo a fracamente negativo, sugerindo interação de magmas de fontes mantélica e crustal.

Tanto os migmatitos arqueanos quanto os paleoproterozoicos exibem leucossomas de composição monzogranítica e sienogranítica, com idades U-Pb em zircão entre 570 e 580 Ma, evidenciando processos de migmatização durante a Orogênese Brasiliana, que atuaram diferencialmente nos segmentos crustais da Província Borborema. Os valores εNd e εHf fortemente negativos sugerem que se trata exclusivamente de retrabalhamento da crosta continental, corroborados ainda pelas razões Th/U >0.01 nos cristais de zircão neoproterozoico. Este evento metamórfico afetou de forma ampla todos os domínios, deformando e metamorfizando as faixas neoproterozoicas e o embasamento com geração de grande quantidade de granitos alcalinos. Os dados isotópicos de U-Pb, Lu-Hf e Sm-Nd demonstram concordantemente a

presença de duas fontes magmáticas para as rochas ao longo do Complexo Patos. O primeiro episódio magmático é representado pelo material mantélico extraído ~3,66 e cristalizado em 3,5 Ga, submetidos a eventos de acresção e crescimento crustal que guardam rochas com idade de cristalização e sobrecrescimento em bordas de cristais de zircão em 3,3, 3,2, 3,0, e 2.6 Ga. Essa rocha apresentam uma coeva linha de evolução gradativa dos parâmetros εHf e εNd durante todo o Arqueano. A rochas estudadas mostram também migmatização riaciana. Essas rochas passaram por intensa atividade de magmatismo juvenil em ~2,2 Ga, com geração de magmatismo cálcio-alcalino com εNd em rocha total negativo e positivo e εHf positivo a levemente negativo, sugerindo que houve a interação de fontes mantélica e crustal. O conjunto foi intensamente retrabalhado no Neoproterozoico (~570 Ma), com a injeção de migmatitos de composição sienogranítica e monzogranítica, formando cristais de zircão metamórficos com baixa razão Th/U e εNd e εHf fortemente negativo.

Com base nos dados isotópicos, geoquímicos e petrogênese das rochas do Complexo Patos, é possível sugerir que se trata de fragmentos de terrenos arqueanos, sugeridos neste trabalho como resquícios do Cráton do São Francisco, que sofreram múltiplos episódios de retrabalhamento e foram afetados pela orogênese riaciana, quando ocorreu a injeção de magma cálcio-alcalino de fonte mantélica com εNd positivo e negativo, culminando com um segundo episódio de migmatização durante a estruturação final no Neoproterozoico.

CAPÍTULO 6

Referências Bibliográficas

Arthaud, M.H., Caby, R., Fuck, R.A., Dantas, E.L., Parente, C.V., 2008. Geology of the Northern Borborema Province NE Brazil and Its Correlation with Nigeria, NW Africa. In: Geological Society of London, Special Publication, vol. 294, pp. 49e67.

Ashworth, J.R., 1985. Migmatites. Blackie, Glasgow.

Blichert-Toft, J., Albarède, F., 1997. The Lu-Hf isotope geochemistry of chondrites and the evolution of the mantle-crust system. Earth and Planetary Science Letters, 148(1-2), 243-258.

Boynton, W.V. 1984. Cosmochemistry of the rare-earth elements: meteorite studies. In: Henderson, P. ed. Rare-earth Elements Geochemistry. Amsterdam, Elsevier. p. 63-114.

Brito Neves, B. B., 1975. Regionalização geotectônica do Pré-Cambriano Nordestino. Tese de Doutorado. Inst. Geoc. USP, 198p.

Brito Neves, B. B., Dos Santos, E. J., Van Schmus, W. R., 2000. Tectonic history of the Borborema Province, Northeastern Brazil. In: Cordani, U., Milani, E. J., Thomaz Filho, A., Campos, D. A., (Eds.). Tectonic evolution of South America. 31st International Geological Congress, Rio de Janeiro, Brazil, pp. 151–182.

Brito Neves, B.B., 2011. The Paleoproterozoic in the South-American continent: Diversity in the geologic time. Journal of South American Earth Sciences. v. 32, pp. 270–286.

Bühn B., Pimentel M.M, Matteini M. e Dantas E. 2009. High spatial resolution analysis of Pb and U isotopes for geochronology by laser ablation multi-collector inductively coupled plasa ass spectroetry (L-C-ICPMS). An Acad Bras Cienc 81: 99-114.

Caby, R., 1989. Precambrian terranes of Benin-Nigeria, and Northeast Brazil and Late Proterozoic South Atlantic fit. Geol. Soc. America, Spec. Paper, v. 230, pp. 145-158.

Chauvel, C., Blichert-Toft, J., 2001. A hafnium isotope and trace element perspective on melting of the depleted mantle. Earth and Planetary Science Letters, 190(3), 137-151.

Cherniak, D.J., Hanchar, J.M., Watson, E.B., 1999. Diffusion of tetravalent cations in zircon. Contrib. Mineral. Petrol. 127, 383–390.

Chu, N.C., Taylor, R.N., Chavagnac, V., Nesbitt, R.W., Boella, M. & Milton, J.A. 2002. Hf isotope ratio analysis using multi-collector inductively coupled plasma mass spectrometry: an evaluation of isobaric interference corrections. Journal of Analytical Atomic Spectrometry, 17: 1567–1574.

Condie, K.C., 2000. Episodic continental growth models: afterthoughts and extensions. Tectonophysics 322, 153–162.

Corsini, M.; Vauchez, A.; Archanjo, C.J.; Jardim De Sá, E.F. 1991. Strain transfer at continental scale from a transcurrent shear zone to a transpressional fold belt: the Patos-Seridd system, northeastern Brazil: Geology, 19: 586-589.

Costa, A.C.D., 2002. Geologia e geocronologia Sm-Nd e U-Pb na região do Lineamento Patos, limite entre os blocos crustais do domínio Rio Grande do Norte e da Zona Transversal, Província Borborema. Tese de PhD, UNESP – Universidade Estadual de São Paulo.

Costa, F.G., Palheta, E.S.M., rodrigues, J.B., Gomes, I.P., Vasconcelos, A.M., 2015. Geochemistry and U-Pb zircon ages of plutonic rocks from the Algodões granite-greenstone terrane, Troia Massif, northern Borborema Province, Brazil: Implications for Paleoproterozoic subduction-accretion processes. Journal of South American Earth Sciences, 59, 45-68

Dantas, E. L., Souza, Z. S., Wernick, E., Hackspacher, P. C., Martin, H., Xiaodong, D., & Li, J. W., 2013. Crustal growth in the 3.4-2.7 Ga São José de Campestre Massif, Borborema Province, NE Brazil. Precambrian Research, 227, 120–156. doi.org/10.1016/j.precamres.2012.08.006

Dantas, E.L., Negrão, M.M., Buhn, B., 2008. 2.3 Ga continental crust generation in the Rio Grande do norte terrane, NE-Brazil, in: 6th South American Symposium on Isotope Geology, Abstract Volume, pp. 40.

Dantas, E.L., Van Schmus W.R., Hackspacher P.C., Brito Neves, B.B.,1995. Terrenos arqueanos e paleoproterozoicos do Maciço Caldas Brandão na Provincia Borborema. Simpósio de Geologia do Nordeste, 16, Boletim 14, Recife-PE, p. 423-427.

Dantas, E.L., Van Schmus W.R., Hackspacher P.C., Fetter A.H., Neves B.B.B., Cordani U.G., Nutman A.P., Williams S., 2004. The 3.4-3.5 São José do Campestre Massif, NE Brazil: remnants of the oldest crust in South America. Precambrian Research 130, 113-137.

DePaolo D. J., 1981. Trace elemento and isptopic effects of combined wallrock assimilation and fractional crystallization. Earth and planetary Science letters 53, 189-202.

Evans, D.A.D., Mitchell, R.N., 2011. Assembly and breakup of the core of Paleoproterozoic–Mesoproterozoic supercontinent Nuna. Geology 39, 443–446.

Faure, G. 1977; Princies of isotope geology. John Wiley & Sond. New York.

Ferreira, C. A. & Santos, E. J.2000. Programa de Levantamento Geológico Básico no Brasil Jaguaribe SE, Folha SB.24-z. Estado do Cerará, Rio Grande do Norte Paraíba e Pernambuco. Escala 1:500.00. Brasília CPRM. CD-ROM: il., mapas.

Fetter, A. H.; Santos, T. J. S.; Van Schmus, W. R.; Hackspacher, P. C.; Britoneves, B. B.; Arthaud, M. H.; Nogueira Neto, J. A.; Wernick, E., 2003, Evidence for Neoproterozoic Constinental Arc Magmatism in the Santa Quitéria Batholith of Ceará State, NW Borborema Province, NE Brazil: Implications for the Assembly of West Gondwana. Gondwana Research, 6 (2): 265-273.

Fetter, A.H., Van Schmus, W.R., Santos, T.J.S., Arthaud, M., J.A.N., Nogueira Neto, J.A., 2000. U-Pb and Sm-Nd geochronological constraints on the crustal evolution and basement architecture of Ceará State, NW Borborema Province, NE Brazil: implications for the existence of the Paleoproterozoic supercontinent Atlantica. Revista Brasileira de Geociências 30, 102-106.

Gerdes, A. & Zeh, A. 2009. Zircon formation versus zircon alteration – New Insights from combined U-Pb and Lu-Hf in-situ LA-ICP-MS analyses, and consequences for the interpretation of archean zircon from the Central Zone of the Limpopo Belt. Chemical Geology, 261: 230-243

Gioia S. M. C. L. e Pimentel M. M., 2000. The Sm-Nd isotopic method in the geochronology laboratory of the University of Brasilia. Annals of the Brazilian Academy of Sciences 72, 219-245.

Guimarães, I. P. & Silva Filho, A. F. 2000. Evidence of multiple source involved in the genesis of the Neoproterozoic Itapetim Granitic Complex, NE Brazil, based on geochemical and isotopic data. Journal os South American Earth Science, vol. 13, n.6, p. 561- 586.

Hollanda, M.H.B.M., Archanjo, C.J., Bautista, J.R., Souza, L.C., 2015. Detrital zircon ages and Nd isotope compositions of the Seridó and Lavras da Mangabeira basins (Borborema Province, NE Brazil): Evidence for exhumation and recycling associated with a major shift in sedimentary provenance. Precambrian Research 258, 186–207.

Irvine I. N. & Baragar W. R. A. 1971. A guide to the chemical classification of the common volcanics rocks. Canadian Journal Earth Science, v. 8, p. 523-548.

Jackson S.E., Pearson N.J., Griffin W.L., Belousova E.A., 2004. The application of laser ablation inductively coupled plasma mass spectrometry to in situ U-Pb zircon geochronology. Chemical Geology 211, 47-69.

Jardim de Sá, E.F., 1994. A Faixa Seridó (Província Borborema, Ne Brasil) e o seu Significado Geodinâmico na Cadeia Brasiliana/Pan-Africana. Tese de Doutorado, Universidade De Brasília, 803pp.

Kinny. P,D,. and Maas. R,. 2003. Lu-Hf and Sm-Nd isotope systems in zircon. In: Hanchar JM and Hoskin PWO (Eds), Zircon, The Geological Society of America (GSA), Washington, USA, p. 327-341.

Kosler J., Fonneland H., Sylvester P., Tubrett M. e Pedersen R. 2002. U-Pb dating of detrital zircons for sediment provenance studies - a comparison of laser ablation ICMPS and SIMS techniques. Chem Geol 182: 605-618.

Le Maitre RW. 1989. A classification of igneous rocks and glossary of terms. Oxford: Blackwell, 193p.

Martins, G., Oliveira, E. P., Lafon, J. M., 2009. The Algodões amphibolite-tonalite gneiss sequence, Borborema Province, NE Brazil: Geochemical and geochronological evidence for Paleoproterozoic accretion of oceanic plateau/back-arc basalts and adakitic plutons. Gondwana Research 15, 71-85.

Matteini, M., Junges, S.L., Dantas, E.L., Pimentel, M.M., Bühn, B., 2010. In situ zircon U–Pb and Lu–Hf isotope systematic on magmatic rocks: insights on the crustal evolution of the Neoproterozoic Goiás Magmatic Arc, Brasília belt, Central Brazil. Gondwana Research, 17(1), 1-12.

McDonough, W.F. & Sun, S.S. 1995. The composition of the Earth. Chem. Geology, 120: 223-253.

Mehnert K. R.; Büsch W. 1982. The initial stage of migmatite formation. Neues Jahrbuch für Mineralogie, Abhandlungen 145: 211– 238.

Mehnert, K. R. 1968. Migmatites and the Origin of Granitic Rocks . Elsevier Publishing Company, Amsterdam, London, New York, Price 393 p.,138 figs.

Morel, M.L.A., Nebel, O., Nebel-Jacobsen, Y.J., Miller, J.S. & Vroon, P.Z. 2008. Hafnium isotope characterization of the GJ-1 zircon reference material by solution and laser-ablation MC-ICPMS. Chemical Geology, 255: 231–235

Nascimento M.A.L., Medeiros V.C., Galindo A.C. 2015. Ediacaran to Cambrian magmatic suites in the Rio Grande do Norte domain, extreme Northeastern Borborema Province (NE of Brazil): current knowldge. Journal of South American Earth Sciences, 58: 281-299.

Nebel, O., Nebel-Jacobsen, Y. J., Mezger, K., & Berndt, J. (2007). Initial Hf isotope compositions in magmatic zircon from early Proterozoic rocks from the

Gawler Craton, Australia: a test for zircon model ages. Chemical Geology, 241, 23-37.

O'Connor J.T. 1965. A classification for quartz-rich igneous rocks based on feldspar ratios. US Geological Survey, 525B, 79-84.

Oliveira F. V., 2015 Chronus: Um novo suplemento para a redução de dados U-Pb obtidos por LAMC-ICPMS. Instituto de Geociências, Universidade Federal de Brasília, Dissertação de Mestrado, 91 pp.

Oliveira, R.G., Medeiros, W.E., 2018. Deep crustal framework of the Borborema Province, NE Brazil, derived from gravity and magnetic data. Precambrian Research, 315: 45-65.

Olsen, S. N. 1985. Mass balance in migmatites, in Migmatites, (ed. J. R. Ashworth., 145–179; Glasgow, Blackie

Patchett, J.P., Kouvo, O., Hedge, C.E., Tatsumoto, M., 1981. Evolution of continental crust and mantle heterogeneity: evidence from Hf isotopes. Contrib. Mineral. Petrol. 78, 279–297.

Patchett, P. J., 1983. Hafnium isotope results from mid-ocean ridges and Kerguelen.Lithos,16,47–51.

Pearce J.A., Harris N.B.W., Tindle A.G. 1984. Trace element discrimination diagrams for the tectonic interpretation of granitic rocks. Journal of Petrology, 25(4):956-983.

Peccerilo A. & Taylor S.R. 1976. Geochemistry of Eoceno Calc-Alkaline Volcanic Rocks from the Kastamonu Area, Northern Turkey. Contributions to Mineralogy and Petrology, 58:63-81.

Ruiz F.V., Della Giustina M.E.S., Oliveira C.G., Dantas E.L., Hollanda M.H.B. 2018. The 3.5 Ga São Tomé layered mafic-ultramafic intrusion, NE Brazil: insights into a Paleoarchean Fe-Ti-V oxide mineralization and its reworking during West Gondwana assembly. Precambriam Research. Available at: <https://doi.org/10.1016/j.precamres.2018.03.011>

Santos E.J. E Medeiros V.C. 1999. Constraints from granitic plutonism on proterozoic crustal growth of the Transverse Zone, Borborema Province, NE Brazil. Revista Brasileira de Geociências, 29: 73-84

Santos, E.J., 1996. Ensaio preliminar sobre terrenos e tectônica acrescionária na Província Borborema, in 39º Congresso Brasileiro de Geologia, Anais, v 1, pp. 47-50.

Sawyer, E.W., 2008. Atlas of migmatites. The CanadianMineralogist Special Publication, 9. Mineralogical Association of Canada, NRC Research Press, Ottawa.

Sawyer, E.W., Brown, M. 2008 (Eds.), Working With Migmatites: Mineralogical Association of Canada, Short Course, vol. 38, pp. 1–28

Scheid, C. & Ferreira, C. A. 1991. Programa de levantamento Geológico Básico do Brasil: cartas geológicas e metalogenética previsional – Escala 1:100.000 (folha SB.24-Z-D-I – Patos), Estado de Pernambuco e Paraíba. Brasília, DNPM/CPRM. 148p.

Scherer, E., Münker, C., Mezger, K., 2001. Calibration of the lutetium-hafnium clock. Science, 293(5530), 683-687.

Shand, S.J. 1943. Eruptive Rocks. Their Genesis, Composition, Classification, and Their Relation to Ore-Deposits with a Chapter on Meteorite. Nova Iorque, John Wiley & Sons, 444 p.

Silva L.C., Armstrong R., Pim entel M.M., Scandolara J., Ram grab G., Wildner W., Angelim L.A.A., Vasconcelos A.M., Rizzoto G., Quadros M.L.E.S., Sander A., Rosa A.L.Z. 2002. Reavaliação da evolução geológica em terrenos precambrianos brasileiros com base em novos dados U-Pb SHRI MP, Parte I I I : províncias Borborema, Mantiqueira Meridional e Rio Negro-Juruena. Rev. Bras. Geoc., 3 2 : 529-544.

Souza, Z.S., Martin, H., Peucat, J.J., Jardim de Sá, E. F., Macedo, M.H.F., 2007. Calc-Alkaline Magmatism at the Archean-Proterozoic Transition: The Caicó Complex Basement (Ne Brasil). Jounal of Petrology 48, 2149-2185.

Van Schmus, W. R., Brito Neves, B.B., Williams, I. S., Hackspacher, P. C., Fetter, A. H., Dantas, E. L., Babinski, M., 2003. The Seridó Group of NE Brazil, a late Neoproterozoic pre- to syn-collisional basin in West Gondwana: insights form SHRIMP U-Pb detrital zircon ages and Sm-Nd crustal residence (TDM) ages. Precambrian Research 127, 287-327.

Van Schmus, W.R., Kozuch, M., Brito Neves, B.B. 2011. Precambrian history of the Zona Transversal of the Borborema Province, NE Brazil: insights from Sm–Nd and U–Pb geochronology. Journal of South American Earth Sciences 31, 227-252.

Vauchez. A; Neves, S.; Caby, R.; Corsini, M.; Egydio-Silva, M.; Arthaud, M. & Amaro, V. 1995. The Borborema shear zone system, NE Brazil. Journal of South America Earth Sciences, vol. 8, 1995, p. 247-266.

Viegas, L. G. F., Arcanjo, C. J., Hollanda, M. H. B. M., Vauchez, A., 2014. Microfabrics and zircon U-Pb (SHIRIMP) chronology of mylonites from the Patos shear zone (Borborema Procince, NE Brazil).

Viegas, L. G. F., Arcanjo, C. J., Vauchez, A., 2013. Fabrics of migmatites and the relationships between partial melting and deformation in high-grade transpressional shear zones: The Espinho Branco anatexite (Borborema Province, NE Brazil). Journal of Structural Geology 48, 45-56.

Wedepohl, K.H., 1995. The composition of the continental crust. Geochimica et cosmochimica Acta, 59(7), 1217-1232.

Whitney, D., Teyssier, C., Vanderhaeghe, O., 2004. Gneiss Domes and Crustal Flow. In: Geological Society of America Special Papers, vol. 380. http://dx.doi.org/10.1130/0-8137-2380-9.15, pp. 15e33.

Woodhead. J, Hergt. J, Shelley. M,. Eggins S,. and Kemp, R. 2004. Zircon Hf-isotope analysis with an excimer laser, depth profiling, ablation of complex geometries and concomitant age estimation. Chem Geol 209: 121-135.

Zeh, A., Gerdes, A., Klemd, R. And Barton Jr. J. M., 2007. Archaean to Proterozoic Crustal Evolution in the Central Zone of the Limpopo Belt (South

Africa-Botswana): Constraints from Combined U-Pb and Lu-Hf Isotope Analyses of Zircon. J Petrol 48: 1605–1639.

Anexo II. Tabelas das análises U-Pb (LA-ICP-MS)

Tabela II.1. Dados da análise U-Pb por LA-ICP-MS da amostra AE-11B (Migmatito).

AMOSTRA	AE-11B											Idades aparentes					
GRÃO	f 206 (%)	Th/U	206Pb/204Pb	207Pb/206Pb	err (%) 1σ	207Pb/235U	err (%) 1σ	206Pb/238U	err (%) 1σ	207Pb/206Pb	2σ	207Pb/235U	2σ	206Pb/238U	2σ	Rho	conc. (%)
ZR18B	0.42	0.15	224613	0.26984	0.9	22.51603	1.2	0.60513	0.8	3305	28	3206	24	3050	38	0.632	92
ZR9B	1.71	0.12	713555	0.27377	0.6	21.18172	1.3	0.56109	1.1	3328	18	3147	25	2871	50	0.848	86
ZR14	3.25	0.14	266153	0.27522	0.8	22.05752	1.4	0.58121	1.1	3336	24	3186	27	2954	52	0.790	89
ZR11	1.27	0.11	4187	0.27867	1.7	21.81334	2.6	0.56767	2.0	3356	51	3175	50	2898	93	0.761	86
ZR2	1.82	0.08	889879	0.27931	0.4	24.68145	0.8	0.64085	0.6	3359	12	3296	16	3192	31	0.748	95
ZR9B2	0.80	0.39	19671	0.27998	0.8	21.84983	2.9	0.56597	2.8	3363	26	3177	56	2891	129	0.949	86
ZR14B	1.51	0.26	179908	0.28428	2.0	25.76517	2.6	0.65729	1.6	3387	63	3338	51	3257	82	0.612	96
ZR12B3	3.83	0.23	49460	0.28614	1.8	22.66767	2.3	0.57450	1.4	3397	57	3213	45	2926	66	0.603	86
ZR9	1.73	0.45	679637	0.28686	0.4	28.07861	1.3	0.70987	1.2	3401	13	3422	26	3458	65	0.908	102
ZR12	0.70	0.45	379205	0.28875	0.5	27.22343	0.9	0.68373	0.6	3411	15	3392	17	3359	33	0.715	98
ZR5	0.63	0.27	319413	0.29625	0.6	27.51625	1.2	0.67360	1.0	3451	18	3402	23	3320	50	0.815	96
ZR12B2	1.79	0.36	344678	0.29656	1.4	28.03299	1.7	0.68553	0.9	3452	42	3420	33	3366	49	0.547	97
ZR18N	0.75	0.30	197538	0.29735	0.5	33.03049	1.5	0.80558	1.4	3456	15	3582	30	3809	80	0.914	110
ZR11B4	2.21	0.10	775212	0.29844	0.7	26.00694	2.0	0.63198	1.9	3462	22	3347	40	3157	94	0.922	91
ZR12B	1.99	0.12	220053	0.31063	0.8	31.86333	1.7	0.74391	1.4	3524	24	3546	33	3585	79	0.858	102
ZR16N	1.72	0.32	684319	0.10405	1.0	2.37605	2.5	0.16553	2.3	1698	36	1235	36	987	42	0.913	58
ZR6B	2.37	0.05	81	0.10516	4.8	0.70673	5.0	0.04874	1.2	1717	172	543	42	307	7	0.248	18
ZR16B	1.64	0.08	298027	0.11128	0.8	2.91705	1.6	0.19016	1.4	1820	27	1387	25	1122	29	0.861	62
ZR13	0.92	0.04	213	0.11552	2.8	1.24952	3.9	0.07844	2.7	1888	100	823	44	487	26	0.692	26
ZR13B	1.75	0.03	241	0.12206	1.0	1.54913	1.3	0.09204	0.7	1987	35	950	15	568	7	0.540	29
ZR17B	0.21	0.19	99221	0.12823	1.0	5.84178	2.0	0.33039	1.6	2074	35	1953	34	1840	52	0.938	89
ZR1B	0.22	0.20	119054	0.13111	0.8	6.97916	1.4	0.38605	1.0	2113	29	2109	24	2105	37	0.752	100
ZR7B	0.81	0.24	374874	0.13122	0.8	5.53605	2.9	0.30595	2.7	2114	27	1906	49	1721	83	0.955	81
ZR1N	0.18	0.18	87429	0.13215	0.9	6.93911	1.4	0.38080	1.0	2127	31	2104	25	2080	37	0.727	98
ZR1B2	0.18	0.19	99906	0.13304	0.8	7.03241	1.3	0.38334	1.0	2138	29	2116	24	2092	35	0.732	98
ZR17	0.28	0.33	124832	0.13581	0.5	7.16859	1.0	0.38279	0.8	2174	19	2133	18	2089	27	0.756	96
ZR7N	0.76	0.27	162951	0.13609	0.5	6.57960	1.1	0.35062	0.9	2178	17	2057	19	1938	30	0.821	89
ZR4	1.05	0.51	700	0.13711	3.0	3.18257	6.4	0.16833	5.7	2191	104	1453	97	1003	105	0.880	46
ZR8B2	0.17	0.32	79385	0.13941	0.8	7.47576	1.5	0.38889	1.1	2220	28	2170	26	2118	41	0.785	95
ZR3	0.86	0.43	457	0.14204	5.9	2.16532	7.3	0.11056	4.3	2252	197	1170	99	676	55	0.584	30
ZR8N	0.88	0.02	536	0.16279	7.5	1.94978	8.1	0.08686	3.0	2485	242	1098	105	537	31	0.369	22
ZR8B	1.19	0.03	143	0.17615	2.5	1.34436	3.2	0.05535	1.9	2617	82	865	37	347	13	0.597	13

continuação Dados da análise U-Pb por LA-ICP-MS da amostra AE-11B (Migmatito).

AMOSTRA	AE-11B																	
										Idades aparentes								
GRÃO	f 206 (%)	$\frac{Th}{U}$	$\frac{^{206}Pb}{^{204}Pb}$	$\frac{^{207}Pb}{^{206}Pb}$	err (%) 1 σ	$\frac{^{207}Pb}{^{235}U}$	err (%) 1 σ	$\frac{^{206}Pb}{^{238}U}$	err (%) 1 σ	$\frac{^{207}Pb}{^{206}Pb}$	2 σ	$\frac{^{207}Pb}{^{235}U}$	2 σ	$\frac{^{206}Pb}{^{238}U}$	2 σ	Rho	conc. (%)
ZR6B3	3.76	0.07	117	0.17721	13.7	1.88702	14.1	0.07722	3.3	2627	424	1077	180	480	31	0.234	18
ZR13B3	2.26	0.03	231	0.17888	2.5	2.34183	2.8	0.09494	1.3	2643	82	1225	40	585	14	0.450	22
ZR11B2	0.83	0.13	475014	0.17957	1.6	8.54260	1.9	0.34500	1.0	2649	53	2290	35	1911	32	0.511	72
ZR11B3	1.40	0.07	401357	0.19205	3.4	12.40153	3.5	0.47171	0.9	2760	100	2642	65	2491	37	0.253	90
ZR13B2	2.07	0.03	200	0.20104	2.6	2.98003	3.1	0.10750	1.7	2835	83	1403	46	658	21	0.537	23
ZR18	1.32	0.09	47140	0.24745	0.7	10.38034	5.8	0.30423	5.7	3169	23	2469	104	1712	170	0.990	54
ZR11B	1.10	0.07	468397	0.24925	0.8	15.34542	1.2	0.44649	0.8	3180	24	2837	22	2380	32	0.686	75
ZR11	1.04	0.06	54626	0.26125	0.7	10.25254	6.6	0.28461	6.5	3254	22	2458	118	1615	185	0.993	50
ZR10	0.56	0.26	186302	0.28619	0.5	20.53141	1.4	0.52028	1.3	3397	16	3117	27	2700	55	0.894	79
ZR15	2.28	0.04	55	0.28790	0.9	2.04330	1.3	0.05147	0.8	3406	28	1130	17	324	5	0.638	9
ZR6	1.86	0.03	91	0.33359	0.7	0.79206	7.1	0.01724	7.1	3634	21	593	63	110	15	0.994	3
ZR6B4	1.32	0.05	71	0.33488	2.2	2.47412	8.6	0.05358	8.3	3640	68	1264	121	336	54	0.965	9
ZR15B	1.47	0.03	99	0.40338	1.8	0.61244	33.4	0.01101	33.4	3922	52	485	243	71	47	0.999	2
ZR6B2	1.18	0.05	48	0.44436	3.8	1.73806	8.1	0.02837	7.1	4066	112	1023	102	180	25	0.878	4

Tabela II.2. Dados da análise U-Pb por LA-ICP-MS da amostra AE-23A (Migmatito).

AMOSTRA	AE-23A																	
										Idades aparentes								
GRÃO	f_{206} (%)	Th/U	206Pb/204Pb	207Pb/206Pb	err (%) 1σ	207Pb/235U	err (%) 1σ	206Pb/238U	err (%) 1σ	207Pb/206Pb	2σ	207Pb/235U	2σ	206Pb/238U	2σ	Rho	conc. (%)
ZR23B2	0.04	0.04	74348	0.05935	0.6	0.72407	1.4	0.08848	1.3	580	26	553	12	547	13	0.876	94
ZR53B2	0.03	0.24	62613	0.05981	1.3	0.76377	1.6	0.09260	0.9	597	54	576	14	571	9	0.548	96
ZR53B	0.01	0.28	44835	0.05994	1.6	0.79545	2.5	0.09624	2.0	601	67	594	23	592	22	0.772	99
ZR23B4	0.40	0.03	409360	0.10650	0.6	3.04700	1.2	0.20749	0.9	1740	22	1419	18	1215	21	0.800	70
ZR19B	0.09	0.16	117536	0.11224	3.2	5.23451	3.9	0.33821	2.1	1836	114	1858	65	1878	68	0.545	102
ZR23	0.46	0.03	29940	0.11995	0.4	5.80319	0.8	0.35085	0.6	1956	15	1947	14	1939	20	0.729	99
ZR19B2	0.11	0.19	393888	0.12129	0.5	5.81459	0.9	0.34766	0.7	1975	19	1949	16	1923	23	0.726	97
ZR50	0.39	0.03	556751	0.19103	3.6	9.68683	4.3	0.36775	2.2	2751	117	2405	77	2019	77	0.519	73
ZR40	0.18	0.04	1441	0.19564	2.4	10.60785	3.2	0.39321	2.1	2790	77	2489	58	2138	75	0.652	77
ZR35B	0.42	0.06	938	0.19726	3.2	12.05437	4.2	0.44318	2.6	2804	103	2609	77	2365	103	0.630	84
ZR9N	0.53	0.03	345230	0.20521	0.4	13.63905	1.0	0.48201	0.9	2868	13	2725	20	2536	37	0.849	88
ZR9B2	0.45	0.03	135542	0.20645	0.5	14.37437	1.0	0.50494	0.8	2878	16	2775	19	2635	35	0.788	92
ZR27B	0.41	0.03	15317	0.20898	0.8	13.61665	1.2	0.47254	0.8	2898	25	2723	22	2495	32	0.663	86
ZR19N	0.38	0.02	747991	0.21199	0.6	15.83400	1.3	0.54168	1.1	2921	19	2867	25	2790	50	0.847	96
ZR24	0.58	0.05	38018	0.21205	0.6	18.68997	4.9	0.60189	4.9	2921	21	2947	35	2985	81	0.993	102
ZR53	0.55	0.03	62624	0.21304	1.5	15.27734	1.9	0.52005	1.1	2929	47	2833	35	2699	47	0.571	92
ZR21B2	0.23	0.35	4738	0.21829	1.3	15.78733	4.7	0.52449	4.5	2968	42	2864	87	2718	196	0.955	92
ZR20B	0.24	0.06	5284	0.21842	0.8	17.22101	1.8	0.58896	1.7	2969	24	2968	64	2967	154	0.917	100
ZR36B	0.15	0.09	6580	0.21949	1.6	12.30138	4.5	0.40645	4.2	2977	52	2628	83	2199	155	0.928	74
ZR33B	0.60	0.02	192450	0.22131	1.0	18.24402	1.7	0.59785	1.3	2990	31	3003	32	3021	65	0.793	101
ZR46B	0.67	0.04	17320	0.22326	0.5	14.82608	1.9	0.48160	1.8	3004	16	2804	35	2534	74	0.941	84
ZR11	0.26	0.08	176798	0.22519	0.5	18.33713	2.0	0.57614	1.8	3018	15	3026	93	3037	235	0.910	101
ZR25N	0.60	0.02	1773430	0.22736	1.4	21.09781	2.2	0.67297	1.6	3034	44	3143	42	3317	83	0.745	109
ZR34B	0.58	0.05	155929	0.22996	2.9	15.78983	3.5	0.49795	1.9	3052	92	2864	66	2605	83	0.547	85
ZR20B2	0.04	0.37	135491	0.23024	0.5	18.78908	1.1	0.59181	0.9	3054	15	3031	21	2997	44	0.836	98
ZR21B	0.39	0.07	11661	0.23082	0.7	17.60370	3.4	0.58450	3.3	3058	23	3008	37	2933	83	0.968	96
ZR13B	0.22	0.02	537818	0.24912	0.4	19.28466	0.8	0.56139	0.6	3179	13	3056	16	2872	30	0.765	90
ZR31	0.09	0.31	268439	0.25590	0.5	20.11942	1.1	0.57019	0.9	3222	17	3097	21	2909	40	0.801	90
ZR2	0.22	0.29	628853	0.25634	0.4	21.68614	0.9	0.61353	0.8	3224	13	3170	18	3084	37	0.810	96
ZR5B	0.45	0.24	624303	0.25902	0.6	23.66122	1.0	0.66248	0.7	3241	19	3255	19	3277	34	0.681	101
ZR1N	0.27	0.23	763850	0.25902	0.4	21.36520	0.9	0.59818	0.7	3241	14	3155	18	3023	34	0.779	93
ZR45	0.23	0.29	643328	0.26030	0.5	22.93281	0.9	0.63893	0.7	3248	15	3224	18	3185	35	0.757	98

continuação Dados da análise U-Pb por LA-ICP-MS da amostra AE-23A (Migmatito).

AMOSTRA	AE-23A										Idades aparentes					
GRÃO	*f* 206 (%)	Th/U	206Pb/204Pb	207Pb/206Pb	err (%) 1 σ	207Pb/235U	err (%) 1 σ	206Pb/238U	err (%) 1 σ	207Pb/206Pb	2 σ	207Pb/235U	2 σ	206Pb/238U	2 σ	Rho	conc. (%)
ZR18B	0.24	0.12	322209	0.26031	0.4	21.83729	0.9	0.60839	0.7	3249	14	3177	18	3064	36	0.783	94
ZR41B	0.20	0.21	228819	0.26163	2.9	23.46315	3.9	0.65038	2.6	3257	91	3246	75	3230	129	0.653	99
ZR31B	0.26	0.07	1041475	0.26198	0.6	23.35255	1.3	0.64645	1.1	3259	18	3242	24	3214	53	0.842	99
ZR43B3	0.21	0.64	438333	0.26269	2.5	24.59481	3.8	0.67899	2.8	3263	78	3292	72	3340	145	0.740	102
ZR43B	0.25	0.57	16387	0.26275	0.5	18.77540	1.4	0.51821	1.2	3263	14	3030	26	2692	55	0.903	82
ZR49	0.21	0.18	11283	0.26340	0.6	25.86004	4.0	0.71199	3.9	3267	20	3341	76	3466	208	0.983	106
ZR4	0.13	0.10	498926	0.26487	0.4	22.71133	0.9	0.62184	0.7	3276	14	3215	17	3117	34	0.774	95
ZR5N	0.17	0.29	501511	0.26671	0.5	24.53601	0.9	0.66715	0.6	3287	16	3290	17	3295	31	0.680	100
ZR4B2	0.22	0.14	647104	0.26739	1.6	23.44617	2.1	0.63590	1.4	3291	49	3246	41	3173	71	0.657	96
ZR43B4	0.11	0.38	410422	0.27018	0.5	21.46502	1.6	0.57616	1.5	3307	16	3160	32	2933	71	0.923	89
ZR10N2	0.04	0.33	49604	0.27076	1.4	22.86113	2.3	0.61231	1.8	3310	43	3221	44	3079	86	0.780	93
ZR43	0.09	0.36	259300	0.27115	1.4	21.29666	1.9	0.56960	1.2	3313	43	3152	36	2906	58	0.656	88
ZR43B2	0.20	0.62	201107	0.27351	1.0	23.25574	1.6	0.61662	1.2	3326	31	3238	31	3096	59	0.753	93
ZR41	0.40	0.47	133818	0.27425	0.8	24.17482	2.5	0.63928	2.4	3330	26	3275	49	3186	119	0.933	96
ZR25B2	0.16	0.14	143608	0.12206	0.4	4.73279	1.4	0.28119	1.3	1987	16	1773	24	1597	36	0.911	80
ZR27N	0.46	0.02	81441	0.15271	1.6	9.23559	2.1	0.43860	1.2	2376	54	2362	37	2344	48	0.601	99
ZR10B	0.29	0.09	2618	0.18708	0.9	5.41200	4.7	0.20980	4.6	2717	30	1887	79	1228	103	0.978	45
ZR9B	0.36	0.03	1062	0.19731	1.0	7.15237	4.3	0.26289	4.1	2804	34	2131	75	1505	111	0.967	54
ZR14N	0.43	0.02	2714	0.19823	0.7	7.25242	3.7	0.26532	3.6	2812	22	2143	65	1517	97	0.977	54
ZR17B	0.46	0.03	14968	0.20030	0.5	11.70728	1.7	0.42388	1.6	2829	17	2581	32	2278	61	0.925	81
ZR30	0.43	0.02	9268	0.20199	1.5	10.67134	4.9	0.38314	4.7	2842	49	2495	89	2091	165	0.949	74
ZR24B	0.67	0.05	1072218	0.20360	1.8	15.79232	2.2	0.56251	1.2	2855	59	2864	42	2877	57	0.553	101
ZR21N	0.22	0.06	16373	0.22201	0.6	15.02367	2.3	0.49077	2.2	2995	18	2817	44	2574	95	0.958	86
ZR7B	0.41	0.02	570879	0.22547	0.6	15.28896	1.3	0.49177	1.1	3020	18	2833	25	2578	48	0.859	85
ZR7N	0.45	0.06	52076	0.23380	1.6	15.24026	4.8	0.47272	4.4	3078	52	2830	89	2495	193	0.935	81
ZR8	0.44	0.02	27422	0.24344	1.7	19.12680	2.9	0.56979	2.3	3143	53	3048	55	2907	109	0.806	93
ZR26	0.34	0.25	441391	0.28377	0.9	29.54541	3.1	0.75507	3.0	3384	27	3472	61	3626	165	0.953	107
ZR10N	0.03	0.30	37273	0.28829	0.8	31.85407	2.6	0.80130	2.5	3408	26	3546	51	3794	141	0.937	111
ZR28B	0.05	0.25	176930	0.29232	1.4	25.59622	1.7	0.63502	0.8	3430	42	3331	32	3169	42	0.506	92
ZR28N	0.18	0.44	93508	0.30141	0.6	26.81201	1.3	0.64511	1.1	3478	17	3377	25	3209	56	0.854	92

Tabela II.3. Dados da análise U-Pb por LA-ICP-MS da amostra AE-24B (Melanossoma).

AMOSTRA	AE-24B										Idades aparentes						
GRÃO	f 206 (%)	Th/U	206Pb/204Pb	207Pb/206Pb	err (%) 1σ	207Pb/235U	err (%) 1σ	206Pb/238U	err (%) 1σ	207Pb/206Pb	2σ	207Pb/235U	2σ	206Pb/238U	2σ	Rho	conc. (%)
ZR29	0.35	0.07	143374	0.05844	0.7	0.70579	1.5	0.08759	1.3	546	29	542	12	541	13	0.862	99
ZR5B	3.24	0.02	1135008	0.05847	0.6	0.76305	1.1	0.09465	0.8	547	28	576	9	583	8	0.715	107
ZR5N	0.63	0.02	170895	0.05860	0.6	0.76055	1.0	0.09412	0.7	552	27	574	9	580	7	0.677	105
ZR70	1.26	0.05	308728	0.05882	0.5	0.75246	0.9	0.09278	0.6	560	21	570	7	572	7	0.704	102
ZR32B	0.47	0.04	137127	0.05888	0.5	0.75493	0.9	0.09299	0.6	563	21	571	7	573	7	0.699	102
ZR55	0.82	0.04	375331	0.05895	0.4	0.75317	0.8	0.09265	0.5	565	18	570	7	571	6	0.685	101
ZR69	0.69	0.11	189500	0.05905	0.7	0.74470	0.9	0.09147	0.6	569	28	565	8	564	6	0.608	99
ZR70B	0.65	0.04	132085	0.05926	0.5	0.75304	0.8	0.09215	0.5	577	22	570	7	568	5	0.625	99
ZR53	0.50	0.08	156786	0.05968	0.4	0.74106	0.8	0.09004	0.5	592	19	563	7	556	6	0.675	94
ZR19	3.35	0.07	653318	0.12138	0.5	5.42051	1.2	0.32386	1.1	1977	17	1888	21	1809	34	0.869	91
ZR71	0.35	0.25	101063	0.12158	0.5	5.39677	0.9	0.32191	0.7	1980	18	1884	15	1799	21	0.732	91
ZR60	0.73	0.35	376558	0.12159	0.5	5.71788	0.8	0.34104	0.6	1980	17	1934	15	1892	19	0.700	96
ZR3	0.65	0.36	558201	0.12183	0.5	5.66593	0.9	0.33727	0.7	1983	17	1926	16	1874	23	0.768	94
ZR63	2.92	0.13	796266	0.12267	0.5	5.50321	0.9	0.32534	0.7	1995	18	1901	15	1816	21	0.727	91
ZR43B	0.73	0.33	337059	0.12281	0.4	5.65572	0.8	0.33398	0.5	1997	14	1925	13	1858	18	0.705	93
ZR9B	0.85	0.31	305088	0.12304	0.5	5.81002	0.9	0.34246	0.7	2001	17	1948	15	1899	22	0.733	95
ZR11B	0.89	0.32	279269	0.12310	0.5	6.14949	0.9	0.36228	0.7	2002	19	1997	16	1993	23	0.720	100
ZR9	0.39	0.25	181514	0.12311	0.6	5.91081	1.0	0.34819	0.7	2002	22	1963	18	1926	24	0.708	96
ZR3B	0.58	0.34	310995	0.12326	0.5	5.83944	1.0	0.34357	0.8	2004	18	1952	18	1904	27	0.791	95
ZR61	1.24	0.22	288782	0.12327	0.6	5.42775	1.3	0.31933	1.1	2004	21	1889	22	1786	34	0.838	89
ZR32	1.52	0.41	1294135	0.12344	0.3	5.82636	0.8	0.34230	0.6	2007	12	1950	13	1898	19	0.754	95
ZR30	3.28	0.04	905890	0.12450	0.5	5.76251	1.3	0.33566	1.1	2022	18	1941	22	1866	36	0.869	92
ZR8B	3.83	0.20	724316	0.12846	0.5	5.77897	0.9	0.32624	0.7	2077	16	1943	15	1820	22	0.758	88
ZR4	2.52	0.20	9103	0.12956	1.0	5.76813	2.3	0.32287	2.0	2092	35	1942	39	1804	64	0.883	86
ZR33	4.24	0.38	478231	0.12967	0.4	6.43858	1.1	0.36008	0.9	2094	15	2038	19	1983	31	0.852	95
ZR13	1.64	0.23	593310	0.12985	0.5	6.34080	1.0	0.35414	0.8	2096	16	2024	18	1954	28	0.813	93
ZR34	2.89	0.40	26573	0.13008	0.5	6.30382	1.3	0.35145	1.1	2099	17	2019	22	1942	37	0.877	92
ZR26	3.92	0.24	44620	0.13026	0.4	6.08081	1.7	0.33856	1.6	2101	13	1987	29	1880	51	0.948	89
ZR23	3.28	0.17	670171	0.13048	0.8	6.39467	1.5	0.35542	1.2	2104	28	2032	26	1960	40	0.801	93
ZR58	2.55	0.23	387503	0.13059	0.4	6.76669	1.5	0.37577	1.4	2106	13	2081	26	2057	48	0.932	98
ZR52	2.35	0.11	254519	0.13067	0.3	6.34758	0.7	0.35228	0.5	2107	10	2025	12	1945	17	0.738	92
ZR17	2.81	0.28	353459	0.13070	0.6	6.16431	1.0	0.34205	0.6	2107	22	1999	17	1897	21	0.658	90

continuação Dados da análise U-Pb por LA-ICP-MS da amostra AE-24B (Melanossoma).

AMOSTRA	AE-24B																	
										Idades aparentes								
GRÃO	*f* 206 (%)	Th / U	206Pb / 204Pb	207Pb / 206Pb	err (%) 1 σ	207Pb / 235U	err (%) 1 σ	206Pb / 238U	err (%) 1 σ	207Pb / 206Pb	2 σ	207Pb / 235U	2 σ	206Pb / 238U	2 σ	Rho	conc. (%)
ZR4	5.45	0.29	1904056	0.13136	0.4	6.89409	0.8	0.38062	0.6	2116	15	2098	15	2079	22	0.728	98
ZR6	3.91	0.31	187344	0.13147	0.7	6.53861	1.1	0.36069	0.7	2118	24	2051	19	1985	25	0.689	94
ZR37	2.59	0.23	90109	0.13152	0.4	5.72120	1.7	0.31547	1.6	2118	14	1935	29	1768	49	0.948	83
ZR22	3.80	0.15	349840	0.13183	0.8	6.83962	1.2	0.37625	0.9	2123	29	2091	22	2059	30	0.686	97
ZR8N	5.19	0.27	1569304	0.13215	0.5	7.13936	0.9	0.39180	0.6	2127	17	2129	16	2131	23	0.721	100
ZR43	3.90	0.23	27715	0.13227	0.4	6.61905	1.3	0.36291	1.2	2128	16	2062	23	1996	41	0.900	94
ZR72	2.96	0.38	6882	0.13252	0.5	7.40717	2.8	0.40536	2.7	2132	16	2162	49	2194	101	0.978	103
ZR54	3.76	0.34	448810	0.13306	1.0	6.35838	1.2	0.34654	0.5	2139	36	2027	21	1918	18	0.448	90
ZR27	1.46	0.31	349819	0.13326	0.7	7.63983	3.2	0.41577	3.1	2141	24	2190	56	2241	116	0.970	105
ZR64	2.74	0.31	75291	0.13335	0.5	6.92069	0.9	0.37638	0.6	2143	16	2101	15	2059	22	0.720	96
ZR14B	3.89	0.28	2738044	0.13381	0.4	7.06165	0.8	0.38273	0.6	2149	16	2119	15	2089	22	0.724	97
ZR48	2.91	0.30	314036	0.13393	0.7	6.63148	2.1	0.35908	2.0	2150	23	2064	37	1978	67	0.933	92
ZR40	3.69	0.43	166329	0.13404	0.5	6.80358	1.2	0.36810	1.1	2152	16	2086	21	2020	37	0.871	94
ZR67	2.14	0.18	864623	0.13420	0.5	6.77751	0.8	0.36625	0.5	2154	19	2083	15	2012	18	0.634	93
ZR35	3.81	0.34	533810	0.13456	0.3	7.24048	1.7	0.39023	1.7	2158	12	2142	31	2124	60	0.956	98
ZR14	1.32	0.38	462535	0.13514	0.5	6.72496	1.0	0.36089	0.8	2166	16	2076	17	1986	27	0.800	92
ZR49	2.28	0.43	355251	0.13588	0.4	6.99540	0.8	0.37334	0.6	2175	13	2111	14	2045	21	0.744	94
ZR20	2.57	0.37	673304	0.13592	0.5	7.65780	0.9	0.40859	0.6	2176	17	2192	16	2208	24	0.725	102
ZR1	2.73	0.39	217028	0.13600	0.6	7.37614	2.6	0.39333	2.5	2177	21	2158	46	2138	90	0.961	98
ZR38	1.33	0.45	141869	0.13637	0.6	7.50885	0.9	0.39931	0.6	2182	20	2174	16	2166	22	0.665	99
ZR68	1.97	0.28	584508	0.13681	0.6	7.70375	0.9	0.40837	0.6	2187	21	2197	17	2207	22	0.644	101
ZR36	1.05	0.35	380836	0.13703	0.4	7.61413	0.8	0.40297	0.6	2190	14	2187	15	2183	22	0.736	100
ZR44	2.50	0.39	241041	0.13842	0.5	7.42950	1.2	0.38926	1.0	2207	18	2165	22	2119	37	0.848	96
ZR47	1.55	0.30	637052	0.13996	0.4	7.93012	0.8	0.41090	0.6	2227	14	2223	14	2219	21	0.706	100
ZR10N	0.28	0.26	1422996	0.18029	1.1	12.26959	1.6	0.49354	1.1	2656	38	2625	30	2586	45	0.665	97
ZR10B	0.42	0.32	161840	0.18343	0.6	12.98735	1.0	0.51348	0.8	2684	21	2679	20	2671	33	0.720	100
ZR18	1.31	0.32	365634	0.21331	0.5	14.52865	0.9	0.49396	0.7	2931	17	2785	18	2588	28	0.711	88
ZR18B	1.05	0.38	412934	0.22317	0.7	16.99431	1.9	0.55226	1.7	3004	21	2935	35	2835	77	0.911	94
ZR7	2.72	0.21	795454	0.22753	0.6	19.89801	1.6	0.63421	1.5	3035	20	3086	31	3166	73	0.894	104
ZR24	2.44	0.45	541383	0.23326	0.4	18.56327	1.1	0.57715	0.9	3075	14	3019	21	2937	43	0.844	96
ZR25	0.45	0.47	107988	0.23680	0.5	18.25543	1.2	0.55909	1.0	3099	16	3003	22	2863	46	0.850	92
ZR12B2	4.58	0.03	1375991	0.24886	0.4	19.42435	1.0	0.56606	0.8	3178	13	3063	19	2892	39	0.829	91

continuação Dados da análise U-Pb por LA-ICP-MS da amostra AE-24B (Melanossoma).

AMOSTRA	AE-24B										Idades aparentes					
GRÃO	*f* 206 (%)	$\frac{Th}{U}$	$\frac{206Pb}{204Pb}$	$\frac{207Pb}{206Pb}$	err (%) 1 σ	$\frac{207Pb}{235U}$	err (%) 1 σ	$\frac{206Pb}{238U}$	err (%) 1 σ	$\frac{207Pb}{206Pb}$	2 σ	$\frac{207Pb}{235U}$	2 σ	$\frac{206Pb}{238U}$	2 σ	Rho	conc. (%)
ZR12B	4.11	0.03	907559	0.25778	0.5	21.13796	0.9	0.59468	0.6	3233	15	3145	17	3008	31	0.728	93
ZR12	0.57	0.12	206192	0.27263	0.6	22.88389	1.4	0.60873	1.2	3321	18	3222	27	3065	59	0.873	92
ZR66B	0.75	0.06	4673540	0.05832	0.5	0.75273	0.8	0.09361	0.6	542	21	570	7	577	6	0.688	107
ZR69B	0.53	0.10	271610	0.06036	0.7	0.73847	1.0	0.08872	0.6	617	20	562	8	548	6	0.628	89
ZR55B	0.99	0.07	33490	0.06345	0.5	0.80587	0.8	0.09210	0.6	723	19	600	8	568	6	0.710	79
ZR56	0.03	0.04	16633	0.07431	5.4	0.98322	7.1	0.09596	4.5	1050	212	695	70	591	51	0.640	56
ZR15	1.22	0.24	186202	0.10159	3.1	4.36456	3.9	0.31156	2.3	1653	114	1706	64	1748	71	0.593	106
ZR41	0.68	0.34	157558	0.11981	0.5	4.82103	0.9	0.29182	0.6	1953	19	1780	15	1651	17	0.669	85
ZR16	2.58	0.19	94924	0.12039	1.0	4.88199	3.6	0.24589	3.4	1962	34	1651	57	1417	86	0.957	72
ZR50	3.37	0.32	29340	0.12747	0.9	5.15150	3.4	0.29309	3.3	2063	31	1845	58	1657	96	0.961	80
ZR2	3.44	0.06	1215280	0.12822	0.5	6.28831	0.8	0.35568	0.6	2074	17	2017	15	1962	19	0.666	95
ZR21	3.71	0.22	140364	0.12865	0.5	6.60441	1.6	0.37228	1.5	2080	16	2060	28	2040	53	0.931	98
ZR28	4.57	0.34	9236	0.13268	0.9	5.94075	3.0	0.32495	2.9	2132	30	1967	52	1814	91	0.962	85
ZR31	1.92	0.40	198970	0.13375	0.4	5.69862	2.0	0.30844	1.9	2148	16	1930	34	1733	58	0.957	81
ZR39	2.26	0.21	15770	0.13473	0.6	6.32244	1.8	0.34033	1.7	2160	22	2022	32	1888	55	0.915	87
ZR11N	2.86	0.34	2837	0.13820	0.9	5.52674	2.9	0.29001	2.7	2205	32	1905	49	1642	78	0.937	74
ZR51	3.88	0.28	29221	0.13878	0.8	8.21030	2.2	0.42905	2.0	2212	29	2254	39	2301	77	0.908	104

Tabela II.4. Dados da análise U-Pb por LA-ICP-MS da amostra AE-24C (Leucossoma).

AMOSTRA	AE-24C											Idades aparentes					
GRÃO	*f* 206 (%)	Th/U	206Pb/204Pb	207Pb/206Pb	err (%) 1 σ	207Pb/235U	err (%) 1 σ	206Pb/238U	err (%) 1 σ	207Pb/206Pb	2 σ	207Pb/235U	2 σ	206Pb/238U	2 σ	Rho	conc. (%)
ZR22	0.45	0.31	7543	0.13311	0.4	6.65274	1.1	0.36245	0.9	2139	15	2066	19	1994	32	0.853	93
ZR17	0.44	0.36	115705	0.13367	0.4	6.89875	1.5	0.37430	1.4	2147	13	2098	26	2050	48	0.937	95
ZR6	0.39	0.33	100745	0.13403	0.3	6.55384	0.9	0.35462	0.8	2151	11	2053	16	1957	26	0.848	91
ZR24	0.29	0.30	57499	0.13450	0.6	7.66933	2.0	0.41351	1.9	2158	20	2193	35	2231	70	0.939	103
ZR8	0.30	0.32	693062	0.13460	0.3	7.13530	1.0	0.38446	0.8	2159	12	2128	17	2097	30	0.855	97
ZR5	0.28	0.24	387536	0.13482	0.5	7.16160	1.6	0.38523	1.5	2162	16	2132	28	2101	52	0.926	97
ZR14	0.29	0.29	116245	0.13515	0.3	7.47024	0.8	0.40085	0.7	2166	11	2169	15	2173	24	0.797	100
ZR32	0.22	0.35	355914	0.13550	0.5	7.64757	0.9	0.40930	0.7	2170	17	2190	16	2212	25	0.729	102
ZR7	0.48	0.28	1935882	0.13593	1.0	7.72189	1.5	0.41197	1.1	2176	34	2199	27	2224	41	0.724	102
ZR29	0.25	0.31	226177	0.13633	0.5	7.51225	0.9	0.39963	0.7	2181	16	2174	17	2167	26	0.762	99
ZR12	0.38	0.31	850084	0.13673	0.3	7.82054	0.7	0.41479	0.6	2186	9	2211	13	2237	21	0.772	102
ZR21	0.17	0.08	21555	0.11641	0.5	3.88056	1.0	0.24175	0.8	1902	18	1610	16	1396	20	0.778	73
ZR32B	0.07	0.19	240780	0.12153	0.5	5.43547	1.1	0.32434	0.9	1979	18	1890	18	1811	28	0.811	92
ZR24	0.30	0.20	218712	0.12211	0.7	6.07375	1.4	0.36071	1.1	1987	24	1986	24	1986	39	0.825	100
ZR28	0.34	0.32	6552	0.12320	1.7	4.39062	3.3	0.25845	2.8	2003	59	1711	54	1482	74	0.854	74
ZR19	0.43	0.04	17628	0.12341	0.9	5.33809	5.5	0.31368	5.4	2006	33	1875	92	1759	166	0.983	88
ZR31	0.27	0.32	4488	0.12453	0.7	4.29877	2.0	0.25034	1.8	2022	26	1693	32	1440	46	0.911	71
ZR27	0.52	0.25	1002505	0.12561	0.5	5.76042	0.9	0.33257	0.7	2037	16	1940	16	1851	23	0.770	91
ZR26	0.33	0.29	2602	0.12798	0.5	4.46067	1.0	0.25329	0.8	2070	16	1725	16	1455	20	0.791	70
ZR18	0.17	0.17	504604	0.12888	0.4	6.44402	0.8	0.36259	0.6	2083	13	2038	13	1994	19	0.721	96
ZR13	0.32	0.26	664450	0.12930	0.4	7.52543	1.0	0.42207	1.0	2089	15	2176	34	2270	71	0.957	109
ZR1	0.25	0.16	419207	0.12952	1.4	7.09141	4.0	0.44745	3.7	2091	48	2230	71	2384	147	0.935	114
ZR6	0.32	0.31	287118	0.12990	1.4	5.90398	3.4	0.32962	3.0	2097	49	1962	58	1837	96	0.901	88
ZR30	0.33	0.35	907665	0.13036	0.4	6.38752	1.0	0.35535	0.8	2103	15	2031	17	1960	26	0.813	93
ZR16	0.36	0.22	172407	0.13067	0.5	7.09389	1.5	0.39371	1.4	2107	16	2123	27	2140	50	0.918	102
ZR25	0.31	0.27	665168	0.13067	0.5	7.68822	3.2	0.42669	3.1	2107	19	2195	57	2291	120	0.979	109
ZR8	0.35	0.31	221520	0.13115	0.5	6.23741	1.1	0.34490	0.9	2113	18	2010	20	1910	31	0.836	90
ZR46	0.28	0.35	20991	0.13160	0.7	6.32692	1.9	0.34893	1.7	2118	26	2022	33	1929	58	0.901	91
ZR20	0.32	0.28	10085	0.13160	0.6	7.13966	2.2	0.39346	2.0	2119	22	2129	38	2139	74	0.940	101
ZR4	0.34	0.28	302517	0.13236	0.3	6.94124	1.0	0.38033	0.8	2129	12	2104	17	2078	30	0.857	98
ZR48	0.33	0.36	7500	0.13253	2.0	6.57181	3.5	0.35963	2.8	2132	70	2056	61	1980	96	0.810	93
ZR10	0.22	0.13	111429	0.13267	0.8	7.03112	1.3	0.38435	1.0	2134	27	2115	23	2097	35	0.744	98

continuação Dados da análise U-Pb por LA-ICP-MS da amostra AE-24C (Leucossoma).

AMOSTRA	AE-24C																		
											Idades aparentes								
GRÃO	*f* 206 (%)	Th/U	206Pb/204Pb	207Pb/206Pb	err (%) 1 σ	207Pb/235U	err (%) 1 σ	206Pb/238U	err (%) 1 σ	207Pb/206Pb	2 σ	207Pb/235U	2 σ	206Pb/238U	2 σ	Rho	conc. (%)
ZR39	0.29	0.27	627545	0.13347	1.6	7.58270	1.9	0.41200	1.1	2144	54	2183	34	2224	40	0.555	104
ZR55	0.17	0.35	506112	0.13365	0.5	7.11275	0.9	0.38597	0.7	2146	17	2126	16	2104	25	0.739	98
ZR47	0.49	0.35	1434393	0.13386	0.4	7.35084	1.2	0.39825	1.1	2149	14	2155	21	2161	39	0.891	101
ZR9	0.24	0.26	112047	0.13465	0.5	8.36939	4.0	0.45077	3.9	2159	17	2272	71	2399	157	0.988	111
ZR34	0.31	0.18	836305	0.13612	0.6	7.36849	1.0	0.39257	0.7	2178	19	2157	17	2135	25	0.717	98
ZR41	0.43	0.36	109591	0.13619	0.6	7.74000	1.3	0.41218	1.1	2179	20	2201	23	2225	42	0.857	102
ZR2	0.24	0.35	774798	0.13633	0.3	7.03073	1.0	0.37399	0.8	2181	12	2115	17	2048	29	0.957	94
ZR3	0.06	0.31	300813	0.13826	0.4	7.55208	0.8	0.39612	0.6	2206	13	2179	15	2151	23	0.755	98
ZR15	0.20	0.24	543136	0.13857	0.5	8.32575	1.2	0.43573	1.0	2209	18	2267	21	2331	37	0.832	106
ZR11	0.28	0.45	1090	0.14104	0.8	4.56501	1.5	0.23473	1.2	2240	27	1743	25	1359	30	0.821	61

Tabela II.5. Dados da análise U-Pb por LA-ICP-MS da amostra JAMES-08 (Paleossoma).

AMOSTRA	JAMES-08																	
										Idades aparentes								
GRÃO	*f* 206 (%)	Th / U	206Pb / 204Pb	207Pb / 206Pb	err (%) 1 σ	207Pb / 235U	err (%) 1 σ	206Pb / 238U	err (%) 1 σ	207Pb / 206Pb	2 σ	207Pb / 235U	2 σ	206Pb / 238U	2 σ	Rho	conc. (%)
ZR3	0.19	0.27	52879	0.16733	2.1	7.94668	2.8	0.34440	1.8	2531	69	2225	50	1908	60	0.650	75
ZR5	0.21	0.09	64452	0.16812	1.5	7.98988	2.6	0.34465	2.1	2539	50	2230	46	1909	68	0.804	75
ZR6	0.03	0.41	117604	0.17171	2.6	10.71669	4.1	0.45261	3.1	2574	85	2499	74	2407	124	0.766	93
ZR18	0.28	0.12	857865	0.17351	0.9	9.46238	1.8	0.39550	1.5	2592	30	2384	33	2148	56	0.842	83
ZR2	0.24	0.30	773166	0.17613	0.9	12.75979	3.3	0.52539	3.1	2617	31	2662	60	2722	137	0.950	104
ZR10	0.17	0.30	416400	0.17873	0.5	11.33456	1.5	0.45992	1.3	2641	17	2551	27	2439	54	0.905	92
~~ZR9~~	~~0.30~~	~~0.80~~	~~2773~~	~~0.07954~~	~~3.3~~	~~1.64424~~	~~5.4~~	~~0.14992~~	~~4.2~~	~~1186~~	~~127~~	~~987~~	~~67~~	~~900~~	~~71~~	~~0.790~~	~~76~~
~~ZR8~~	~~0.09~~	~~0.06~~	~~57854~~	~~0.08890~~	~~5.4~~	~~1.50038~~	~~7.2~~	~~0.12239~~	~~4.8~~	~~1402~~	~~200~~	~~931~~	~~86~~	~~744~~	~~67~~	~~0.663~~	~~53~~
~~ZR22~~	~~0.23~~	~~0.23~~	~~14476~~	~~0.09907~~	~~5.3~~	~~1.79834~~	~~5.8~~	~~0.13164~~	~~2.3~~	~~1607~~	~~193~~	~~1045~~	~~75~~	~~797~~	~~34~~	~~0.392~~	~~50~~
~~ZR15~~	~~0.25~~	~~0.22~~	~~16789~~	~~0.10717~~	~~1.0~~	~~2.91003~~	~~2.3~~	~~0.19693~~	~~2.1~~	~~1752~~	~~36~~	~~1385~~	~~35~~	~~1159~~	~~44~~	~~0.888~~	~~66~~
~~ZR20~~	~~0.08~~	~~0.03~~	~~92316~~	~~0.10754~~	~~5.0~~	~~2.56508~~	~~8.1~~	~~0.17299~~	~~6.3~~	~~1758~~	~~179~~	~~1291~~	~~115~~	~~1029~~	~~120~~	~~0.781~~	~~59~~
~~ZR19~~	~~0.11~~	~~0.14~~	~~5188~~	~~0.11468~~	~~4.1~~	~~2.91725~~	~~5.4~~	~~0.18448~~	~~3.4~~	~~1875~~	~~146~~	~~1386~~	~~80~~	~~1091~~	~~68~~	~~0.631~~	~~58~~
~~ZR12~~	~~0.25~~	~~0.17~~	~~16721~~	~~0.11569~~	~~0.6~~	~~3.45356~~	~~6.1~~	~~0.21649~~	~~6.0~~	~~1891~~	~~20~~	~~1517~~	~~93~~	~~1263~~	~~138~~	~~0.994~~	~~67~~
~~ZR25~~	~~0.30~~	~~0.49~~	~~23787~~	~~0.11834~~	~~1.3~~	~~3.62581~~	~~1.6~~	~~0.22220~~	~~0.8~~	~~1931~~	~~46~~	~~1555~~	~~25~~	~~1294~~	~~18~~	~~0.503~~	~~67~~
~~ZR28~~	~~0.30~~	~~0.41~~	~~320339~~	~~0.11913~~	~~0.5~~	~~4.68961~~	~~1.4~~	~~0.28549~~	~~1.3~~	~~1943~~	~~18~~	~~1765~~	~~23~~	~~1619~~	~~36~~	~~0.897~~	~~83~~
~~ZR14~~	~~0.34~~	~~0.20~~	~~539404~~	~~0.11971~~	~~1.7~~	~~4.67863~~	~~2.0~~	~~0.28345~~	~~0.9~~	~~1952~~	~~60~~	~~1763~~	~~33~~	~~1609~~	~~26~~	~~0.461~~	~~82~~
~~ZR31~~	~~0.37~~	~~0.35~~	~~941100~~	~~0.12069~~	~~0.5~~	~~5.27568~~	~~1.3~~	~~0.31700~~	~~1.2~~	~~1966~~	~~19~~	~~1865~~	~~23~~	~~1775~~	~~36~~	~~0.870~~	~~90~~
~~ZR13~~	~~0.29~~	~~0.32~~	~~546972~~	~~0.12117~~	~~1.1~~	~~5.08404~~	~~2.7~~	~~0.30429~~	~~2.5~~	~~1974~~	~~40~~	~~1833~~	~~46~~	~~1713~~	~~74~~	~~0.902~~	~~87~~
~~ZR1~~	~~0.27~~	~~0.24~~	~~285566~~	~~0.12890~~	~~4.2~~	~~4.47035~~	~~6.7~~	~~0.25150~~	~~5.2~~	~~2083~~	~~143~~	~~1725~~	~~108~~	~~1446~~	~~135~~	~~0.780~~	~~69~~
~~ZR21~~	~~0.24~~	~~0.29~~	~~71733~~	~~0.12961~~	~~1.7~~	~~6.01969~~	~~2.9~~	~~0.33682~~	~~2.4~~	~~2093~~	~~58~~	~~1979~~	~~50~~	~~1871~~	~~77~~	~~0.813~~	~~89~~
~~ZR17~~	~~0.37~~	~~0.14~~	~~90781~~	~~0.14369~~	~~0.6~~	~~5.58803~~	~~1.1~~	~~0.28204~~	~~0.9~~	~~2272~~	~~21~~	~~1914~~	~~19~~	~~1602~~	~~24~~	~~0.767~~	~~70~~
~~ZR29~~	~~0.20~~	~~0.20~~	~~193154~~	~~0.15144~~	~~2.1~~	~~10.05654~~	~~3.4~~	~~0.48159~~	~~2.6~~	~~2362~~	~~70~~	~~2440~~	~~61~~	~~2534~~	~~110~~	~~0.781~~	~~107~~
~~ZR32~~	~~0.22~~	~~0.02~~	~~578705~~	~~0.15321~~	~~0.6~~	~~9.04768~~	~~1.7~~	~~0.42826~~	~~1.5~~	~~2382~~	~~21~~	~~2343~~	~~30~~	~~2298~~	~~57~~	~~0.898~~	~~96~~
~~ZR16~~	~~0.25~~	~~0.34~~	~~101836~~	~~0.16704~~	~~0.7~~	~~7.05960~~	~~1.7~~	~~0.30650~~	~~1.5~~	~~2528~~	~~24~~	~~2119~~	~~30~~	~~1723~~	~~46~~	~~0.882~~	~~68~~
~~ZR4~~	~~0.29~~	~~0.67~~	~~19253~~	~~0.18061~~	~~1.9~~	~~11.09929~~	~~3.0~~	~~0.44568~~	~~2.3~~	~~2658~~	~~63~~	~~2531~~	~~55~~	~~2376~~	~~90~~	~~0.757~~	~~89~~
~~ZR24~~	~~0.21~~	~~0.56~~	~~57112~~	~~0.18469~~	~~0.9~~	~~9.95827~~	~~3.4~~	~~0.39102~~	~~3.3~~	~~2695~~	~~29~~	~~2431~~	~~62~~	~~2128~~	~~119~~	~~0.960~~	~~79~~
~~ZR26~~	~~0.07~~	~~0.38~~	~~279389~~	~~0.19474~~	~~2.9~~	~~15.24168~~	~~5.7~~	~~0.56761~~	~~4.9~~	~~2783~~	~~95~~	~~2830~~	~~106~~	~~2898~~	~~226~~	~~0.854~~	~~104~~
~~ZR11~~	~~0.13~~	~~0.15~~	~~36320~~	~~0.19564~~	~~1.8~~	~~9.81784~~	~~2.1~~	~~0.36394~~	~~1.1~~	~~2790~~	~~58~~	~~2418~~	~~39~~	~~2001~~	~~37~~	~~0.512~~	~~72~~
~~ZR7~~	~~0.20~~	~~0.48~~	~~30503~~	~~0.19657~~	~~2.5~~	~~12.26886~~	~~5.3~~	~~0.45264~~	~~4.7~~	~~2798~~	~~79~~	~~2625~~	~~98~~	~~2407~~	~~188~~	~~0.884~~	~~86~~
~~ZR27~~	~~0.23~~	~~0.52~~	~~46266~~	~~0.20927~~	~~1.6~~	~~11.48880~~	~~2.9~~	~~0.39813~~	~~2.4~~	~~2900~~	~~50~~	~~2564~~	~~53~~	~~2160~~	~~88~~	~~0.831~~	~~74~~
~~ZR30~~	~~0.19~~	~~0.21~~	~~363241~~	~~0.21304~~	~~2.8~~	~~19.57526~~	~~5.7~~	~~0.66637~~	~~5.0~~	~~2929~~	~~89~~	~~3071~~	~~107~~	~~3292~~	~~254~~	~~0.870~~	~~112~~
~~ZR23~~	~~0.11~~	~~0.33~~	~~2460898~~	~~0.22047~~	~~2.8~~	~~20.21929~~	~~4.9~~	~~0.66508~~	~~4.0~~	~~2984~~	~~88~~	~~3102~~	~~93~~	~~3287~~	~~207~~	~~0.823~~	~~110~~

Tabela II.6. Dados da análise U-Pb por LA-ICP-MS da amostra JAMES-39 (Migmatito Espinho

ranco).

AMOSTRA	JAMES-39																	
										Idades aparentes								
GRÃO	*f* 206 (%)	Th/U	206Pb/204Pb	207Pb/206Pb	err (%) 1 σ	207Pb/235U	err (%) 1 σ	206Pb/238U	err (%) 1 σ	207Pb/206Pb	2 σ	207Pb/235U	2 σ	206Pb/238U	2 σ	Rho	conc. (%)
ZR13	1.33	0.23	187559	0.12749	0.4	4.90004	0.8	0.27873	0.6	2064	15	1802	14	1585	17	0.732	77
ZR18	0.91	0.30	194352	0.12933	1.0	5.26546	4.2	0.29525	4.1	2089	35	1863	70	1668	119	0.967	80
ZR8	0.93	0.32	153747	0.13156	0.9	5.99399	3.7	0.33042	3.6	2119	31	1975	64	1840	115	0.966	87
ZR17	1.35	0.38	468328	0.13333	0.5	6.21749	0.9	0.33817	0.7	2142	16	2007	16	1878	23	0.767	88
ZR2	1.11	0.37	201304	0.13375	0.8	6.60961	1.1	0.35838	0.7	2148	27	2061	20	1974	25	0.651	92
ZR29	1.23	0.37	194307	0.13461	1.2	6.63770	4.9	0.35761	4.7	2159	43	2064	84	1971	159	0.965	91
ZR16	1.00	0.31	348507	0.13480	0.6	6.57212	1.2	0.35357	0.9	2161	21	2056	21	1952	32	0.801	90
ZR23	1.01	0.33	417023	0.13525	0.4	6.61182	1.0	0.35452	0.9	2167	14	2061	18	1956	30	0.846	90
ZR28	1.08	0.39	768122	0.13539	0.3	6.51471	0.7	0.34897	0.5	2169	10	2048	12	1930	17	0.748	89
ZR24	0.97	0.41	320350	0.13560	0.5	6.65050	1.2	0.35567	1.0	2172	18	2066	21	1962	34	0.843	90
ZR31	0.83	0.21	330971	0.13584	0.9	6.48201	1.5	0.34606	1.2	2175	31	2043	26	1916	38	0.769	88
ZR4	0.91	0.28	206616	0.13585	0.7	6.59274	2.1	0.35194	2.0	2175	23	2058	37	1944	67	0.935	89
ZR15	1.23	0.37	423959	0.13640	0.7	7.00677	2.7	0.37254	2.6	2182	25	2112	48	2041	91	0.954	94
ZR25	0.49	0.47	227344	0.13762	0.4	6.84197	0.9	0.36055	0.7	2197	14	2091	16	1985	24	0.789	90
ZR30	1.04	0.25	162165	0.13763	0.6	7.81598	2.9	0.41185	2.9	2198	19	2210	52	2223	108	0.974	101
ZR1	0.82	0.36	438342	0.13799	0.8	8.06447	3.5	0.42383	3.4	2202	28	2238	62	2278	128	0.968	103
ZR14	0.90	0.34	182613	0.14039	0.8	8.44377	2.2	0.43619	2.1	2232	28	2280	40	2334	80	0.915	105
~~ZR5~~	~~0.88~~	~~0.02~~	~~221480~~	~~0.05909~~	~~0.5~~	~~0.77196~~	~~1.4~~	~~0.09475~~	~~1.2~~	~~570~~	~~20~~	~~581~~	~~12~~	~~584~~	~~14~~	~~0.903~~	~~102~~
~~ZR22~~	~~0.01~~	~~0.37~~	~~202880~~	~~0.10747~~	~~1.4~~	~~2.03367~~	~~7.6~~	~~0.13723~~	~~7.5~~	~~1757~~	~~50~~	~~1127~~	~~101~~	~~829~~	~~116~~	~~0.982~~	~~47~~
~~ZR11~~	~~0.89~~	~~0.28~~	~~55105~~	~~0.10985~~	~~1.4~~	~~2.76629~~	~~4.4~~	~~0.18263~~	~~4.2~~	~~1797~~	~~49~~	~~1346~~	~~65~~	~~1081~~	~~83~~	~~0.948~~	~~60~~
~~ZR21~~	~~1.13~~	~~0.33~~	~~132956~~	~~0.11018~~	~~0.6~~	~~2.61963~~	~~1.4~~	~~0.17242~~	~~1.2~~	~~1802~~	~~21~~	~~1306~~	~~21~~	~~1025~~	~~23~~	~~0.870~~	~~57~~
~~ZR32~~	~~0.76~~	~~0.29~~	~~202248~~	~~0.11482~~	~~0.9~~	~~3.10588~~	~~3.0~~	~~0.19616~~	~~2.8~~	~~1877~~	~~32~~	~~1434~~	~~46~~	~~1155~~	~~60~~	~~0.946~~	~~62~~
~~ZR26~~	~~0.74~~	~~0.21~~	~~2172~~	~~0.11549~~	~~2.0~~	~~3.19126~~	~~4.1~~	~~0.20039~~	~~3.6~~	~~1888~~	~~73~~	~~1455~~	~~63~~	~~1177~~	~~77~~	~~0.865~~	~~62~~
~~ZR3~~	~~0.01~~	~~0.37~~	~~169789~~	~~0.12396~~	~~2.2~~	~~4.50630~~	~~7.8~~	~~0.26363~~	~~7.5~~	~~2014~~	~~77~~	~~1732~~	~~126~~	~~1508~~	~~200~~	~~0.958~~	~~75~~
~~ZR10~~	~~0.29~~	~~0.17~~	~~110125~~	~~0.12403~~	~~2.3~~	~~4.30937~~	~~5.0~~	~~0.25197~~	~~4.4~~	~~2015~~	~~79~~	~~1695~~	~~81~~	~~1449~~	~~115~~	~~0.889~~	~~72~~
~~ZR27~~	~~0.01~~	~~0.27~~	~~255105~~	~~0.12599~~	~~2.3~~	~~4.76344~~	~~7.0~~	~~0.27419~~	~~6.6~~	~~2043~~	~~79~~	~~1778~~	~~115~~	~~1562~~	~~183~~	~~0.945~~	~~76~~
~~ZR7~~	~~0.88~~	~~0.13~~	~~113390~~	~~0.12725~~	~~1.9~~	~~5.51545~~	~~3.7~~	~~0.31434~~	~~3.2~~	~~2060~~	~~65~~	~~1903~~	~~63~~	~~1762~~	~~98~~	~~0.859~~	~~86~~
~~ZR6~~	~~1.32~~	~~0.19~~	~~394651~~	~~0.12809~~	~~0.9~~	~~5.84322~~	~~2.1~~	~~0.33083~~	~~1.9~~	~~2072~~	~~32~~	~~1953~~	~~36~~	~~1842~~	~~59~~	~~0.881~~	~~89~~
~~ZR12~~	~~1.36~~	~~0.36~~	~~316386~~	~~0.12938~~	~~0.9~~	~~5.79894~~	~~3.7~~	~~0.32505~~	~~3.6~~	~~2090~~	~~32~~	~~1946~~	~~64~~	~~1814~~	~~114~~	~~0.964~~	~~87~~
~~ZR19~~	~~0.01~~	~~0.20~~	~~242123~~	~~0.13142~~	~~2.8~~	~~6.44543~~	~~5.3~~	~~0.35567~~	~~4.5~~	~~2117~~	~~98~~	~~2038~~	~~91~~	~~1962~~	~~150~~	~~0.842~~	~~93~~
~~ZR9~~	~~1.33~~	~~0.38~~	~~491782~~	~~0.13507~~	~~0.6~~	~~7.24893~~	~~3.2~~	~~0.38920~~	~~3.1~~	~~2165~~	~~20~~	~~2143~~	~~56~~	~~2119~~	~~113~~	~~0.977~~	~~98~~
~~ZR20~~	~~0.95~~	~~0.30~~	~~227739~~	~~0.14599~~	~~1.8~~	~~8.87370~~	~~4.0~~	~~0.44081~~	~~3.6~~	~~2299~~	~~61~~	~~2325~~	~~73~~	~~2354~~	~~142~~	~~0.892~~	~~102~~

Tabela II.7. Dados da análise U-Pb por LA-ICP-MS da amostra JAMES-10 (Migmatito).

AMOSTRA	JAMES-10										Idades aparentes					
GRÃO	f 206 (%)	$\frac{Th}{U}$	$\frac{^{206}Pb}{^{204}Pb}$	$\frac{^{207}Pb}{^{206}Pb}$	err (%) 1 σ	$\frac{^{207}Pb}{^{235}U}$	err (%) 1 σ	$\frac{^{206}Pb}{^{238}U}$	err (%) 1 σ	$\frac{^{207}Pb}{^{206}Pb}$	2 σ	$\frac{^{207}Pb}{^{235}U}$	2 σ	$\frac{^{206}Pb}{^{238}U}$	2 σ	Rho	conc. (%)
ZR16	0.23	0.82	672604	0.12935	0.6	5.12009	4.0	0.28706	4.0	2089	19	1839	67	1627	113	0.986	78
ZR3	0.22	0.66	701885	0.13206	0.4	6.03357	2.6	0.33133	2.5	2126	13	1981	44	1845	80	0.979	87
ZR13	0.20	0.48	772468	0.13453	0.3	6.76015	0.9	0.36442	0.7	2158	10	2081	15	2003	24	0.832	93
ZR28	0.56	0.65	271725	0.13467	0.6	7.03947	2.0	0.37907	1.8	2160	22	2116	35	2072	65	0.928	96
ZR12	0.36	0.70	421916	0.13487	0.6	7.37149	2.7	0.39636	2.7	2162	20	2158	48	2152	97	0.967	100
ZR27	0.60	0.52	254269	0.13516	1.9	7.13951	2.2	0.38309	1.1	2166	64	2129	39	2091	40	0.514	97
ZR9	0.25	0.64	614942	0.13547	0.5	7.05556	1.7	0.37770	1.6	2170	18	2118	31	2066	57	0.930	95
ZR24	2.68	0.47	56302	0.13586	2.0	7.40385	3.3	0.39522	2.6	2175	70	2161	58	2147	93	0.780	99
ZR29	0.57	0.48	265083	0.13631	0.4	7.20274	1.0	0.38321	0.8	2181	13	2137	17	2091	28	0.827	96
ZR8	0.25	0.49	596002	0.13669	0.5	7.34763	0.8	0.38984	0.6	2186	16	2155	15	2122	22	0.714	97
ZR31	0.32	0.64	471937	0.13710	0.3	7.52782	0.8	0.39820	0.7	2191	12	2176	15	2161	25	0.800	99
ZR20	0.43	0.49	354367	0.13736	0.3	7.51200	0.8	0.39660	0.6	2194	11	2174	14	2153	22	0.768	98
ZR25	1.51	0.50	99603	0.13750	0.8	7.75243	3.5	0.40889	3.3	2196	28	2203	61	2210	124	0.966	101
ZR23	0.35	0.69	433928	0.13949	0.5	8.19689	2.0	0.42615	1.9	2221	18	2253	37	2288	75	0.952	103
ZR1	0.24	0.52	621140	0.14213	1.2	8.74070	4.4	0.44599	4.2	2253	41	2311	78	2377	166	0.958	106
ZR4	0.14	0.46	1102313	0.14298	1.1	9.09010	3.2	0.46106	3.0	2264	38	2347	58	2444	121	0.930	108
~~ZR30~~	~~0.25~~	~~0.06~~	~~612854~~	~~0.05922~~	~~0.4~~	~~0.76210~~	~~0.9~~	~~0.09333~~	~~0.8~~	~~575~~	~~16~~	~~575~~	~~8~~	~~575~~	~~9~~	~~0.832~~	~~100~~
~~ZR14~~	~~0.63~~	~~0.66~~	~~244759~~	~~0.12117~~	~~3.2~~	~~4.29777~~	~~5.8~~	~~0.25724~~	~~4.8~~	~~1973~~	~~112~~	~~1693~~	~~93~~	~~1476~~	~~126~~	~~0.830~~	~~75~~
~~ZR11~~	~~0.21~~	~~0.82~~	~~731166~~	~~0.12228~~	~~2.3~~	~~4.39460~~	~~4.5~~	~~0.26063~~	~~3.8~~	~~1990~~	~~82~~	~~1711~~	~~73~~	~~1493~~	~~101~~	~~0.849~~	~~75~~
~~ZR22~~	~~1.45~~	~~1.05~~	~~195495~~	~~0.12472~~	~~5.3~~	~~5.13027~~	~~5.7~~	~~0.29830~~	~~2.1~~	~~2025~~	~~181~~	~~1841~~	~~94~~	~~1683~~	~~61~~	~~0.365~~	~~83~~
~~ZR2~~	~~0.09~~	~~0.91~~	~~1770711~~	~~0.12812~~	~~3.5~~	~~5.99070~~	~~3.8~~	~~0.33090~~	~~1.2~~	~~2072~~	~~122~~	~~1974~~	~~64~~	~~1802~~	~~40~~	~~0.329~~	~~91~~
~~ZR19~~	~~0.11~~	~~1.02~~	~~1329103~~	~~0.13233~~	~~2.6~~	~~6.69503~~	~~2.7~~	~~0.36692~~	~~0.7~~	~~2129~~	~~90~~	~~2072~~	~~47~~	~~2015~~	~~23~~	~~0.241~~	~~95~~
~~ZR15~~	~~6.73~~	~~0.42~~	~~22565~~	~~0.13282~~	~~1.7~~	~~6.63598~~	~~2.1~~	~~0.36233~~	~~1.2~~	~~2136~~	~~58~~	~~2064~~	~~36~~	~~1993~~	~~40~~	~~0.559~~	~~93~~
~~ZR10~~	~~0.17~~	~~0.80~~	~~871636~~	~~0.13377~~	~~1.5~~	~~6.52206~~	~~1.8~~	~~0.35359~~	~~0.8~~	~~2148~~	~~54~~	~~2049~~	~~31~~	~~1952~~	~~27~~	~~0.451~~	~~91~~
~~ZR32~~	~~0.78~~	~~0.86~~	~~190884~~	~~0.13430~~	~~1.3~~	~~8.24281~~	~~2.8~~	~~0.44512~~	~~2.5~~	~~2155~~	~~45~~	~~2258~~	~~51~~	~~2374~~	~~99~~	~~0.878~~	~~110~~
~~ZR21~~	~~0.21~~	~~0.53~~	~~715876~~	~~0.13535~~	~~4.0~~	~~8.43635~~	~~4.6~~	~~0.45203~~	~~2.2~~	~~2169~~	~~136~~	~~2279~~	~~82~~	~~2404~~	~~90~~	~~0.487~~	~~111~~
~~ZR7~~	~~0.12~~	~~0.56~~	~~1307092~~	~~0.13535~~	~~1.3~~	~~7.23833~~	~~1.5~~	~~0.38703~~	~~0.6~~	~~2169~~	~~45~~	~~2141~~	~~26~~	~~2113~~	~~23~~	~~0.426~~	~~97~~
~~ZR17~~	~~0.30~~	~~0.66~~	~~511981~~	~~0.13658~~	~~2.1~~	~~6.96088~~	~~2.4~~	~~0.36962~~	~~1.0~~	~~2184~~	~~73~~	~~2106~~	~~42~~	~~2028~~	~~35~~	~~0.422~~	~~93~~
~~ZR5~~	~~0.49~~	~~0.34~~	~~309565~~	~~0.13658~~	~~0.8~~	~~6.60899~~	~~3.4~~	~~0.35517~~	~~3.3~~	~~2184~~	~~29~~	~~2071~~	~~59~~	~~1959~~	~~109~~	~~0.963~~	~~90~~
~~ZR6~~	~~0.17~~	~~0.57~~	~~895338~~	~~0.13689~~	~~1.8~~	~~7.26813~~	~~2.0~~	~~0.38506~~	~~0.7~~	~~2188~~	~~63~~	~~2145~~	~~36~~	~~2100~~	~~26~~	~~0.366~~	~~96~~
~~ZR18~~	~~0.28~~	~~0.49~~	~~530191~~	~~0.14282~~	~~1.2~~	~~7.32584~~	~~1.5~~	~~0.37198~~	~~0.9~~	~~2262~~	~~40~~	~~2152~~	~~27~~	~~2039~~	~~33~~	~~0.612~~	~~90~~
~~ZR26~~	~~0.48~~	~~0.44~~	~~313463~~	~~0.14633~~	~~1.7~~	~~9.24923~~	~~4.0~~	~~0.45834~~	~~3.6~~	~~2303~~	~~57~~	~~2363~~	~~71~~	~~2432~~	~~144~~	~~0.903~~	~~106~~

Tabela II.8. Dados da análise U-Pb por LA-ICP-MS da amostra JAMES-11 (Migmatito).

AMOSTRA	JAMES-11											Idades aparentes					
GRÃO	*f* 206 (%)	Th/U	206Pb/204Pb	207Pb/206Pb	err (%) 1σ	207Pb/235U	err (%) 1σ	206Pb/238U	err (%) 1σ	207Pb/206Pb	2σ	207Pb/235U	2σ	206Pb/238U	2σ	Rho	conc. (%)
ZR29	0.00	0.07	452923	0.06039	1.9	0.77684	2.2	0.09329	1.2	618	79	584	20	575	13	0.542	93
ZR38	0.01	0.48	261854	0.12954	0.7	5.09823	1.1	0.28541	0.8	2092	24	1836	18	1619	22	0.701	77
ZR24	0.00	0.40	373755	0.13124	0.7	5.35784	2.0	0.29607	1.8	2115	25	1878	34	1672	53	0.915	79
ZR12	0.00	0.50	468222	0.13288	0.5	5.49947	1.4	0.30013	1.3	2136	17	1901	24	1692	37	0.900	79
ZR9	0.00	0.21	345258	0.13397	0.5	5.69837	0.9	0.30847	0.6	2151	18	1931	15	1733	19	0.704	81
ZR37	0.01	0.48	173619	0.13569	0.7	6.21711	1.7	0.33227	1.5	2173	23	2007	29	1849	49	0.896	85
ZR25	0.00	0.62	423427	0.13591	0.6	6.29989	1.2	0.33616	0.9	2176	21	2018	20	1868	30	0.793	86
ZR10N	0.01	0.33	147949	0.13614	0.5	6.15786	1.1	0.32803	0.9	2179	19	1998	20	1829	29	0.815	84
ZR3	0.00	0.76	356765	0.13705	0.5	6.55706	1.5	0.34698	1.3	2190	17	2054	25	1920	44	0.909	88
ZR21	0.00	0.53	411970	0.13706	0.5	6.45284	1.0	0.34143	0.7	2190	18	2039	17	1894	24	0.758	86
ZR18	0.00	0.53	348493	0.13758	0.7	7.21283	1.2	0.38021	0.9	2197	25	2138	21	2077	31	0.733	95
ZR10B	0.00	0.47	501576	0.13769	0.5	6.84599	0.9	0.36059	0.7	2198	17	2092	16	1985	24	0.755	90
ZR14N	0.00	0.45	374619	0.13771	0.4	6.95026	0.8	0.36602	0.6	2199	15	2105	14	2011	19	0.709	91
ZR6	0.00	0.56	318236	0.13776	0.4	6.82731	0.9	0.35941	0.7	2199	13	2089	15	1979	24	0.804	90
ZR34	0.00	0.84	738395	0.13781	0.5	6.96111	0.9	0.36633	0.7	2200	18	2106	16	2012	22	0.718	91
ZR11	0.00	0.55	778571	0.13800	0.4	6.88909	1.1	0.36203	1.0	2202	15	2097	20	1992	33	0.853	90
ZR31	0.00	0.52	422716	0.13824	0.7	6.81652	1.0	0.35761	0.7	2205	23	2088	18	1971	24	0.687	89
ZR39	0.00	0.64	366112	0.13853	0.7	7.26931	1.0	0.38056	0.6	2209	25	2145	18	2079	22	0.610	94
ZR32	0.00	0.48	432950	0.13865	0.8	7.05675	1.2	0.36910	0.8	2210	26	2119	21	2025	28	0.688	92
ZR26	0.00	0.56	481591	0.13872	0.7	6.68513	1.0	0.34950	0.6	2211	24	2071	17	1932	20	0.606	87
ZR40	0.00	0.74	303192	0.13882	0.7	7.37073	1.6	0.38507	1.4	2212	24	2157	29	2100	50	0.875	95
ZR14B	0.00	0.30	341692	0.13907	0.4	7.06285	0.8	0.36830	0.5	2216	15	2119	14	2021	19	0.695	91
ZR27	0.00	0.51	441248	0.13908	0.9	6.99555	1.9	0.36477	1.6	2216	30	2111	33	2005	56	0.866	90
ZR36	0.00	0.66	559526	0.13935	0.5	7.23733	0.9	0.37664	0.7	2219	18	2141	16	2061	23	0.718	93
ZR19	0.01	0.94	144272	0.13937	0.6	7.33970	1.1	0.38191	0.8	2219	22	2154	19	2085	27	0.719	94
ZR33	0.00	0.76	687194	0.13944	0.8	7.33866	1.1	0.38167	0.7	2220	27	2154	20	2084	26	0.648	94
ZR1	0.00	0.52	696520	0.13965	0.5	7.84662	0.9	0.40749	0.6	2223	16	2214	15	2203	24	0.734	99
ZR20	0.00	0.53	952502	0.13990	0.7	7.24812	1.1	0.37572	0.7	2226	25	2142	19	2056	24	0.653	92
ZR17	0.00	0.63	382932	0.13994	0.7	7.25735	1.0	0.37610	0.7	2226	24	2144	19	2058	24	0.660	92
ZR8	0.01	0.68	281097	0.14012	0.5	7.58288	0.9	0.39247	0.7	2229	16	2183	16	2134	25	0.765	96
ZR35	0.00	0.51	625759	0.14117	0.5	7.74990	0.9	0.39813	0.6	2242	18	2202	16	2160	22	0.680	96
ZR2	0.01	0.63	223533	0.14163	0.8	8.27747	1.3	0.42384	0.9	2247	29	2262	23	2278	33	0.683	101

continuação Dados da análise U-Pb por LA-ICP-MS da amostra JAMES-11 (Migmatito).

AMOSTRA	JAMES-11										Idades aparentes					
GRÃO	*f* 206 (%)	Th/U	206Pb/204Pb	207Pb/206Pb	err (%) 1 σ	207Pb/235U	err (%) 1 σ	206Pb/238U	err (%) 1 σ	207Pb/206Pb	2 σ	207Pb/235U	2 σ	206Pb/238U	2 σ	Rho	conc. (%)
ZR23	0.14	0.06	10848	0.04983	10.7	0.54464	12.6	0.07927	6.5	187	464	441	88	492	62	0.519	263
ZR15	0.01	0.30	261268	0.09281	1.9	0.84728	7.1	0.06620	6.9	1484	71	623	65	413	55	0.963	28
ZR16	0.12	0.37	12932	0.10973	2.0	1.91279	3.2	0.12642	2.5	1795	71	1086	42	767	35	0.774	43
ZR7	0.00	0.01	347008	0.12540	0.4	4.66286	0.9	0.26966	0.7	2034	14	1761	14	1539	18	0.765	76
ZR28	0.00	0.40	382886	0.12946	0.9	4.47556	1.2	0.25071	0.7	2091	31	1726	20	1442	19	0.605	69
ZR30	0.00	0.64	397087	0.13299	2.1	5.41833	2.2	0.29546	0.8	2138	72	1888	38	1669	22	0.339	78
ZR5	0.00	0.35	492732	0.13484	1.0	6.73174	2.0	0.36205	1.6	2162	36	2077	36	1992	56	0.829	92
ZR13	0.01	0.62	231057	0.13722	1.9	6.84496	2.2	0.36175	0.8	2192	67	2092	38	1990	29	0.395	91
ZR22	0.00	0.56	344018	0.16149	2.7	12.89959	3.4	0.57929	2.0	2471	88	2672	62	2946	96	0.606	119
ZR4	0.01	0.38	163353	0.17130	4.0	14.12377	5.0	0.59705	3.0	2570	131	2758	93	3022	146	0.603	118

Tabela II.9. Dados da análise U-Pb por LA-ICP-MS da amostra JAMES-49

AMOSTRA	JAMES-49									Idades aparentes						
GRÃO	f 206 (%)	$\frac{Th}{U}$	$\frac{206Pb}{204Pb}$	$\frac{207Pb}{206Pb}$	err (%) 1 6	$\frac{207Pb}{235U}$	err (%) 1 6	$\frac{206Pb}{238U}$	err (%) 1 6	$\frac{207Pb}{206Pb}$	2 6	$\frac{207Pb}{235U}$	2 6	$\frac{206Pb}{238U}$	2 6	Rho	conc. (%)
ZR20	1.30	0.14	20215	0.07552	1.5	1.03407	2.8	0.09930	2.3	1082	59	721	28	610	27	0.834	56
ZR19	0.74	0.12	15722	0.07578	1.4	1.10287	2.2	0.10554	1.6	1089	57	755	23	647	19	0.727	59
ZR18	0.82	0.32	15334	0.09312	1.4	1.55555	2.8	0.12115	2.5	1490	51	953	35	737	34	0.867	49
ZR17	0.98	0.25	7253	0.10307	1.0	2.08823	2.2	0.14694	2.0	1680	37	1145	31	884	32	0.875	53
ZR16	1.06	0.22	4146	0.11522	1.8	2.91231	2.9	0.18331	2.3	1883	65	1385	44	1085	45	0.772	58
ZR14	1.42	0.05	7914	0.11552	1.7	3.04678	3.7	0.19127	3.3	1888	62	1419	56	1128	68	0.880	60
ZR13	0.86	0.27	2117	0.11986	1.5	3.38358	2.0	0.20473	1.2	1954	54	1501	30	1201	26	0.597	61
ZR11	1.04	0.27	12341	0.12002	2.4	3.01096	4.2	0.18193	3.4	1957	84	1410	63	1078	68	0.820	55
ZR10	1.15	0.27	8108	0.12144	2.4	3.48365	4.8	0.20804	4.1	1977	85	1524	74	1218	91	0.859	62
ZR8	0.98	0.22	197036	0.12903	0.7	4.83627	2.2	0.27183	2.0	2085	26	1791	36	1550	55	0.925	74
ZR7	0.77	0.28	52660	0.13098	1.0	4.47620	2.9	0.24783	2.7	2111	34	1727	47	1427	68	0.930	68
ZR6	0.86	0.40	132661	0.13213	1.3	5.33832	2.4	0.29299	1.9	2127	47	1875	40	1656	55	0.806	78
ZR5	0.91	0.23	211471	0.13271	0.6	5.65590	1.5	0.30907	1.3	2134	20	1925	25	1736	39	0.883	81
ZR3	0.81	0.36	328798	0.13592	0.6	6.21108	2.0	0.33139	1.9	2176	21	2006	34	1845	59	0.936	85
~~ZR15~~	~~1.63~~	~~0.06~~	~~142316~~	~~0.04694~~	~~3.9~~	~~0.46550~~	~~6.3~~	~~0.07102~~	~~5.0~~	~~46~~	~~180~~	~~388~~	~~41~~	~~448~~	~~43~~	~~0.791~~	~~968~~
~~ZR32~~	~~1.62~~	~~0.01~~	~~401612~~	~~0.05270~~	~~2.2~~	~~0.61409~~	~~3.0~~	~~0.08464~~	~~2.0~~	~~316~~	~~99~~	~~487~~	~~23~~	~~524~~	~~20~~	~~0.673~~	~~166~~
~~ZR31~~	~~1.25~~	~~0.05~~	~~32903~~	~~0.05312~~	~~2.4~~	~~0.56294~~	~~4.0~~	~~0.07686~~	~~3.2~~	~~334~~	~~107~~	~~463~~	~~29~~	~~477~~	~~30~~	~~0.800~~	~~143~~
~~ZR30~~	~~1.29~~	~~0.10~~	~~5333~~	~~0.05538~~	~~1.5~~	~~0.55449~~	~~4.3~~	~~0.07261~~	~~4.0~~	~~428~~	~~65~~	~~448~~	~~31~~	~~452~~	~~35~~	~~0.935~~	~~106~~
~~ZR29~~	~~1.79~~	~~0.03~~	~~381033~~	~~0.05555~~	~~1.5~~	~~0.67087~~	~~2.1~~	~~0.08875~~	~~1.4~~	~~435~~	~~67~~	~~527~~	~~17~~	~~548~~	~~14~~	~~0.663~~	~~126~~
~~ZR28~~	~~1.56~~	~~0.03~~	~~140533~~	~~0.05593~~	~~1.0~~	~~0.68269~~	~~1.3~~	~~0.08852~~	~~0.7~~	~~450~~	~~43~~	~~528~~	~~11~~	~~547~~	~~8~~	~~0.575~~	~~122~~
~~ZR26~~	~~1.36~~	~~0.01~~	~~307288~~	~~0.05722~~	~~0.7~~	~~0.75207~~	~~1.1~~	~~0.09532~~	~~0.8~~	~~500~~	~~31~~	~~569~~	~~10~~	~~587~~	~~9~~	~~0.693~~	~~117~~
~~ZR25~~	~~2.36~~	~~0.01~~	~~1409344~~	~~0.05900~~	~~0.4~~	~~0.75366~~	~~0.8~~	~~0.09263~~	~~0.6~~	~~567~~	~~15~~	~~570~~	~~7~~	~~571~~	~~6~~	~~0.750~~	~~101~~
~~ZR24~~	~~1.73~~	~~0.00~~	~~694786~~	~~0.05918~~	~~0.4~~	~~0.76604~~	~~0.8~~	~~0.09387~~	~~0.6~~	~~574~~	~~19~~	~~577~~	~~7~~	~~578~~	~~6~~	~~0.713~~	~~101~~
~~ZR27~~	~~0.81~~	~~0.06~~	~~63674~~	~~0.05923~~	~~6.3~~	~~0.69005~~	~~9.0~~	~~0.07959~~	~~6.3~~	~~576~~	~~264~~	~~509~~	~~70~~	~~494~~	~~60~~	~~0.705~~	~~86~~
~~ZR23~~	~~1.49~~	~~0.15~~	~~35727~~	~~0.06178~~	~~0.8~~	~~0.76006~~	~~2.7~~	~~0.08993~~	~~2.6~~	~~666~~	~~34~~	~~577~~	~~24~~	~~555~~	~~27~~	~~0.946~~	~~83~~
~~ZR22~~	~~1.31~~	~~0.05~~	~~67318~~	~~0.06309~~	~~0.6~~	~~0.76075~~	~~1.1~~	~~0.08745~~	~~0.9~~	~~711~~	~~24~~	~~574~~	~~10~~	~~540~~	~~9~~	~~0.790~~	~~76~~
~~ZR9~~	~~1.50~~	~~0.18~~	~~2901~~	~~0.06340~~	~~2.1~~	~~0.85973~~	~~2.4~~	~~0.09834~~	~~1.1~~	~~722~~	~~88~~	~~630~~	~~23~~	~~605~~	~~13~~	~~0.465~~	~~84~~
~~ZR21~~	~~0.87~~	~~0.01~~	~~308369~~	~~0.06974~~	~~1.1~~	~~1.05510~~	~~1.6~~	~~0.10973~~	~~1.1~~	~~921~~	~~45~~	~~731~~	~~17~~	~~671~~	~~14~~	~~0.691~~	~~73~~
~~ZR1~~	~~0.90~~	~~0.50~~	~~2279~~	~~0.08795~~	~~2.0~~	~~1.24190~~	~~5.7~~	~~0.10241~~	~~5.3~~	~~1381~~	~~77~~	~~820~~	~~63~~	~~629~~	~~63~~	~~0.931~~	~~46~~
~~ZR12~~	~~1.20~~	~~0.19~~	~~4509~~	~~0.09916~~	~~3.3~~	~~2.17564~~	~~6.8~~	~~0.15913~~	~~5.9~~	~~1608~~	~~122~~	~~1173~~	~~92~~	~~952~~	~~104~~	~~0.870~~	~~59~~
~~ZR2~~	~~0.74~~	~~0.62~~	~~3709~~	~~0.11033~~	~~1.3~~	~~2.45572~~	~~5.3~~	~~0.16142~~	~~5.1~~	~~1905~~	~~47~~	~~1259~~	~~75~~	~~965~~	~~92~~	~~0.967~~	~~53~~
~~ZR4~~	~~0.90~~	~~0.36~~	~~215601~~	~~0.13588~~	~~0.5~~	~~5.23793~~	~~0.9~~	~~0.27955~~	~~0.7~~	~~2175~~	~~17~~	~~1959~~	~~15~~	~~1589~~	~~19~~	~~0.745~~	~~73~~